Titre: Title:	Implantable Asynchronous Epilectic Seizure Detector
Auteur: Author:	Marjan Mirzaei
Date:	2013
Type:	Mémoire ou thèse / Dissertation or Thesis
Référence: Citation:	Mirzaei, M. (2013). Implantable Asynchronous Epilectic Seizure Detector [Mémoire de maîtrise, École Polytechnique de Montréal]. PolyPublie. https://publications.polymtl.ca/1187/

URL de PolyPublie: PolyPublie URL:	https://publications.polymtl.ca/1187/
Directeurs de recherche: Advisors:	Mohamad Sawan
Programme: Program:	génie électrique

UNIVERSITÉ DE MONTRÉAL

IMPLANTABLE ASYNCHRONOUS EPILEPTIC SEIZURE DETECTOR

MARJAN MIRZAEI

DÉPARTEMENT DE GÉNIE ÉLECTRIQUE

ÉCOLE POLYTECHNIQUE DE MONTRÉAL

MÉMOIRE PRÉSENTÉ EN VUE DE L'OBTENTION

DU DIPLÔME DE MAÎTRISE ÈS SCIENCES APPLIQUÉES

(GÉNIE ÉLECTRIQUE)

MAI 2013

UNIVERSITÉ DE MONTRÉAL

ÉCOLE POLYTECHNIQUE DE MONTRÉAL

Ce mémoire intitulé:

IMPLANTABLE ASYNCHRONOUS EPILEPTIC SEIZURE DETECTOR

présenté par: MIRZAEI Marjan

en vue de l'obtention du diplôme de : Maîtrise ès sciences appliquées

a été dûment accepté par le jury d'examen constitué de :

M. LANGLOIS Pierre, Ph.D., président

M. SAWAN Mohamad, Ph.D., membre et directeur de recherche

M. YAHIA L'Hocine, Ph.D., membre

ACKNOWLEDGEMENTS

I would like to thank my advisor Professor Mohamad Sawan for his support, guidance, and encouragement during my M.A.Sc studies in Polytechnique Montréal. I would like to acknowledge the contribution of the project epileptologist Dr. Dang Khoa Nguyen in this research work. Special thanks to Mohamad Tariq Salam for his valuable discussion and advice along the way. I would like to acknowledge the support and technical advices of Mona Safi-Harb, Masood Karimian, Faycal Mounaim, and Guillaume Simard during the project research.

I would like to thank my office colleagues Nicolas, Jérôme, Bahareh, Marzieh, Ghazal, Mahya, Axelle, Geneviève, Étienne, Sébastien, and Jonathan who provided a friendly and pleasant atmosphere. I am also grateful to all faculty members and other colleagues of the group who helped me during my research.

I would like to thank the members of my committee, Drs. Pierre Langlois and L'Hocine Yahia for taking time to review my work. In addition, I am grateful the Natural Sciences and Engineering Research Council of Canada (NSERC) and Canada Research Chair in Smart Medical Devices for their support.

Finally, I wish to thank my parents and husband for their emotional support and love.

RÉSUMÉ

Plusieurs algorithmes de détection à faible consommation ont été proposés pour le traitement de l'épilepsie focale. La gestion de l'énergie dans ces microsystèmes est une question importante qui dépend principalement de la charge et de la décharge des capacités parasites des transistors et des courants de court-circuit pendant les commutations. Dans ce mémoire, un détecteur asynchrone de crise pour le traitement de l'épilepsie focale est présenté. Ce système fait partie d'un dispositif implantable intégré pour stopper la propagation de la crise. L'objectif de ce travail est de réduire la dissipation de puissance en évitant les transitions inutiles de signaux grâce à la technique du « clock tree » ; en conséquence, les transistors ne changent pas d'état transitoire dans ce mode d'économie d'énergie (période de surveillance des EEG intracrâniens), sauf si un événement anormal est détecté.

Le dispositif intégré proposé comporte un bio-amplificateur en amont (front-end) à faible bruit, un processeur de signal numérique et un détecteur. Un délai variable et quatre détecteurs de fenêtres de tensions variables en parallèles sont utilisés pour extraire de l'information sur le déclenchement des crises. La sensibilité du détecteur est améliorée en optimisant les paramètres variables en fonction des activités de foyers épileptiques de chaque patient lors du début des crises.

Le détecteur de crises asynchrone proposé a été implémenté premièrement en tant que prototype sur un circuit imprimé circulaire, ensuite nous l'avons intégré sur une seule puce dans la technologie standard CMOS 0.13µm. La puce fabriquée a été validée in vitro en utilisant un total de 34 enregistrements EEG intracrâniens avec la durée moyenne de chaque enregistrement de 1 min. Parmi ces jeux de données, 15 d'entre eux correspondaient à des enregistrements de crises, tandis que les 19 autres provenaient d'enregistrements variables de patients tels que de brèves crises électriques, des mouvements du corps et des variations durant le sommeil. Le système proposé a réalisé une performance de détection précise avec une sensibilité de 100% et 100% de spécificité pour ces 34 signaux icEEG enregistrés. Le délai de détection moyen était de 13,7 s après le début de la crise, bien avant l'apparition des manifestations cliniques, et une consommation d'énergie de 9 µW a été obtenue à partir d'essais expérimentaux.

ABSTRACT

Several power efficient detection algorithms have been proposed for treatment of focal epilepsy. Power management in these microsystems is an important issue which is mainly dependent on charging and discharging of the parasitic capacitances in transistors and short-circuit currents during switching. In this thesis, an asynchronous seizure detector for treatment of the focal epilepsy is presented. This system is part of an implantable integrated device to block the seizure progression. The objective of this work is reducing the power dissipation by avoiding the unnecessary signal transition and clock tree; as a result, transistors do not change their transient state in power saving mode (icEEG monitoring period) unless an abnormal event detected.

The proposed integrated device contains a low noise front-end bioamplifier, a digital signal processor and a detector. A variable time frame and four concurrent variable voltage window detectors are used to extract seizure onset information. The sensitivity of the detector is enhanced by optimizing the variable parameters based on specific electrographic seizure onset activities of each patient.

The proposed asynchronous seizure detector was first implemented as a prototype on a PCB and then integrated in standard 0.13 µm CMOS process. The fabricated chip was validated offline using a total of 34 intracranial EEG recordings with the average time duration of 1 min. 15 of these datasets corresponded to seizure activities while the remaining 19 signals were related to variable patient activities such as brief electrical seizures, body movement, and sleep patterns. The proposed system achieved an accurate detection performance with 100% sensitivity and 100 % specificity for these 34 recorded icEEG signals. The average detection delay was 13.7 s after seizure onset, well before the onset of the clinical manifestations. Finally, power consumption of the chip is 9 µW obtained from experimental tests.

TABLE OF CONTENTS

LIST OF TABLES

LIST OF FIGURES

LIST OF ABBREVIATIONS

ANNs	Artificial Neural Networks
ASD	Asynchronous Seizure Detector
CMFB	Common-Mode Feedback
CHUM	Centre Hospitalier De l'Université De Montréal
DBS	Deep Brain Stimulation
DFF	D Flip Flop
DDA	Differential Difference Amplifier
DAC	Digital to Analog Converter
EEG	Electroencephalogram
ECOG	Electrocorticogram
EMU	Epilepsy Monitoring Unit
EEC	Earliest Electrographic Change
EEG-FMRI	EEG-Functional MRI
FN	False Negative
FP	False Positive
FDA	Food and Drug Administration
HFD	High Frequency Detector
ICA	Independent Component Analysis
IEI	Inter Event Intervals
IcEEG	Intracerebral EEG
SPECT	Single Photon Emission Computed Tomography
MEG	Magnetoencephalographic
MRI	Magnetic Resonance Imaging

NSERC	Natural Sciences and Engineering Research Council of Canada
OTA	Operational Transconductance Amplifier
PCB	Printed Circuit Board
PET	Positron Emission Tomography
RNS	Responsive Neurostimulator
F_{SZ}	Seizure Onset Frequency
TN	True Negative
TP	True Positive
T_f	Time Frame
UCO	Unequivocal Clinical Onset
UEO	Unequivocal Electrographic Onset
VNS	Vagus Nerve Stimulator
VWD	Voltage Window Detector

INTRODUCTION

Many methods are investigated for treatment of the refractory patients who suffer from focal epilepsy. Deep brain stimulation (DBS) for Parkinson and vagus nerve stimulation (VNS) for epilepsy disease are the examples of the open loop seizure therapies. In these techniques, the electrical stimulation is applied to deep brain (DBS therapy) or to extracranial vagus nerve (VNS therapy). Commercially available VNS are implantable devices that provide scheduled stimulation at predetermined time intervals to reduce seizure frequency. However, only 30 to 40% of the patients have attenuation in seizure frequency and usually seizure freedom is rare. In contrast to these open-loop systems, the closed-loop devices (detection and treatment) provide seizure alarms prior to clinical manifestations and further triggers focal treatment in order to abort seizures at their onset. Local therapy, such as automatically cooling, injecting fast-acting drug, or using electrical stimulation can be used by closed-loop systems at certain necessary times. This may increase the efficiency and safety of these systems compared to open-loop devices due to effectively use of therapy and reduce the amount of the medications. To do so, it is necessary to have a reliable seizure detection algorithm that can be implemented in an integrated circuit and perform effectively.

Research objectives

Recently, several methods for detecting seizures have been published. These works usually suffer from some limitations addressed below.

- The algorithms suffer from high complexity or power consumption that makes it harder to implement them in an integrated circuit.
- Seizure detection is not accurate or it is required to tune a large number of variable parameters to detect seizure precisely.
- Seizure detection is not early enough before clinical manifestation.

The great progress of technologies let us overcome these limitations and propose new applicable methods for better detection of the epilepsy. The objectives of this thesis are addressed below.

- Propose a new asynchronous seizure detector that is part of an implantable integrated device intended to identify onset seizure and trigger focal treatment to block seizure progression.

- Provide a count-based detection algorithm to minimize the false recognition of the unrelated seizure activities.
- Obtain a reliable detection delay prior to seizure emergence, which provides sufficient time for preparing proper medications.
- Consider the system's complexity as well as power consumption, and sensitivity.

Contributions

The algorithm of the asynchronous seizure detector is verified by using discrete components on a printed circuit board (PCB). The performance of the device was tested using EEG signals recorded from 7 patients with different electrical seizures [1].

To improve the power consumption, noise, and performance of the system, the seizure detector is implemented in an integrated CMOS chip. Post-layout simulation and validation results had promise of the proper detection [2]. The experimental tests on two samples of the microchip are done by using various signals recorded from two epileptic patients that also corresponded to post-layout simulations and approved the performance of the microchip [3].

Thesis organization

This thesis is organized as follows. In chapter 1, brief description of the epileptic seizures and some background information on electroencephalogram (EEG) signals are provided. An introduction of the basic theories, problems, and criteria of the epilepsy therapy are discussed.

Chapter 2 provides literature review of the related seizure detection systems. The design issues and criteria of the implantable devices such as power consumption, complexity, and reliability are discussed. The factors limiting and improving the performance of the epileptic seizure detectors are highlighted.

In chapter 3, we present an asynchronous algorithm to reduce the total power consumption of the system. Also presented here are the design and implementation of the asynchronous seizure detector on discrete component circuit board and the integrated microchip in 0.13 µm CMOS process.

Chapter 4 outlines experimental tests and case study results of the microchip. Results are discussed and compared to other methods of the seizure detections. Also, the optimized features,

patient-specific detection criteria, and power consumption are highlighted in the design of the microchip. These results demonstrate the efficiency of the proposed system using the EEG signals of 2 epileptic patients including the normal neural signals and epileptic seizure activities.

Chapter 5 provides the results of the asynchronous seizure detector that was implemented on PCB as well as post-layout simulation and validation results of the asynchronous seizure detector integrated in 0.13 µm CMOS process.

Finally, the conclusions of this research followed by discussion and future work are summarized.

CHAPTER 1 AN INTRODUCTION TO EPILEPSY

About 50 million people suffer from epilepsy which is approximately 0.75% of the world population. Epilepsy is a neurological disorder characterized by a tendency to unprovoked recurrent seizure. A seizure is the violent disturbance of the cerebral electrical activity due to abnormal discharge of the cortical neurons in the brain. Epileptic seizure can occur equally in both males and females but usually very young and elderly people experience it more than other population. Several causes may provoke epilepsy, such as genetic abnormalities, tumors, head injury, central brain infection, and ischemia. Epileptic seizures may be recognized by clinical symptoms like shaking of the body, disability of the motor functions, loss of the consciousness, teeth clenching and other behavioural changes followed by excessive fatigue. Based on these clinical manifestations and the EEG recordings of the patients, physicians are able to evaluate and analyze the epileptic seizures.

1.1 Treatments of the epilepsy

The most common treatment of the epilepsy is antiepileptic drug but this therapy is not useful for one-third (30%) of the epileptic patients who are drug resistant. Furthermore, some patients whose epilepsy is treated by these anticonvulsant medications are suffering from system side effects such as depression and behavioral changes [4].

Epilepsy surgery is another common treatment for the drug resistant (refractory) patients to remove the epileptogenic area. An accurate localization and identification of the epileptogenic zone increases the success of the surgery. However, the patients who have multifocal epilepsy or have the risk of the surgery with permanent sequelae or loss of the functionalities cannot benefit from this therapy.

In spite of all these available therapies, there are some patients with focal epilepsy who suffer from untreatable seizures. Since the electrical seizures are unpredictable, they may damage the patient's lives and put them in dangerous situations (e.g. when driving a car). Therefore providing a reliable method to diagnose and detect seizures prior to clinical manifestation could significantly improve the quality of these epileptic patient lives. Such a predictive device can provide some time to release fast acting medications in order to suppress the seizure before any clinical symptoms.

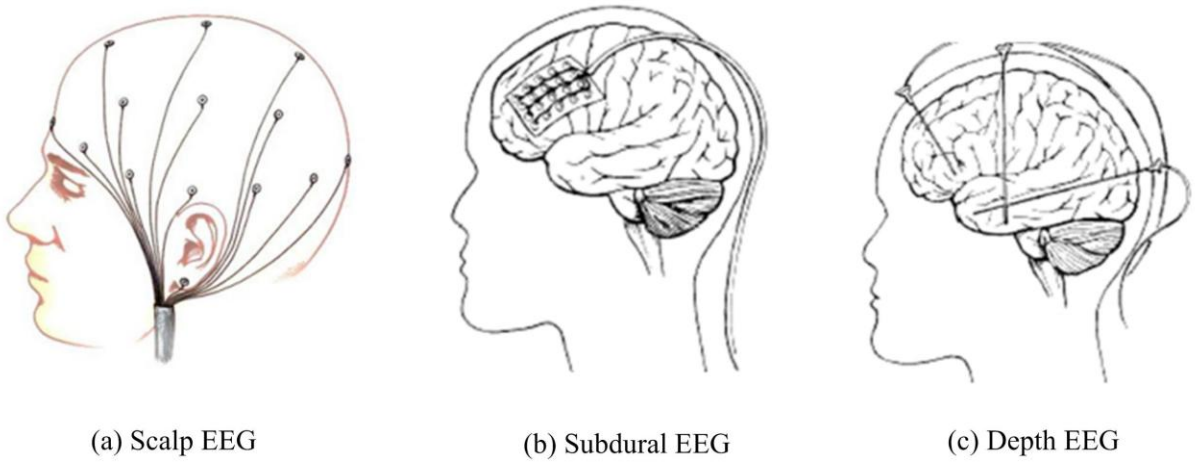

Figure 1.1: Different placement of electrodes for recording EEG signals. Image obtained from [4].

1.2 Epilepsy and EEG recordings

The electroencephalogram (EEG) signals are the electrical activities recorded from brain. Either the scalp EEG (signals from surface of the head) and invasive EEG (signals from brain) are used to diagnose epilepsy. Scalp EEG signals contain physiological artifacts which may combine with environmental interfaces. The physiological artifacts originated from body activities such as tongue movement, arms movement, or eye blinking while the environmental artifact comes from electrode movements, power line interfaces, etc. Whereas scalp EEG is used to diagnose the region of the seizure activities from surface of the head, the invasive techniques are required to record potential changes occurred inside the brain. Hence, the invasive approaches have the advantage of placing subdural or depth electrodes directly on the brain to overcome the noise that could be recorded by scalp electrodes.

EEG signals are used to localize seizures before epilepsy surgery or analyze brain activities to indicate seizure emergence. Depending on the electrode location (Fig. 1.1), different types of the EEG signals are introduced such as electrocorticogram (ECoG), depth EEG, and scalp EEG. These methods are described below [4].

- Scalp EEG is the recorded signals from the surface of the head.
- ECoG signals are the recorded activities from cortex using subdural grid or strip electrodes.

- Depth EEG is the recorded signals of the brain using penetrating electrodes.

Since a seizure is unpredictable and may occur from seconds to minutes, patients must be under long-term EEG monitoring to collect various data of the brain including normal neural activities and multiple seizures. The normal brain signals are recognized by rhythmic activities in specific frequency ranges while seizures are described in terms of variable frequency, phase and amplitude activities. Recording these signals helps neurologists to analyze different patterns of the EEG signals and improve the diagnoses and treatment of the epilepsy. Video monitoring is used in addition to EEG recordings to provide the behavioural reaction of the patient in order to have a better evaluation of the seizure activities.

This work focuses on the design of an effective seizure detector to assist physician in such a challenging task.

1.3 Classification of the epileptic seizures

An epileptic seizure is recognized by abnormal discharge of cortical neurons in brain that may lead to signs or symptoms. The epileptic seizures are identified by brain EEG recordings and can be categorized into two main groups, focal (partial) and generalized seizures.

- Focal seizure

Focal seizures occur in the brain locally and are diagnosed by a few channels of the EEG recording. The focal seizure is simple partial if it affects a small area of the brain without loss of consciousness. Otherwise, it is known as complex partial seizure that causes loss of consciousness in patients.

- Generalized seizure

The generalized seizures affect both hemispheres of the brain and are diagnosed by many channels of the EEG recording. This type of the seizure often causes loss of consciousness.

1.4 Brain waves

EEG signals are classified in four main categories in terms of the most frequency bands of the brain activities that are described below [5].

- Delta rhythm

The lowest frequencies in the brain are categorized as delta wave (0 - 4 Hz). These signals usually have highest amplitude and occur when high focus and attention is required. Delta rhythm is also the dominant wave during deep sleep states.

- Theta rhythm

The slow rhythm of the brain in frequency range of 4 - 8 Hz is categorized as theta wave. These signals are the dominant waves during the sleep of children up to 13 years. Theta waves are usually found during behavioural activations, pain, emotions, and creative states.

- Alpha rhythm

The brain signals in the frequency range of 8 - 13 Hz are categorized as alpha wave. These signals are found in normal adults and usually are associated with states reflecting mental resourcefulness, sense of relaxation, and conscious mind. The alpha waves are usually found in the posterior region of the head during resting or eyes closed while excitement or eyes opened will stop these signals.

- Beta rhythm

The fast brain activities in the frequency ranges above 13 Hz are recognized as beta wave. These signals are recorded from frontal region of the brain. The people who are alert, apprehensive, and busy usually have the symmetrical distribution of the beta waves on both sides of their brain.

1.5 Epileptic states

A continuous interval of the EEG recording is called a segment or epoch. In a broad classification, ictal EEG refers to the segments of the EEG with seizure activity while the rest of the EEG is named interictal EEG. The different states of the EEG signals are described below.

- Interictal state

Interictal state indicates normal resting condition with no seizure activity. Some EEG recordings may contain irregular neural activities which are not seizures. But these abnormalities are known as subclinical seizures and can be useful to diagnose epileptic condition.

- Preictal state

Preictal state refers to the time prior to a seizure that doesn't show the normal state of the brain. Researchers discuss the presence of this state that helps seizure prediction [6]. The preictal state

indicates an upcoming seizure in a certain period of time that can occur from few minutes to hours before seizure onset [7]. Onset of the clinical seizure is characterized by sudden change in amplitude or frequency of the neural signals at the transient time between interictal and preictal states [8].

- Ictal state

Ictal state refers to the time that EEG recordings show abnormal activity of the brain such as significant change in frequency and amplitude. The transition period from preictal to ictal state may be different depending on patient and type of the epilepsy. During the ictal state, EEG patterns become unpredictable and some symptoms such as teeth clenching, loss of consciousness, shaking of the body, eye rolling towards back of the head, and facial twitches are very common during this period.

- Postictal state

Postictal state refers to the time following a seizure which represents the recovery period of the patient. The required time for transition from ictal to postictal state depends on the severity of the seizure and may last few seconds or hours. The postictal dysfunctions are prevalent during this state and disturbances are a consequence of the focal or generalized neurological shortage. Behavioural reactions including poor memory, low attention, and concentration, postictal migraine headaches, and decreased verbal skills are very common. Patients are usually unaware of their seizure but an epileptic patient, who had this situation several times, is able to realize these symptoms.

The additional terms described by epileptologists are unequivocal clinical onset (UCO), unequivocal electrographic onset (UEO), and earliest electrographic change (EEC) [8].

- Unequivocal clinical onset

The earliest time that seizure is recognized clearly by visual or clinical observing a patient is called UCO.

- Unequivocal electrographic onset

Proving the EEG signals, the earliest time that it is evident a seizure occurs without prior knowledge if seizure follows is known as UEO.

- Earliest electrographic change

The earliest time that it is evident a seizure occurs with prior knowledge that a seizure follows, is known as EEC.

1.6 Evaluation of the seizure detector

To characterize and evaluate the performance of the seizure detector, the following parameters must be declared.

- True Negative (TN)

True negative shows that the output of the seizure detector declares the normal activity of the brain in a time interval and that interval demonstrates no seizure activity.

- False Negative (FN)

False negative shows that the output of the seizure detector declares normal activity of the brain in a time interval while that interval includes seizure activity.

- True Positive (TP)

True positive shows that the output of the seizure detector declares seizure activity in a time interval and that interval demonstrates a seizure activity.

- False Positive (FP)

False positive shows that the output of the seizure detector declares seizure activity of the brain in a time interval but that interval demonstrates no ictal activity.

- Sensitivity

This parameter is calculated by Eq. (1.1). It demonstrates the ability of the seizure detector to detect true positive ratio as the diagnosis of the expert neurologists.

$$\text{Sensitivity} = \frac{\text{TP}}{\text{TP} + \text{FN}} \times 100 \quad \% \tag{1.1}$$

- Specificity

This parameter is calculated by Eq. (1.2). It demonstrates the ability of the seizure detector to detect true negative ratio as the diagnosis of the expert neurologists. The goal of the researchers is designing a seizure detector that exhibits maximum sensitivity and specificity.

$$\text{Specificity} = \frac{\text{TN}}{\text{TN} + \text{FP}} \times 100 \quad \% \tag{1.2}$$

CHAPTER 2 LITERATURE REVIEW

2.1 Automated seizure detection methods

In the early 1970s, the analysis of the EEG recordings began to assist the diagnosis and treatment of the epilepsy. As it is shown in Fig. 2.1, these methods can be classified in two main directions; (a) analysis of the ictal spikes and (b) analysis of the epileptic seizures which are described below.

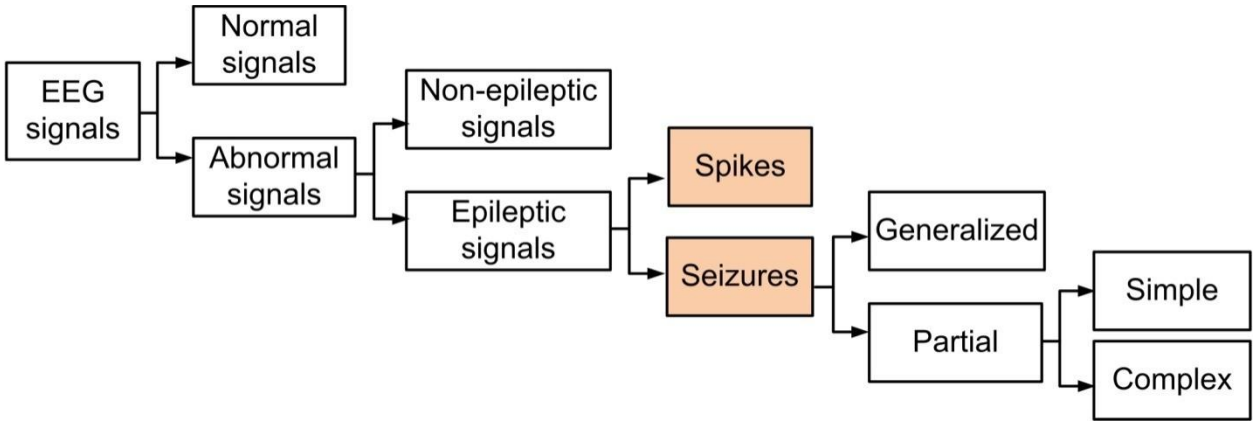

Figure 2.1: Analysis and classification of the EEG recordings, adapted from [9].

2.1.1 Analysis of the ictal spikes

Since epileptic spikes happen more frequently than seizures, several researchers have proposed methods to detect and classify spike activities. Moreover, a better diagnosis of the epileptic spike zones helps surgeons to remove the source of the frequent interictal spikes that are linked to the epileptic seizures [10, 11].

The most common methods for spike detection are [12]:

- Mimetic techniques

  In this traditional technique, the slope, duration, and amplitude attributes of the spikes are analyzed and compared with provided values of the neurophysiologists [13, 14]. In 1985

Faure [15] proposed a new method where the EEG waveforms were decomposed into two half waves and classified based on distinctive attributes of the half signals.

- Morphological analyses methods

  These methods used the structural features of spike to characterize the raw EEG waveforms into several physical parts. Pon et al. introduced mathematical morphology to detect spikes [16]. In [17], Xu et al. proposed a morphological filter to separate the background activity from spikes components.

- Independent component analysis (ICA) methods

  This approach is used to isolate spikes from EEG data [18, 19]. In this method, the abnormal spike activities are selected visually and analyzed by neurologists. A multidimensional ICA analysis to define a mixing matrix, which corresponds to epileptic components, was proposed in [20].

- Artificial neural networks

  In the artificial neural networks (ANNs) either raw data or select features are used to simulate the behaviour of the neurons and detect spikes [21, 22]. Selecting features are based on two approaches, (a) waveform features and (b) context features. The characteristics obtained from duration, sharpness, and amplitude of the spike are known as waveform features while the characteristics obtained from EEG activity surrounding the spikes (EEG variance and baseline crossings) are known as context features.

In the spike detection methods, there is a trade-off between sensitivity and selectivity. This means providing a suitable approach to obtain all spikes usually comes with a large number of the false detections [23, 24]. On the other hand, proposing systems with low false detection rate are usually accompanied by low sensitivity and loss of the seizures. Since the false detections can be checked and analyzed by neurophysiologists, it is preferable for researchers to increase the sensitivity of the system.

Despite the proposed techniques that use features extraction and classification stages to detect inter-ictal spikes (Fig. 2.2), few methods proposed that a spike enhancement stage can be used prior to the spike detection stage [25, 26, 27]. These methods have the same point of view of (a) using spike enhancement stage to attenuate the background events and leave the EEG waveforms from the rest of the data and (b) providing spike detection stage to analyze the waveforms and

classified them as spikes or non-spikes events. In these methods the spikes, artifacts, and background events are enhanced to increase sensitivity and minimize the missed data. Based on the enhancement strategy, the spike detector can be classified in three categories [12]:

- Time domain approaches [28, 29]
- Transform domain techniques [30]
- Signal modeling methods [31, 32]

In the following, some of the recent and remarkable methods for spike detection are explained with more details [33].

In [34], an algorithm is introduced based on detecting the amplitude of the spikes data. This method consists of four channels spike sorting classifier. In this method, the spikes are categorized in the same class if their peak amplitude was in a specific predefined interval. Due to the signal to noise ratio and variation of the spike waveforms, the windowing-based methods exhibit a better performance compared to template matching classifiers [33].

In [35], Chandra et al. introduced a clustering based algorithm to detect spike activities. This

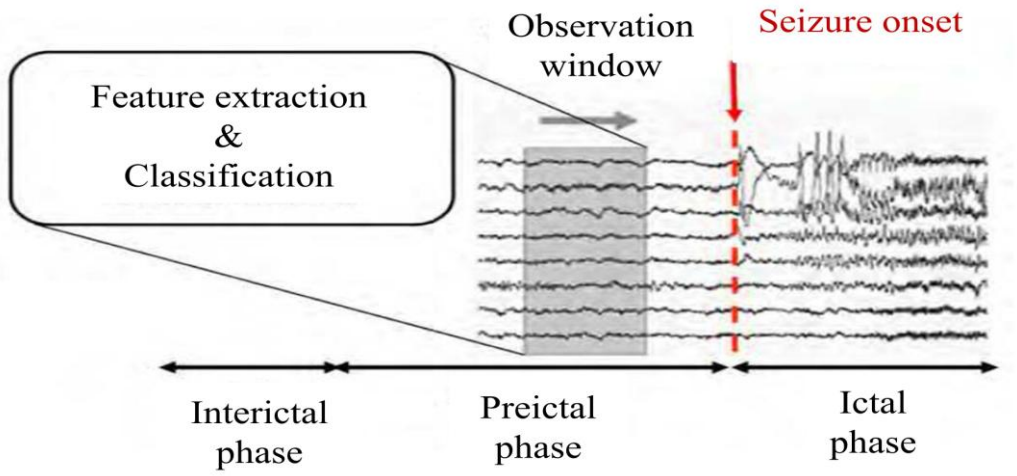

Figure 2.2: The feature extraction and classification are used in some of spike detection methods to improve the sensitivity. Feature extraction obtained from a moving-window observation then the classification stage is used to decide whether the extracted data is seizure or non-seizure activity. Figure is adapted from [12].

method is based on comparing the amplitude of the spikes with a predefined threshold level. When spikes pass this positive or negative threshold, the system detects abnormal spike activities. The detected spikes are clustered together and sorted as initial clusters, and then the best clusters are chosen to provide noise-free templates. In this algorithm, the selection of the clusters depends on some parameters such as inter-distance and sensitivity of the clusters. This method is performed on simulated data.

In [36], a seizure detector is introduced using manual sort of the data. This study exhibited some difficulties for manual spike sorting specially on multi-channel data and illustrated the importance of a robust spike sorting detector.

Kaneko et al. proposed a spike detector based on template matching classifier [37]. This method provided a better sorting result due to tracking the amplitude-change of the spikes. The amplitude variation of the waveforms provides spike-amplitude vectors and every vector allocated to a cluster. The clusters are combined and tracked which resulted in better analysis of the multi-channel data.

Wolf et al. introduced a method for spike detection assuming neuron activities provide spike waveforms [38]. It is supposed that some neurons generate a mixture model but generally, the feature of the waveforms is changed based on a probability distribution. In this approach, the action potential of the neurons are tracked and arranged from multi-channel recordings. The long recordings are divided to short intervals and the detected spikes are clustered using the Gaussian mixture model. The study reports a better clustering and tracking performance compared to other traditional approaches [33].

In[39], Chan et al. introduced a template-matching based spike detector. In this method, it is not required to have a complete prior knowledge of the recording to extract the template. Data sorting depends on wavelet coefficient and spike alignment. Wavelet coefficients are used as vector and by using significant vectors near alignment points, the spike sorting is enhanced.

2.1.2 Analysis of the epileptic seizures

The seizure onset detectors use the feature of the onset in order to detect epileptic seizure. Since this method may cause false detection, some researchers introduced the algorithms for seizure pattern detection, which may reduce the false alarms but increases the detection delay. Recently,

the epileptic seizure prediction methods are interested for researchers since detecting seizure activities prior to clinical manifestation could warn patients and moreover provide the release of the medication in order to suppress seizure activities. Therefore, the automatic pre-seizure detector must exhibit high sensitivity and low false alarms.

So far, many algorithms for epileptic seizure detection are introduced. These algorithms usually are based on classical signal processing methods, which detect different patterns of the seizure activities [40]. The selection of the features could be based on waveform or morphological parameters such as amplitude, frequency, and shape of the waveforms or time domain features like nonlinear characteristics, statistical features, and correlation dimension [12].

Fast Fourier transform based [41], wavelet based [42, 43, 44], frequency based [45, 46, 47] and time-frequency based features [48] also were used for rhythmic discharges. Genetic programming is another method to detect epileptic seizure, which is not based on physiological features [49]. Once the feature of the EEG signal was extracted, it is required to analyze whether the EEG signal is related to a seizure or non-seizure activity. In literature, different methods have been proposed such as logistic regression [50], linear classifiers [51, 52], Gaussian mixture model [53], etc.

A general classifying of the automated seizure detector is based on the age group of the patients, which is categorized to adult seizure detection and newborn (neonate) seizure detection. The detection for neonate is different from adults due to slower discharge of the cortical neurons (down to 0.5 Hz) and gradual seizure onset, which can last couple of minutes [12]. In another classification, the automated seizure detectors may be used for each patient (patient-specific system) or be optimized as generic (non-patient-specific system) which are described below [4].

2.1.2.1 Generic seizure detection

Pauri et al. introduced a seizure detection system and evaluated it by using the EEG signals of twelve patients that were under video monitoring [54]. The system was adjusted with several settings and showed the best sensitivity of 81.4 %. Results demonstrated that tunable detection thresholds are required to improve the performance of their system.

In [55], a system that detects seizures based on half wave amplitude features is proposed. In this method, seizures were detected when the defined features passed the detection thresholds. The

improved method [56] provided better detection of the low amplitude seizures and exhibited lower false detections due to increasing the distance between the background and seizure activities. The system performed sensitivity in the range of 70 - 80%.

Harding introduced a seizure detector using the magnitude difference of the samples and time difference of the large spikes. The number of the high amplitude events was counted in 5 s time periods and if the counter passed a defined level, seizure was detected. This method was tested on 40 patients and exhibited a sensitivity of 92.6 % [57].

In [58], Osorio et al. introduced a seizure detector where the EEG signals in the frequency range between 5 and 50 Hz were filtered. The system was based on a real-time detection method and exhibits short detection delay with 100 % sensitivity and no false positive alarms. Although the authors mentioned that, the seizure detector is not for a patient-specific application but it seems the patients with mesial temporal seizure could have benefit of this method [33].

Khan et al. introduced a multichannel seizure detector that divided the EEG signals in frequency bands. For each band, the features of the signal are obtained and applied to decision stage. This method used for 11 patients and exhibited a sensitivity of 85.6 % [59]. In [60] an improved method is presented which used a tunable threshold and provided a trade-off between false alarm detection and sensitivity of the detector. In the improved system, the feature vector is composed of five features obtained from each frequency band and then applied to decision stage. Results showed sensitivity of 86.4 %.

Iasemidis introduced a seizure detector based on neural network [61]. Futures in addition to a set of spatial information provide the neural network rules. In this method, The EEG signals are decomposed and analyzed in time and frequency domains. The system is tested on EEG signals for 1046 hours and showed a sensitivity of 76%. This method is accepted to be used in the epilepsy monitoring unit (EMU) [33].

Navakatikyan et al. introduced a neonate seizure detector [62]. The algorithm is based on waveform morphology where the amplitude and shape of the EEG signals are used for feature extraction. EEG waveforms decomposed in two half waves, the negative and positive half waves which defined as trough-wave and peak-wave, respectively. The average of two sequent half waves is compared with a threshold level in order to define the increase of the EEG waveforms and detect seizure. The validation results on 55 neonate signals showed sensitivity between 83

and 95 % and suggested a better performance for morphological-based methods compared to other popular features for classification.

Arabi et al. introduced an algorithm to analyze data from depth EEG recordings. This seizure detector composed of the individual channels and seizure was detected in each channel using rule-based classifier. The detection of the individual channels was combined to provide the final detection. Validation results on 21 patients exhibited a sensitivity of 98.7 % [63]. To be noted is that detecting clinical seizures was the target of this work while all short seizures and other abnormal activities, which don't lead to clinical manifestation, are not excluded in this method [33].

Duun-Henriksen et al. introduced a method to detect seizure based on wavelet feature of the signals. This method used few recording channels for detection. The first step is selecting the channels, which provide analyses of the features. The next step is using support vector classifier in order to detect seizure [64]. The EEG signals of 10 patients are used to evaluate the performance of the seizure detector, which demonstrated minimum improvement in sensitivity. Moreover, the focal and subclinical seizures are not used to determine the performance of this study, which cannot claim its generic application for all types of the seizures [4].

Majumdar and Vardhan introduced a seizure detector using waveform features [65]. This method is based on window variation detector, which diagnoses the abnormal activities of depth EEG recording. Validation results on 15 patients exhibited a sensitivity of 91.5 % but subclinical seizures are not included in this study.

2.1.2.2 Patient-specific seizure detection

Que and Gotman proposed a method based on template matching approach to provide patient-specific seizure detection. In this approach, the onset and a large background data prior to the seizure signals are selected and used to train a modified nearest-neighbor classifier. The template seizure patterns and background EEG data are selected manually and a complex classifier is used for seizure detection [66]. Note that this study introduced the new concept of the patient-specific seizure detection.

Wendling et al. introduced a method for detecting seizures. This system provided segments of the EEG signals and then characterized these segments in order to extract the similar data between

observations [67]. The seizure detector is evaluated on depth EEG signals of the medically refractory patients who have partial seizures. The authors claimed that this study is useful to have a better understanding of the epileptogenic networks [68], [69].

Shoeb et al. presented a method based on morphological information of the EEG signals. The multichannel seizure detector comprised of the feature vector and support vector machine classifier. The classifier is trained based on prior knowledge of 2 - 4 seizures and non-seizure EEG signals in order to diagnose epileptic seizures during recording. A remote computer is used for classification to reduce the power consumption of the device and improve the battery life [70]. The authors claimed that the computational cost is reduced due to the remote classifier. However, designing such a seizure detector with an external remote system as a classifier could not be a practical method [4]. In comparison with other patient-specific seizure detectors that required a single template seizure pattern, this study used more seizure patterns to train the remote classifier. The validation results of this method on scalp EEG signals of 36 patients exhibited a sensitivity of 94 %.

Wilson introduced a patient-specific seizure detector. This system used a classifier that required a single seizure pattern for training. A learning algorithm proposed for improving the errors of the classifier [71], [72]. Although training the classifier is based on minimum sample data, but it required long background data that is extracted from the end of the preceding seizure to the start of the next seizure and this limited the application of this method.

Shi et al. introduced a patient-specific seizure detector based on prior knowledge of a single seizure data. This method used sinusoidal wavelet function to provide the template seizure. Validation results on two patients resulted in a sensitivity of 100 % and no false alarm was detected in this study [73]. However, the seizure detector is not an automated system. Moreover, a few data is used to evaluate this method while the practical systems provide an automated detection on large dataset of the EEG recording.

Zandi et al. introduced a seizure detector using the scalp EEG recording of 14 patients [74]. This method is using a large background and providing a moving window with 2 s time frame to analyze the EEG signals. The seizure and non-seizure patterns are recognized based on the energy density function. The energy of the individual channels in addition to multichannel information is used to diagnose the epileptic seizures. This study exhibited 90.5 % sensitivity,

however this method suffers from the non-automated seizure detection, and it is not a practical seizure detector due to selecting specific type of the seizure that is limited to temporal lobe epilepsy [33].

2.2 Implantable devices for seizure therapy

Epileptic patients with refractory to antiepileptic drugs are good candidates for surgical operation. Since this therapy is not useful for multifocal epileptic patients and can cause some permanent sequelae near eloquent areas, other supplemental treatments are required. In recent years, there was a growing interest to introduce algorithms for treatment of the epilepsy. Some of these algorithms aimed to be implantable on microelectronic devices.

Vagus nerve stimulator (VNS) is the only implantable device accepted for FDA (Food and Drug Administration) for treatment of the epileptic seizures [75]. This device is composed of an implantable stimulator, an external pulse programmer, and two bipolar electrodes, which provide a non-responsive (open loop) therapy. The stimulator is implantable under the skin of the left chest and the lead is delivered to neck. The bipolar electrodes are used near the vagus nerve. Once the stimulator is implemented in the body of the patient, the programmer can turn on the device, which stimulates the vagus nerve directly to attenuate the duration and severity of the seizure. This open loop therapy provides the electrical stimulation at a predetermined time intervals [76]. The stimulator is usually set for frequency range of 20 - 30 Hz, time on and time off around 250 - 500 μs [75]. This method doesn't need the exact definition of the epileptogenic area of brain. However, it reduces the seizure frequency only in 30 - 40 % of the epileptic patients [77].

Recently, the closed loop therapies (detect and treatment) are in the interest of researchers, these devices detect epileptic seizure before evaluating into clinical manifestations and then trigger therapy to stop seizure activities. As a result, less medication is required, which reduces the side effects on the patients. In general, a responsive (closed-loop) device is composed of two main parts; the seizure detector and seizure controller. The methods that could be used to control and suppress the seizure are:

- Electrical stimulation
- Cooling

- Drug release

High-frequency electrical stimulation can be used in a responsive device to stop seizure activities. It is important to provide a limited charge density in order to prevent human tissue damages. Focal drug delivery is another approach to block seizure activities in a responsive device. This therapy may improve the effects of the drugs and reduce the system side effects due to limiting the drug releases only onto epileptogenic areas. However, the delivery system and refilling procedure is another concern in this method [75]. The other method used in a closed-loop device to stop seizure is focal cooling. After detecting seizure onset, the area of the brain that shows a rise in temperature is recognised by sensors. Then subdural grid electrodes that contain integrated micro-tubes are used in order to provide water circulation. The cooling therapy affects the magnitude of the neuronal action and as a result, reduces the potential of the upcoming abnormal electrical activities [75]. This method has the advantage of reducing the brain damages and prevents the disturbance of the normal brain activities. However, the cooling system and the efficiency to release seizure are the concerns of these seizure therapy methods.

Responsive Neurostimulator (RNS) is an implantable device for treatment of the epilepsy. This device is useful on patients with both simple and complex focal seizure. The device is composed of the internal and external parts. The internal part contains the implantable neurostimulator and intracranial electrodes while the external part is composed of the telemetry interface, programmer, and laptop computer [75]. Physicians use the external device to provide the tuneability of the detection and use wireless communication to send data to neurostimulator. The neurostimulator is implanted in the cranium and after detecting seizure activities, it releases electrical pulses to the epileptogenic area. The RNS is designed to recognize high frequency and amplitude variation of the EEG signals and provide seizure detection based on feature extraction and data reduction approaches. However, this device is under clinical trial and its power consumption and detection performance aren't published yet [75]. Fig. 2.3 shows the RNS and VNS devices including their feature description.

VNS			RNS		
FDA approved			Clinical trial		
 Vagal Nerve Stimulation Cyberonic Inc. Houston, USA			 Neuropace RNS-300 Mountain Biew, California, USA		
Features: • Battery powered • Stimulate vagus nerve • External remote • Applicable for refractory generalized and focal epilepsy.			**Features**: • Battery powered • Controlled by microcontroller • Store neural signal • Detect signature of seizure onset • Applicable for motor simple partial seizure and complex partial seizure		
	Min dose	Max dose		Min dose	Max dose
Stimulation Parameters	0.25 mA 30 Sec ON 3 hr OFF 130 μsec PW	3.5 mA 30 sec ON 5 min OFF 500 μsec PW	Stimulation Parameters	1 mA 40 μsec PW	12 mA 1000 μsec PW
Frequency	0.25 Hz	30 Hz	Frequency	1 Hz	333 Hz
 www.cyberonics.com			 www.neuropace.com		

Figure 2.3: The feature description of RNS and VNS devices available for seizure therapy, adapted from [75].

The closed-loop systems require an efficient and reliable seizure detector to provide an accurate detection with minimum false alarms. Moreover, the device should be implantable in an integrated circuit to reduce the power consumption, which helps reducing the thermal tissue

damage on epileptic patients. Several models are proposed for seizure detection using desktop computers to process data off-time [78, 79, 80, 81, 82]. These methods can't be implemented on a low power microchip because of the long-term data processing and heavy computations. Recently, a few implantable seizure detectors are proposed for clinical applications such as [83, 84, 85, 86, 87].

In the following, the implantable low power CMOS-based methods are introduced and compared to this work.

The low-power method in [83] proposed a mixed-signal seizure onset detector which could be implemented in a microchip. This count-based algorithm provides patient-specific seizure detection using one variable parameter. This seizure detector is designed using 0.18 µm CMOS process including front-end amplifier, comparators, and digital signal processor stages. The front-end amplifier is used to amplify low amplitude icEEG signals. It is composed of two amplifier blocks and provides a total gain of 62 dB and 3 dB bandwidth of 0.5 to 215 Hz. A voltage window is used with two threshold levels. One of the threshold levels is set to the mean of the icEEG signals while the second one is tunable for specific patient application. The digital signal processor contains counter and 10 bit digital comparators. A total of 13 epileptic seizures from two patients with focal epilepsy are used to validate the performance of this method. The post-layout simulation results exhibited 100 % sensitivity and an average detection delay of 9.7 s was obtained after seizure onset. In this method, the signal is counted in a time window length. Choosing a longer window provides a higher sensitivity but increases the detection delay. The author proposed a two-path system in order to minimize the detection delay. However, selecting a fixed window length (5 s) could affect the tuneability of the device specified for each patient. Moreover, the 60 Hz power line interference is not filtered and all the results are based on simulations.

Salam et al. [84] introduced a low power device for seizure detection using a set of the voltage level and high frequency detectors. The system is customized for patient-specific EEG signals to increase the specificity of the detection and reduce the unwanted false alarms. The seizure detector is composed of a chopper stabilized preamplifier, filtering stage, voltage comparators, demodulators, and high frequency detectors. The proposed system modulates and amplifies icEEG signals and extracts the progressive increase in amplitude by using voltage level detectors,

and then the signals are demodulated and passed through high frequency detectors to extract the original frequency and detect epileptic seizures. Tuneable detection thresholds are used to identify the voltage variation of the EEG signals for each patient. The circuit is implemented using 0.18 µm technology and power consumption of 6.7 µw is obtained from simulation results. The experimental tests showed that the power consumption of the device is about 50 µw. This system provided accurate patient-specific seizure detection due to increasing the number of the variable parameters. The validation results on seven patients provided 100 % specificity and an average detection delay of 13.5 s is obtained after seizure onset [84]. However, this method is using a synchronous algorithm where the building blocks are sharing a common clock. Switching in transistors causes additional power consumption and transistors that are switching more rapidly will consume more power. As a result, power consumption of the synchronous seizure detectors are increased because of these unwanted clock transitions.

In [85], an implantable method is proposed to detect epileptic seizures and a multiple stage algorithm is used to reduce the false alarms. The detection method is based on marking out the icEEG data into events and measuring the inter-event-intervals (IEI). Threshold levels are used to identify events and the events are related to high-frequency discharges. DC offset and artifacts are removed by capacitive blocking and low-pass filtering stages. Then the amplified and filtered data is compared to amplitude thresholds and IEI extraction blocks. The level of these thresholds is adjustable to adjust the false positive rate less than 5 % and provide patient-specific detection. The detector circuit is designed in 180 nm SOI technology and the data acquisition system is interfaced to desktop computer. The previously recorded data of 6 animals are used to evaluate the performance of the circuit design which resulted in 95 % sensitivity. However, the sensitivity is based on simulation results and furthermore, such event detection methods exhibit more false negative and false positive detection rates due to the increase of the non-seizure detections compared to the count-based algorithms [83].

Power management, safety, tuneability, and performance of the seizure detector are the issues in the design of these systems. Unlike the synchronous methods [84, 85, 86, 87] that share a common clock, the asynchronous techniques eliminate clock trees to reducing power consumption in long-term applications.

CHAPTER 3 A NOVEL ASYNCHRONOUS EPILEPTIC SEIZURE-ONSET DETECTOR

In previous chapters, a review of the seizure detection algorithm including performance, drawback, and limitation were explained. Some of these methods are designed for special purposes such as patient age groups (neonatal and adult) or clinical use (prediction or detection). The other methods are classified based on type of the EEG recordings (scalp, depth, etc) and detection application (patient-specific or non-patient-specific).

This work proposes a new asynchronous seizure detector that is part of an implantable integrated device intended to identify seizure onset and trigger focal treatment to block seizure progression. In the design of the asynchronous seizure detector, the system's complexity is considered as well as power consumption, and sensitivity. Moreover, a reliable detection delay prior to the seizure attack is verified.

3.1 Synchronous versus asynchronous epileptic seizure detector

Power management of the automatic seizure detectors is one of the major issues of the implantable devices. Since power consumption could be managed by two main parameters, short circuit currents due to transistor switching and signal transitions in parasitic capacitances [91], this work proposes an asynchronous system to reduce power consumption of the seizure detector by eliminating unnecessary clock tree. The general structure of the synchronous method [84] is shown in Fig. 3.1(a). In this structure, the input signals are modulated and then amplified and analyzed in high frequency bands (100–6500 Hz). The time frame is generated by an internal frequency divider and the detection stage is applied after demodulating the input signals to original frequency bands. Fig. 3.1(b) illustrates the block diagram of the asynchronous method (this work) where an external device on the top of the skin generates the time frame and the input signals are analyzed directly without using modulation or demodulation stages. Table 3.1 explains the differences and similarities of these two methods.

3.2 Asynchronous epileptic seizure detection algorithm

In the algorithm of the integrated seizure detector (Fig. 3.2), an analog stage is used in order to amplify and filter the input signal. The output of the analog part passes through four voltage

window detectors (VWDs). $V_{TL\text{-}TH,i}$ is the threshold voltage of the VWDs to determine the strength of the neural signal activities. Due to unpredictable behaviour of the epileptic seizures, a large number of the voltage window detectors (threshold levels) are required. Increasing the number of the VWDs results in higher sensitivity and specificity but at the cost of increasing the detection complexity and power consumption. Using four VWDs provides maximum detection performance; two of these VWDs are used to detect epileptic activities while two others monitor basal activities [1]. The high frequency detectors measure the signal frequency and extract fast activities. The variable parameters ($V_{TL\text{-}TH,\ Tf)\ and\ I}$ are tuned based on specific patient seizures to minimize false alarms and enhance sensitivity and specificity of the system.

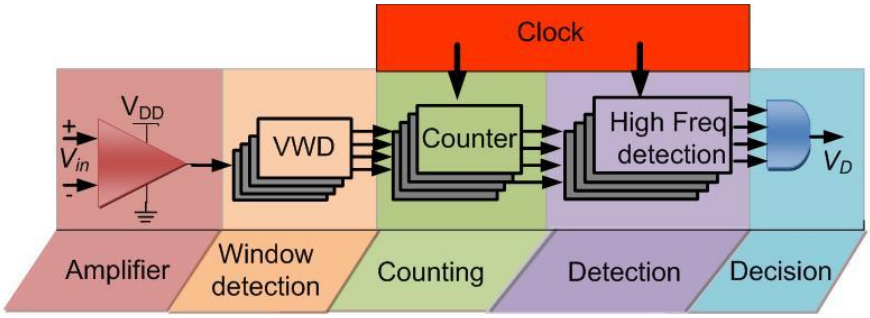

(a)

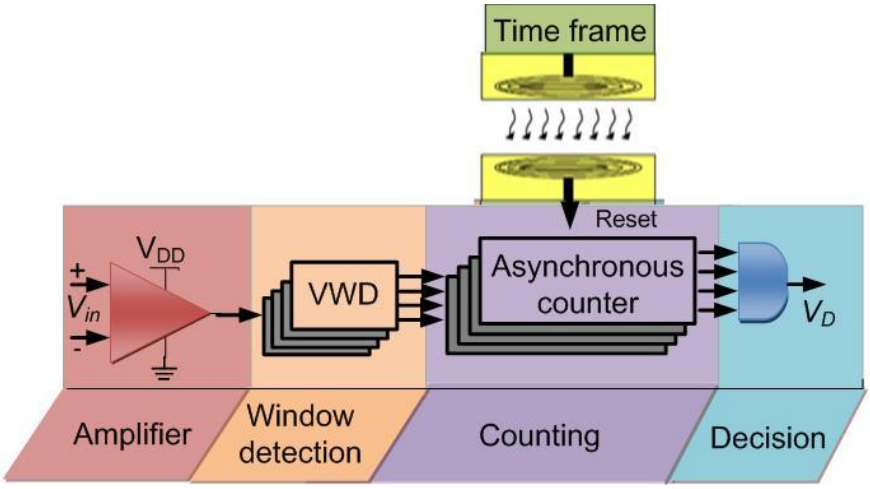

(b)

Figure 3.1: Block diagram of the seizure detector, (a) The general structures of the synchronous method in [84], and (b) The general structure of the proposed asynchronous method.

Table 3.1: Comparison of the synchronous and asynchronous seizure detector

Parameter	**Synchronous method [84]**	**Asynchronous method (this work)**
Variable parameters (threshold levels and time frame) to provide tuneability in detection	Yes	Yes
Applicable for all patients with partial seizure	Yes	Yes
Complexity in circuit design	Low	Medium
Clock used	Yes	No
Comparative power dissipation	High	Low
Modulation stage	Yes	No
Frequency divider	Yes	No
Demodulation stage	Yes	No
Time frame generated	Internal	External
Window detection	Positive amplitude	Positive and negative amplitudes

3.3 Circuit implementation

3.3.1 Prototype-based asynchronous seizure detector

An asynchronous device for automated diagnoses of the focal epilepsy is presented. This device is assembled with discrete components on a PCB. As block diagram of the asynchronous seizure detector is shown in Fig. 3.2, it contains a front-end amplifier, filtering stages, VWDs, and high-frequency detectors. The circular PCB is shown in Fig. 3.3. The performance of this device was verified using icEEG signals recorded from 7 patients with different electrical seizures. The power consumption of the detector was reduced in power saving mode compared to similar synchronous architectures [1]. The results persuaded us to design an integrated version of our previous system to improve power management, noise, and performance of the asynchronous seizure detector, which is described in chapter 4. Details of the PCB design are described below.

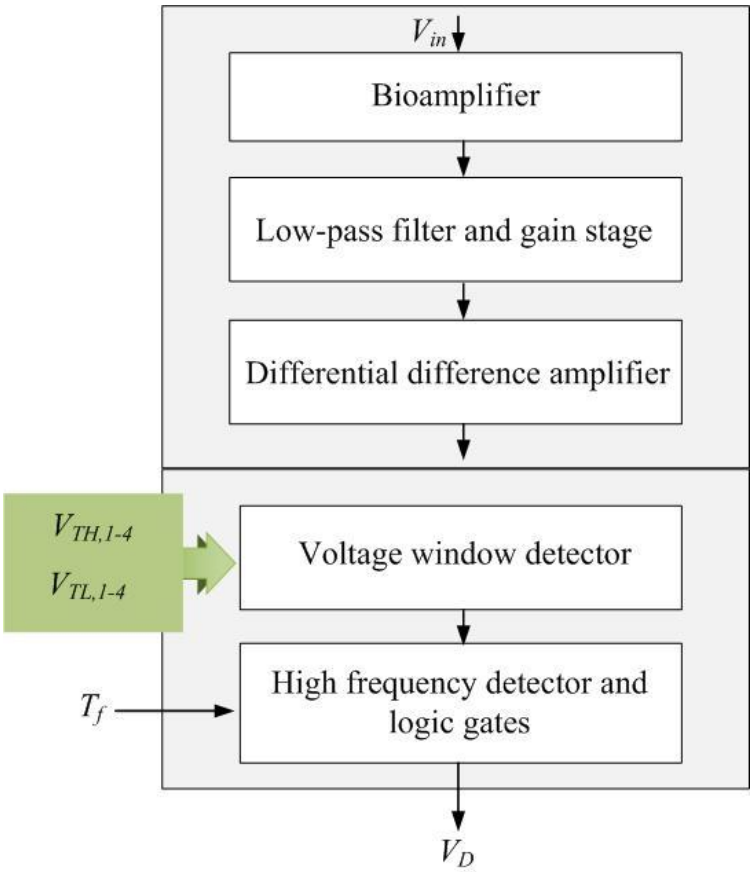

Figure 3.2: High-level diagram of the asynchronous seizure detector.

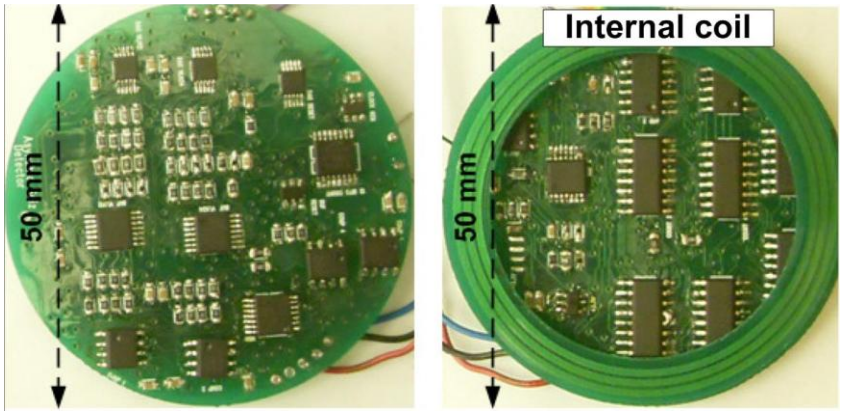

Figure 3.3: The top and bottom views of the discrete components based prototype including the internal and external coils for transferring time frame (T_f).

3.3.1.1 Front-end amplifier

Structure of the bioamplifier is shown in Fig. 3.4. It contains two stages; an instrumentation amplifier (A_1) which is used to amplify low-amplitude neural signals (microvolts) and an inverting Miller integrator. The proposed front-end amplifier has the advantage of the low-noise performance for biomedical applications. Moreover, this design provides Dc offset suppression due to using the inverting Miller integrator. The Dc offset is produced by mismatches of the recording electrodes and has relatively high and random amplitude compared to neural signals. As a result, a low-frequency rejection circuit is required to eliminate the Dc offset and prevent saturation of the instrumentation amplifier. In this structure, the Miller integrator works as Dc suppression circuit. It is composed of a high gain amplifier (A_2), high resistor (R_2), and a capacitor (C_1). The integrators time constant ($\tau = R_2.C_1$) is very long to set the lower 3-dB cut-off frequency of the bioamplifier less than 1 Hz.

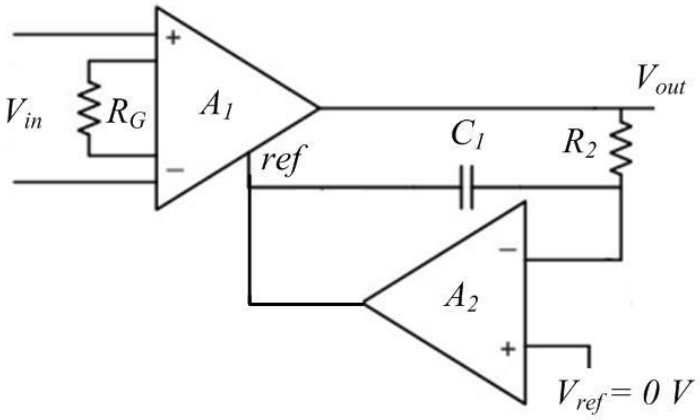

Figure 3.4: The structure of the bioamplifier.

Amplifier A_1 plays a main role to determine the total noise of the device. Hence, the low noise instrumentation amplifier INA 118 is used to implement the discrete component A_1. Moreover, setting higher gain for this amplifier results in lower total input referred noise. The adjustable resistor R_G determines gain of A_1 (Gain = 1+ 50 kΩ / R_G) and as it is shown in Table 3.2, for R_G around 50 Ω the amplifier gain is set to 60 dB (1000 V/V) [92].

Table 3.2: The adjustable resistor determines the gain of A_1 [92]

Desired gain	R_G (Ω)	Nearest 1 % R_G (Ω)
1	NC	NC
2	50.00k	49.9k
5	12.50k	12.4k
10	5.556k	5.62k
20	2.632k	2.61k
50	1.02k	1.02k
100	505.1	511
200	251.3	249
500	100.2	100
1000	50.05	49.9
2000	25.01	24.9
5000	10.00	10
10000	5.001	4.99

Fig. 3.5 explains the application of the low-frequency rejection circuit where both open-loop gain (noted A_{02}) and closed-loop (integrator) gain of the amplifier A_2 are demonstrated. As it is shown, the Miller structure attenuates both bandwidth and unity gain frequency of A_2. As a result, the integrator samples the output of the main amplifier (A_1), then for very low frequencies provides the maximum gain and cancels out any Dc offsets while features a very small bandwidth and lets the low frequency neural signals pass through the front-end amplifier without suppression. It is important to note, an ideal integrator exhibits infinite gain at Dc but practical one has a Dc gain equal to open loop gain (A_{02}) [93]. By selecting capacitor C_1 and resistor R_2 around 0.1 µF and 1 MΩ, a high cut-off frequency around 1.5 Hz is obtained. V_{ref} sets the Dc output of the bioamplifier in the middle range of the positive and negative supply voltages, which provides the maximum swing of the output signals.

3.3.1.2 Filtering stage

A band-pass filter is used to reduce the flicker noise and thermal noise of the circuit. Moreover, the bandwidth of the analog stage is reduced by this filtering stage from 3 Hz to 50 Hz. This structure attenuates the 60 Hz power line interference to avoid the unwanted false alarms during seizure detection.

A Sallen-Key topology is used to implement the filtering stage. This structure is shown in Fig. 3.6 and the value of the parameters is illustrated in Table 3.3.

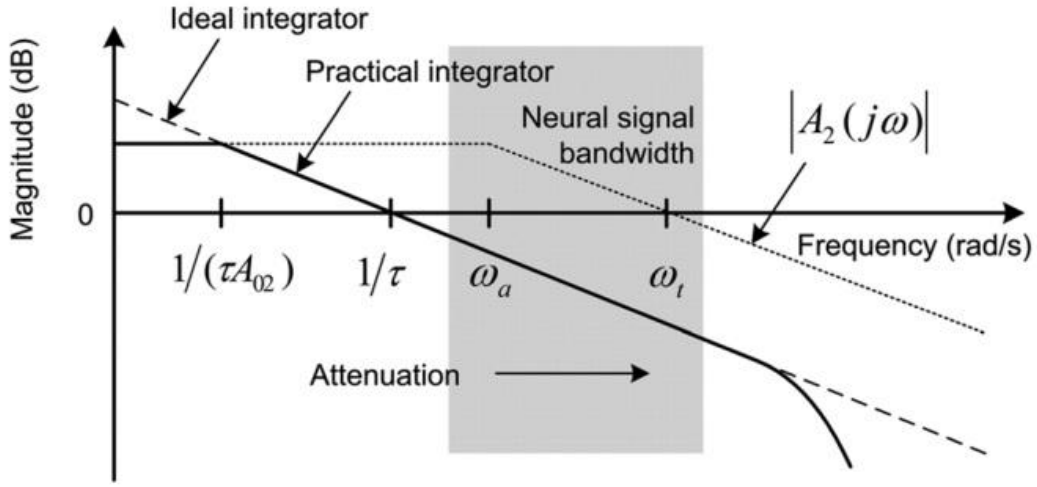

Figure 3.5: Magnitude plot of the Miller integrator, adapted from [93].

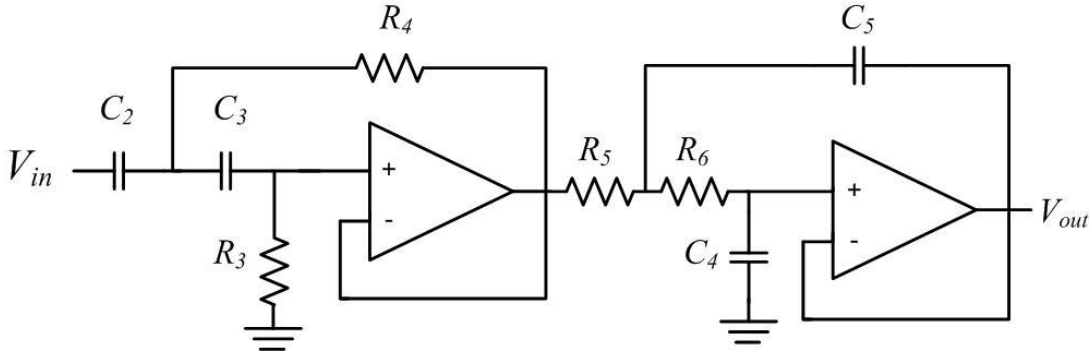

Figure 3.6: The band-pass filter using Sallen-Key topology.

Table 3.3: Value of the parameters used in the design of the Sallen-Key filtering stage

Parameters	C2	C3	R3	R4	R5	R6	C5	C4
Value	100 nF	100 nF	375 kΩ	750 kΩ	1 MΩ	750 kΩ	4.7 nF	2.2 nF

3.3.1.3 Asynchronous seizure detector

The detection stage contains four VWDs and four high-frequency detectors. The VWDs detect the progressive increase in the magnitude of the icEEG signals. The threshold voltages of the

VWDs are adjusted externally. These threshold voltages divide the amplified and filtered icEEG signals into delimited intervals named voltage windows. Instead of using the significant number of windows, two windows are used to analyze the positive side and two are used to analyze the negative part of the signals. These four voltage windows are adjusted based on observation of the off-line icEEG waveforms specified for each patient. This allows selection of the windows based on the activity variation for each patient, and thus, offers the advantage of optimizing the number of the windows, reducing the power consumption and complexity of the integrated device. For this system, the VWDs are able to present the magnitude variation of the signals with minimum steps of 20 mV precisely. The high frequency detectors contain asynchronous counters and logic gates. The counters detect high-frequency events by counting the number of the neural activities in a variable time frame. The time frame is tuned externally based on the specific seizure onset frequency of each patient.

3.3.2 Micro-chip asynchronous seizure detector

The integrated version of the asynchronous seizure detector is implemented in a CMOS 0.13 µm process with total die area of 1.5 × 1.5 mm^2. Fig. 3.7 illustrates the different blocks of the asynchronous seizure detector.

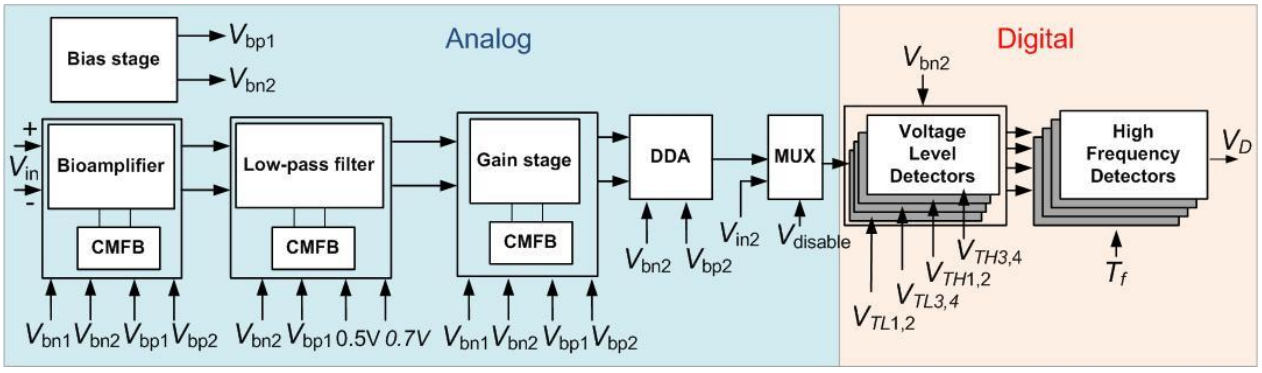

Figure 3.7: The analog and digital building blocks of the ASD.

3.3.2.1 Starter and bias circuit

The starter circuit, which consists of transistors M_{k1}, M_{k2}, and M_{k3} doesn't affect the operation of the integrated seizure detector (Fig. 3.8). It is used to avoid the unwanted operating point, where zero current flows in the circuit and doesn't let the system to start-up. After starting the system,

transistor M_{k1} works continuously. To reduce the power consumption of the starter circuit, the size of the transistor M_{k1} is adjusted to large length and small width. Transistor M_{k3} will be off and transistor M_{k2} works in the linear region, which means that transistor M_{k2} works as a resistor.

The Beta-multiplier design is used to provide the biasing levels (Vbp1 and Vbn2). In this circuit, resistor R_1 has an important role to determine the stability. For example, by decreasing the value of this resistor, the bias circuit is closer to instable condition or by using the resistor out of the chip, the bias circuit could oscillate [94].

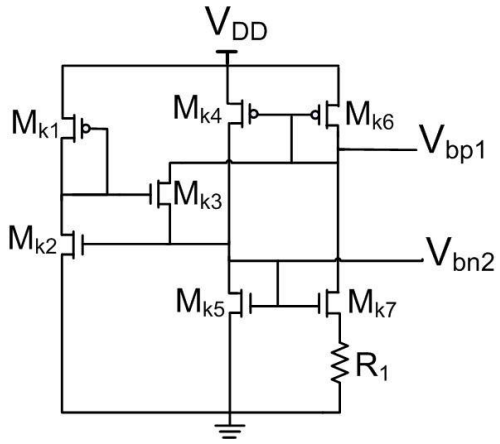

Figure 3.8: The integrated design of the starter and bias circuit [94].

3.3.2.2 Analog building blocks

Fig. 3.9(a) shows the block diagram of the bioamplifier, which rejects the large and random Dc offset voltages caused by electrode mismatches. In Fig. 3.9(b) the schematic design of the operational transconductance amplifier is demonstrated. The ratio of the capacitors C_1/C_2 determines the midband gain of the bioamplifier. Transistors Ma-Md, are the MOS-bipolar (pseudo-resistors) elements. With this configuration, for small input signals ($|\Delta V| < 100$ mV) the equivalent resistance is very high [95]. For negative gate to source voltage, these transistors act as diode- connected PMOS transistors and for positive V_{GS} they behave like diode connected BJTs [95]. The size of the transistors M_1-M_{13} determines the noise of the bioamplifier. To minimize thermal noise of the circuit at low current, transistors M_1 and M_2 are designed in weak inversion (large W/L ratio) and transistors M_3-M_8 are used with small W/L ratio (strong inversion). This sizing must not affect the low-power consumption and stability of the bioamplifier.

Fig 3.9(c) demonstrates the schematic of the CMFB used for bioamplifier stage. By connecting the inputs of the CMFB circuit to the outputs of the bioamplifier, this circuit will adjust the output bias points to avoid them to drift into the supply rails. For example, when the common mode output voltages of the amplifier are increased, the current through transistors M_{a1} and M_{a4} will increase and as a result, the current of the transistors M_{a2} and M_{a3} will decrease. This causes the increase in V_{CMFB} and decrease in common mode output voltages of the bioamplifier [95].

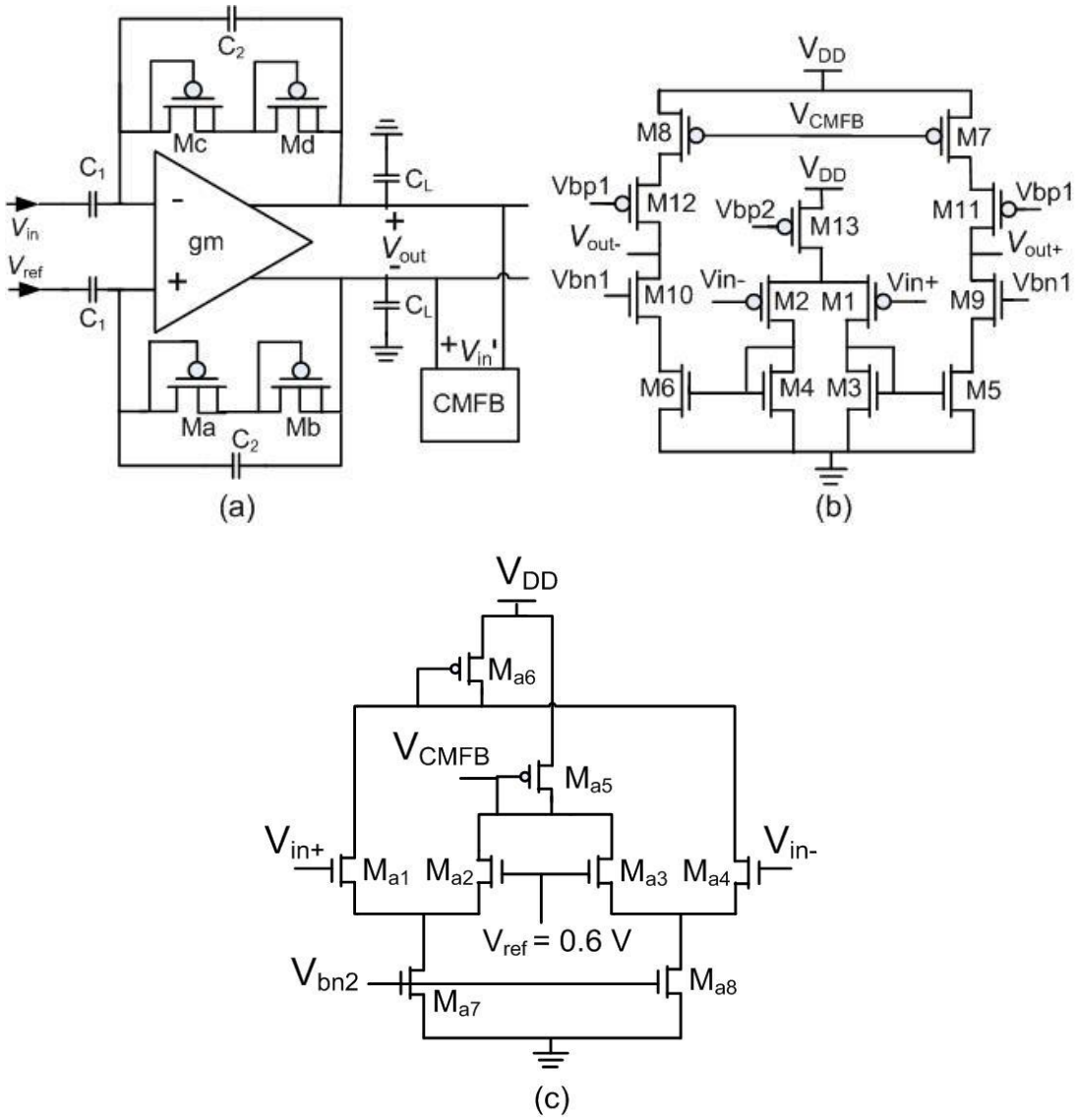

Figure 3.9: (a) Block diagram of the bioamplifier, (b) Operational transconductance amplifier, and (c) Common mode feedback circuit. Adapted from [95].

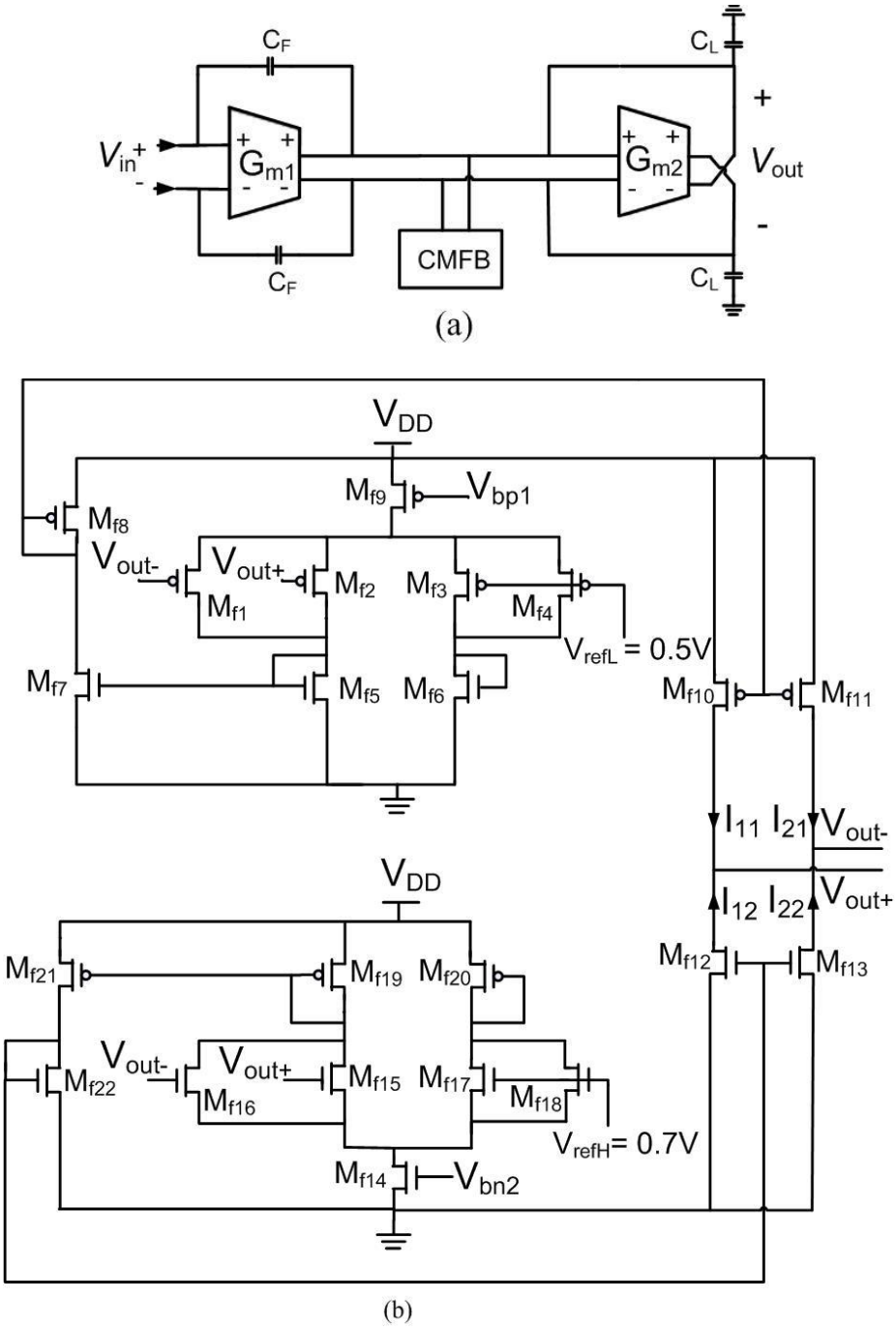

Figure 3.10: (a) Block diagram of the Gm-C low pass filter and (b) Schematic design of the common mode feedback circuit [96].

The structure of the fully differential Gm-C filter is shown in Fig. 3.10(a). This low-pass filter is added at the output of the front-end amplifier to attenuate the 60 Hz power-line interference. The structure of the transconductance cell is shown in Fig. 4.5 (b). The CMFB circuit is used to set the

bias points of the fully differential low-pass filter in order to avoid them drifting into the supply rails. Since a single supply voltage (0 to 1.3V) is used, the operation point of the differential output is stabilized between two supply rails or 600 mV. To do this, Fig. 3.10(b) is used where the top part of the CMFB circuit adjusts the common mode voltage (V_{CM}) if it drops below 500 mV (V_{refL}) and the bottom part works conversely if the common mode voltage rises above 700 mV (V_{refH}). The adjustment is based on using currents I_{11} and I_{12} that load or discharge node V_{out+} connected to capacitor C_L. While the current I_{21} and I_{22} load or discharge the node of V_{out-} connected to capacitor C_L. If $V_{CM} > V_{refH}$ the currents I_{12} and I_{22} increases and currents I_{11} and I_{21} decreases which discharge the capacitors C_L and as a result reduces V_{CM}. For $V_{CM} < V_{refL}$ the currents I_{11} and I_{21} increases and currents I_{12} and I_{22} decreases which charges capacitor C_L and as a result increases V_{CM}. Since there is only one differential pair of the independent nodes (common output of the G_{m1} and G_{m2}), one CMFB block is required.

3.3.2.3 Digital building block

Fig. 3.11 shows the schematic of the switch used to provide the test point in order to verify the performance of the analog and digital building blocks separately. For $V_{disable}$ connected to high voltage, the output of the DDA (V_{in1}) will pass through transistor M_{s1} while for $V_{disable}$ connected to low voltage, an external signal (V_{in2}) passes through transistor M_{s2}.

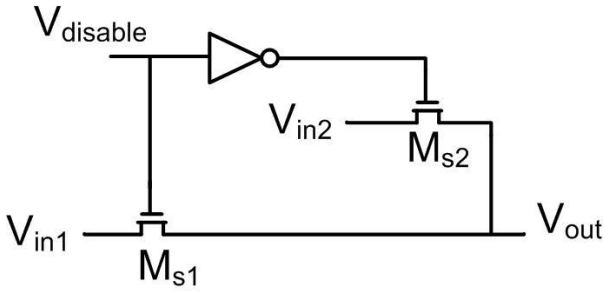

Figure 3.11: Schematic of the switch used to provide test point between analog and digital stages of the ASD.

XOR gates are used in the comparators and full adders to perform the arithmetic operations [97]. The issues in the design of the XOR gate are; avoiding any decrease of the output voltage, consuming less power, rejecting noise, and improving the delay of the XOR gate. However, for low supply voltages the performance of the XOR gate could be affected. When input "B" is low,

the circuit produces bad logic levels in a noisy environment [97].

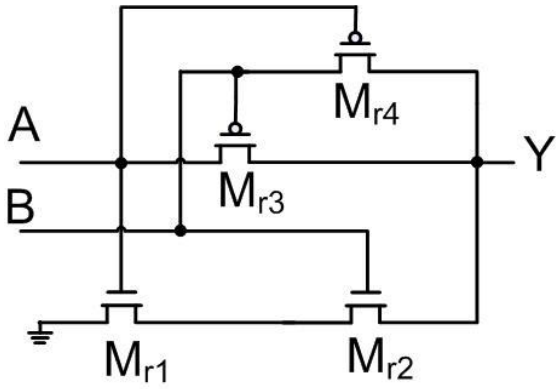

Figure 3.12: Schematic design of the XOR gate [97].

Fig. 3.13 shows the block diagram of the counter using four D flip-flops and Fig. 3.14 demonstrates the implementation of the D flip-flop using NAND gates.

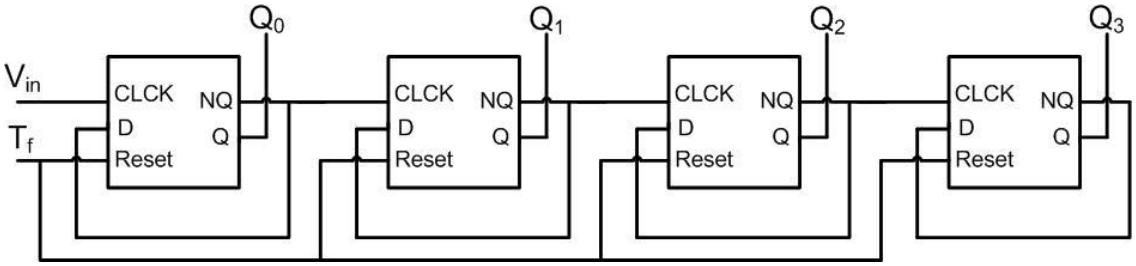

Figure 3.13: Schematic diagram of the counter [98].

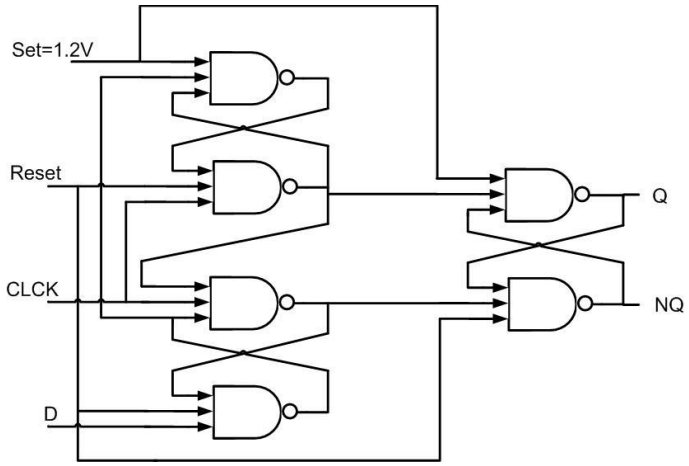

Figure 3.14: Schematic diagram of the D flip-flop using NAND gates [99].

Moreover, the number of the transistors should be minimized to achieve low power consumption. There are several structures for XOR logic gates. A design with four transistors is used in the output of the comparators (Fig. 3.12) [97]. This configuration is simulated in a 0.13 µm CMOS technology with 1.2 V supply voltage. It contains four transistors, exhibits very low power dissipation, and has low voltage drop in the output.

CHAPTER 4 CMOS-BASED ASYNCHRONOUS SEIZURE DETECTOR

In this chapter, the main design and implementation of the asynchronous seizure detector in 0.13 µm CMOS process is presented. The optimized features, patient-specific detection criteria and power consumption are highlighted. Moreover, experimental tests and case study results of the Micro-chip are provided and compared to other methods of the seizure detections. These results demonstrate the efficiency of the proposed system using the EEG signals of two epileptic patients including normal neural signals and epileptic seizure activities.

The content of this chapter is a manuscript that was submitted to the IEEE Transactions on Biomedical Circuits and Systems " in March 2013 and it is reproduced as follow.

4.1 ARTICLE 1 – A Fully-Asynchronous Low-Power Implantable Seizure Detector for Self-Triggering Treatment

Marjan Mirzaei[1], Muhammad T. Salam[1], Dang K. Nguyen[2], and Mohamad Sawan[1], Fellow, IEEE

[1]Polystim Neurotechnologies Laboratory, Polytechnique Montréal, Québec

[2]Neurology service, Notre-Dame Hospital (Centre Hospitalier de l'Université de Montréal)

Abstract–In this paper, we present a new asynchronous seizure detector that is part of an implantable integrated device intended to identify electrographic seizure onset and trigger a focal treatment to block the seizure progression. The proposed system has a low-power front-end bioamplifier and a seizure detector with intelligent mechanism to reduce power dissipation. This system eliminates the unnecessary clock tree during normal neural activity monitoring mode and reduces power dissipation in the seizure detector; as a result, this device is suitable for long-term implantable applications. The proposed system includes analog and digital building blocks with programmable parameters for extracting electrographic seizure onset information from real-time EEG recordings. Sensitivity of the detector is enhanced by optimizing the variable parameters based on specific electrographic seizure onset activities of each patient. The detection algorithm was validated using Matlab tools and implemented in standard 0.13µm CMOS process with total die area of 1.5×1.5 mm^2. The fabricated chip was validated offline using intracranial EEG recordings from two patients with refractory epilepsy. Total power consumption of the chip is 9

μW and average detection delay is 13.7 s after seizure onset, well before the onset of the clinical manifestation. The proposed system achieves an accurate detection performance with 100% sensitivity and no false alarms during the analyses of 15 seizures and 19 non-seizure datasets.

Index Terms—Asynchronous, seizure detector, and implantable device.

4.2 Introduction

Epileptic patients suffer from a tendency to recurrent seizures as the result of the abnormal neuronal discharges. First line of the treatment for epilepsy is oral antiepileptic drugs; however, many of them have systemic side effects and remaining of the patients are drug resistant [100]. Epilepsy surgery is an alternative treatment option for the drug resistant (refractory) patients. An accurate localization of the epileptogenic zone and precise analysis may increase success in the surgery. However, patients who have multifocal epilepsy or have risks from surgery due to loss of the brain functionalities are continuously disabling due to the lack of the treatment option. Thus, researchers are looking for other alternative treatments for conventionally untreatable patients, such as implantable devices delivering focal treatment upon automated detection of the electrographic seizures.

Over the last decade, there has been a growing interest on implantable self-triggering Microsystems for treatment of the refractory patients. Efficacy of the self-triggering treatment depends on precise evaluation of the EEG and accurate identification of the predefined electrographic patterns. The automated evaluation and detection performance can be improved by using intracerebral EEG (icEEG), which is advantageous over scalp EEG due to less motion/muscle artifacts and lower sensitiveness for brain signal recordings. However, several other noises may degrade the icEEG recordings and subsequent self-triggering treatment may not be effective. The front-end bioamplifier has a low dynamic input range (microvolt) and the Dc offset due to electrode-tissue interface and 60 Hz noise may saturate the bioamplifier [101]. Moreover, flicker noise due to fundamental physics property of the instrumentation and thermal noise due to internal resistance of the instrumentation and wire resistance contribute major amount.

Following the amplification and filtering stages, recordings need to be further evaluated to detect abnormal electrographic patterns. From patient to patient, seizure onset patterns may vary in terms of the onset morphology, discharge frequency, and spread pattern. The most common

seizure onset pattern is characterized by a low-voltage high-frequency discharge [100]. In patients with simple partial epilepsy, electrographic seizure activities begin from epileptogenic zone and spread to adjacent regions while in patients with generalized seizure, the electrographic seizure activities spread to a broad region of the brain and usually lead to visible clinical manifestations. As a result, the behavioral changes such as shaking of the body, disability of the motor functions, and loss of the consciousness are evident.

So far, several techniques are investigated for the treatment of the refractory patients who suffer from focal epilepsy. Deep brain stimulation (DBS) for Parkinson and vagus nerve stimulation (VNS) for epilepsy disease are examples of the open loop seizure therapies. In these techniques the electrical stimulation is applied to deep brain (DBS therapy) or to extracranial VNS (VNS therapy), respectively. The commercially available VNS provide scheduled stimulation at predetermined time intervals to reduce seizure frequency. However, seizure freedom is rare and only 30 to 40% of the patients have attenuation in seizure [101]. In contrast to these open-loop systems, the closed-loop devices (detection and treatment) provide seizure alarms prior to clinical manifestations and further triggers focal treatment in order to abort seizures at their onset. Delivering focal treatment (e.g. drug, electrical stimulation, cooling) can be used by closed-loop systems at certain necessary times to provide effectively use of the therapy and reduce the amount of the medications. This may increase the efficiency and safety of these systems compared to open-loop devices. Responsive Neurostimulator (RNS) is a responsive implantable device that has been recently submitted for FDA approval [83]. This device is useful on patients with simple or complex focal seizures. As such, in the last few years a growing interest for developing seizure detection methods can be seen. Some of them are desktop computer-based algorithm for offline detection [102], [66], [78], [79], [103], [104] and the remaining are integrated microsystems for real-time evaluation and detection [1], [2], [83], [85], [86], [101], [105]. Generally, the computer-based algorithms use heavy mathematic computations to increase the sensitivity and specificity of the detectors [66], [78], [79], [102], [103], [104]. However, trade-off between their accuracy in detection and complexity in analysis makes it complicated to implement them in an integrated circuit due to the high power dissipation.

Recently, several power efficient detection algorithms have been proposed which were implemented in CMOS-based microsystems and suitable for implantation [1], [2], [83], [85], [86], [87], [101], [105]–[109]. In [107], the patient-specific seizure onset activities are recorded and detected using 8 analog front-end channels and a machine-learning seizure classification. The seizure detector is implemented in 0.18 µm 1P6M CMOS process with total die area of 25 mm^2. The functionality of the detector is verified with rapid eye blink patterns and children's database that showed 84.4% accuracy in classification test. However, power consumption of 66 µW is obtained only from analog front-end channels. The seizure detector in [108] proposed patient specific seizure detection with multichannel feature extraction. This system is trained with rapid-eye blinks characterized by 10 eye blinks within a 5 s window. The proposed system exhibited more than 95% detection accuracy and less than 1% false alarm. However, the total power consumption of the seizure detector is not mentioned. In [109], fully integrated seizure detection with an adaptive neural stimulation is presented. This system is implemented in 0.18µm CMOS occupying 13.47 mm^2. It shows detection accuracy more than 92% within 0.8 s and power dissipation of 2.798 mW. Power management in these microsystems is an important issue for the implantation. The power consumption is mainly dependent on signal transitions in a device, such as charging and discharging of parasitic capacitances in transistors and short-circuit currents

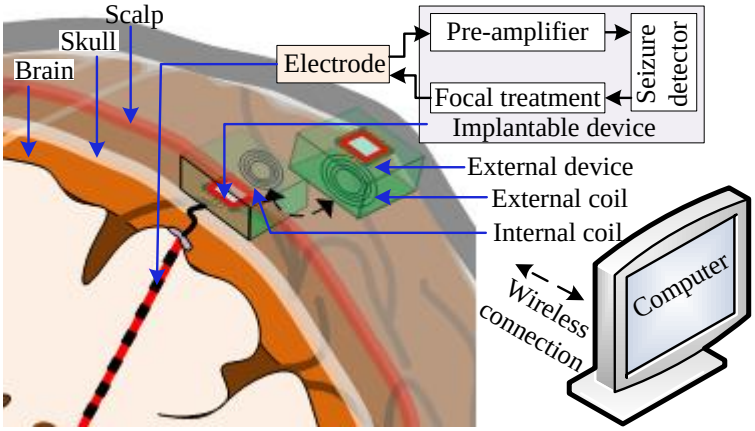

Figure 4.1: A diagram showing the application of proposed ASD in a closed-loop seizure detection and therapy. Seizure detector identifies the progress increase of low-voltage fast-activity at seizure onset and then triggers local therapy in order to abort seizure prior to clinical manifestations.

during switching [91]. Thus, power consumption can be further reduced by avoiding the unnecessary signal transitions [91]. All modules of the synchronous designs [85], [86], [87], [101], [105]–[109] share a common clock signal distributed throughout the circuit, and the unnecessary signal transitions arise from clock gating. Because of these limitations in the conventional synchronous circuit design, an asynchronous technique (data-dependent analysis) is likely to become more popular.

In this paper, a low-power asynchronous seizure detector (ASD) is proposed for a self-triggering treatment microsystem. Power dissipation in the detector is managed by eliminating unnecessary clock skew and clock tree; as a result, transistors do not change their transient state in power saving mode (icEEG monitoring period) unless an abnormal event detected. This system contains low noise front-end bioamplifier, digital signal processor and a detector. This microsystem can identify electrographic seizure onset precisely and trigger an electrical stimulator for focal treatment prior to clinical manifestations. Fig. 4.1 shows the high-level diagram of the proposed ASD in a closed loop detection and therapy system.

In the following sections, the background work and algorithm of the proposed integrated ASD are described in section 4.3. Section 4.4 highlights the design and implementation of the proposed circuits. The experimental tests and validation results are illustrated in section 4.5 and conclusion is summarized in section 4.6.

4.3 Proposed system

4.3.1 Background works

Our previous work proposed several low-power seizure detectors and stimulator/inhibitor for self-triggering treatment in refractory epilepsy patients [1]. Time-frequency and time-amplitude analysis were the main tools for detecting electrographic seizure onset while minimizing the false recognition of the unrelated seizure activities. Moreover, compared to synchronous design [105], asynchronous design [1] reduces the total power dissipation. These systems were assembled with discrete components on printed circuit board (PCB) illustrated in Fig. 4.2(a)–(b). Furthermore, the synchronous design was fabricated in microchip (Fig. 4.2(c)) in order to reduce power dissipation and size of the microchip [101]. These detectors monitor icEEG recordings using electrodes (Fig. 4.2(e)) in real-time and upon seizure onset detection, trigger a current stimulator (Fig. 4.2(d))

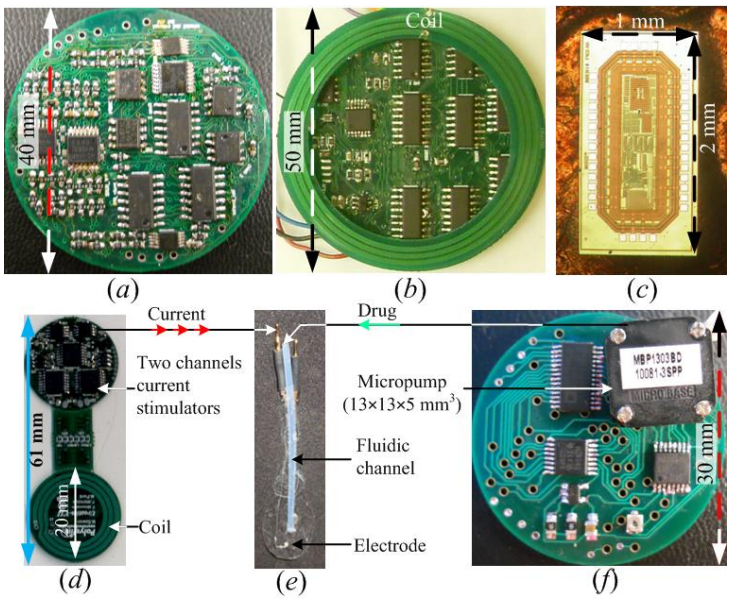

Figure 4.2: Background works on seizure detection and stimulation/inhibition: (a) Synchronous seizure detection prototype made up of discrete components [103], (b) Asynchronous seizure detection prototype made up of discrete components [1], (c) Synchronous seizure detection microchip [99], (d) Two channels current stimulator [106], (e) Hybrid surface electrodes compatible for stimulation and drug delivery [1], and (f) Drug delivery system [1].

[106] or direct drug delivery system (Fig. 4.2(f)) [1] in order to suppress the seizure. Among these detectors, the asynchronous detector has demonstrated smart power saving technique (reduced 45% in power saving mode compared to synchronous prototyped architectures) [1]. However, the PCB-based asynchronous seizure detector was neither implantable (area 1963.5 mm2) nor low-power (47200 µW) for long-term implantable device therapies. Thus, a novel integrated circuit design is used to improve the power management, noise, size, and performance of the proposed asynchronous seizure detector.

4.3.2 Detection algorithm

The proposed power efficient detection algorithm processes analog and digital signals and detects an electrographic seizure onset (Fig. 4.3(a)). At first, input analog signals are amplified to the desired amplitude range and filtered of all unnecessary frequency contents and noises. The output of the processed signals (V_a) passes through four voltage window detectors (VWDs) to find neural activities in lower and higher amplitudes, in both positive and negative sides of the signal

amplitudes. Outputs of the VWDs ($V_{w,\ i}$) define the strength of the neural signal activities in different amplitude ranges (Eq. (4.1)).

$$V_{w,i} = \begin{cases} '1', & for \quad |V_{TH,i}| > V_a > |V_{TL,i}| \\ '0', & otherwise \end{cases} \tag{4.1}$$

Where i = 1, 2, 3, 4. $V_{TL\text{-}TH,\ i}$ is the threshold voltage of the VWDs. Several frequency analyzers extract $V_{w,\ i}$ and measure signal frequency ($F_{H,\ i}$) using a time frame (T_f), as shown in Eq. (4.2).

$$F_{H,i} = \frac{1}{T_f} \sum_{t=0}^{t=T_f} V_{w,i}(t) \tag{4.2}$$

If $F_{H,\ i}$ is greater than specific seizure onset frequency (F_{SZ}) in both lower and higher amplitudes, the output $V_{D,\ i}$ is considered fast activity (Eq. (4.3)).

$$V_{D,i} = \begin{cases} '1', & for \quad F_{H,i} > F_{SZ} \\ '0', & otherwise \end{cases} \tag{4.3}$$

Seizure detection logic analyzes $V_{D,\ i}$ and quantifies specific features characterized by a progressive increase in amplitude and high frequency. Thus, a seizure onset is declared on the

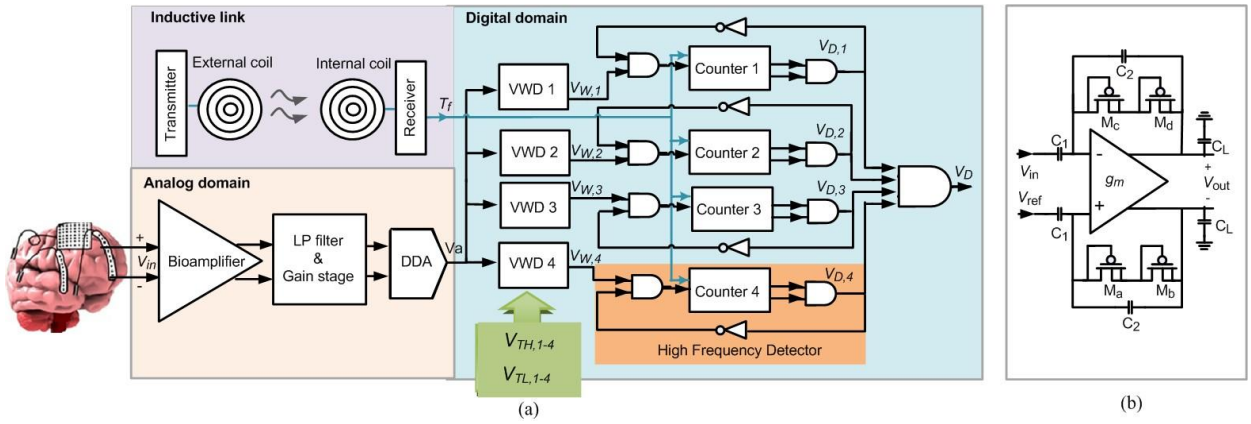

Figure 4.3: Proposed integrated seizure detector: (a) Block diagram of the asynchronous system, where V_{in} is the recorded icEEG signal in the input of the system, Va is the amplified signal in the output of the analog stage, $V_{W,1\text{-}4}$ are the outputs of the voltage window detectors (VWDs), $V_{D,1\text{-}4}$ are the outputs of the high-frequency detectors, and V_D is the final output of the integrated ASD, (b) General structure of the bioamplifier stage [110].

basis of the following conditions (Eq. (4.4)).

$$V_D = \begin{cases} '1', & for \quad V_{D1}.V_{D2}.V_{D3}.V_{D4} = 1 \\ '0', & otherwise \end{cases} \tag{4.4}$$

$V_{\text{TL-TH, i}}$ and T_f are tuned to the specific patient F_{SZ} to minimize false alarms. These parameters can optimize the decision boundary and enhance the sensitivity and specificity of the system.

4.4 Implementation of the proposed algorithm

This ASD consists of two main analog and digital building blocks. The analog one is composed of the bioamplifier, filtering level, gain stage, and fully differential to single-ended converter. The digital part contains VWDs and high-frequency detectors. Details are given below.

4.4.1 Bioamplifier stage

A fully differential bioamplifier with standard continuous-time common-mode feedback (CMFB) is used to amplify low-voltage icEEG input signals. Although the fully differential structures are used with CMFB circuits and occupy more area compared to similar single-ended designs, they exhibit less noise and show better performances. Fig. 4.3(b) shows the schematic of the used bioamplifier that is able to reject the large and random Dc offset voltages caused by electrode mismatches [110].

4.4.2 Filtering and gain stage

The architecture of the fully differential G_m-C filter is shown in Fig. 4.4(a). Analyzing the frequency range of the seizure signals [101], this low-pass filter is added at the output of the front-end amplifier to attenuate the 60 Hz noise. Designing a low-pass filter with very low cut-off frequency requires an operational transconductance amplifier (OTA) with lower transconductances or larger integrated capacitors. Concerning the chip area, low value transconductances are used. This leads to design transistors with long lengths to minimize the current of the OTAs. Since matching such geometries is difficult from a layout perspective, current splitting and source degeneration techniques are used. Fig. 4.4(b) shows the schematic of a fully differential low-transconductance OTA where small-signal currents in transistors M_A, M_B and M_C are divided by ratio in their sizes. The source degeneration technique increases the linearization of the filter. For this structure, the source-degeneration resistors are realized by

designing transistors M_{14} and M_{15} in triode region. V_{SG} of these transistors, and thus, their resistance is controlled by M_{12}, M_{16}, and M_{17}.

An additional amplification stage is used at output of the G_m-C filter. This amplifier uses the same structure in Fig. 4.3(b) with small capacitor ratio (C_1/C_2) that provides the overall gain of 60 dB for analog building block.

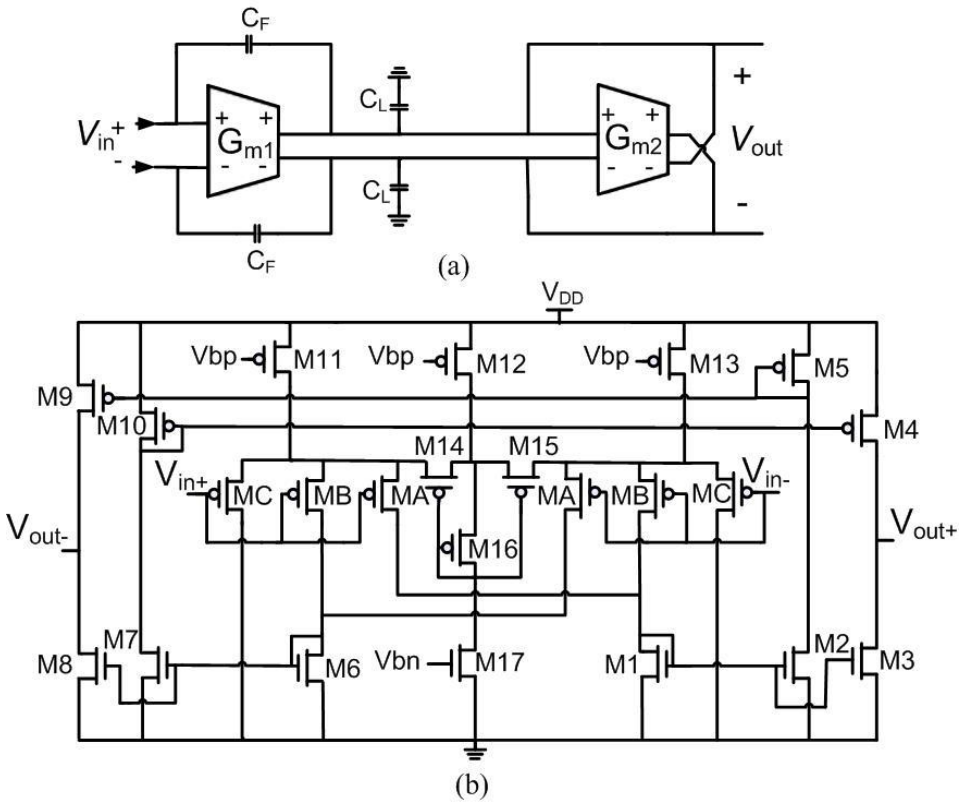

Figure 4.4: Schematic diagram of low-pass filter: (a) G_m-C low-pass filter, (b) Operational transconductance amplifier (G_{m1}, G_{m2}) used to implement the filter.

4.4.3 Differential difference amplifier

The fully differential inputs are converted to single ended output using a differential difference amplifier (DDA). This block also works as a buffer between analog and digital stages to minimize the effect of the jitter and kickback noise. Fig. 4.5 is a schematic diagram of the DDA, which consists of two main parts, 1) a differential-input single-ended output transconductance stage that converts two pairs of the differential input voltages into a single subtracted output current and 2) a gain stage which provides the output voltage [111]. The compensating capacitor and resistor (C_C and R_C) are used to stabilize the circuit.

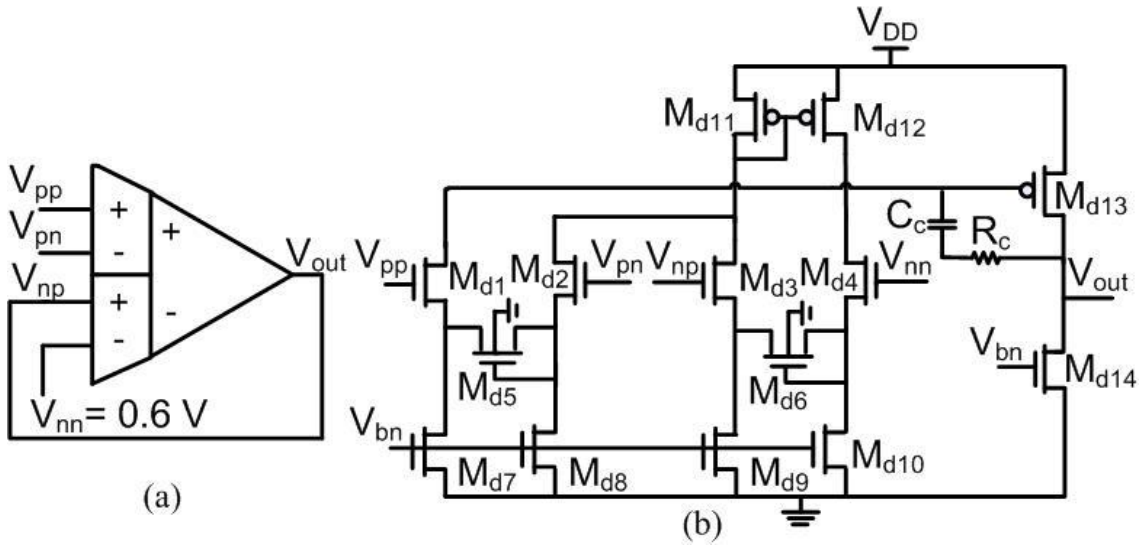

Figure 4.5: Schematic diagram of differential difference amplifier: (a) Symbol of DDA where the first port is used as an front-end op-amp and the second port consists of a voltage adder, (b) The circuit design of DDA.

4.4.4 Seizure detector

The detection stage contains four VWDs and four high-frequency detectors. The VWDs (Fig. 4.6) detect progressive increases in amplitude of the icEEG recordings. The threshold voltages ($V_{TH/TL,1\text{-}4}$) of the VWDs are widely programmable which are generated digitally using digital-to-analog converters and buffers. These threshold voltages divide the amplified and filtered icEEG signals into delimited intervals named voltage windows. Our previous studies showed that instead of using significant number of the VWDs, two VWDs in positive side of the icEEG and another two in negative side are sufficient to detect seizure onset [1]. The VWDs are adjusted to the patient-specific seizure onset to prevent false seizure detections. Moreover, the implemented tuning separates normal and hyperexcited activities; as a result, some modules of the detection stage are turned off during normal icEEG recordings. This processing method allows saving power dissipation in detection stage. Furthermore, the VWDs can detect small magnitude variation in the icEEG recordings that enhances the sensitivity and specificity (100 % for two patients) of the system for detecting the seizure activities with variable patterns, magnitude, and spectral contents.

The high frequency detectors contain the asynchronous counters (using four D flip flops) and various logic gates. The counters detect high-frequency events by counting the number of the

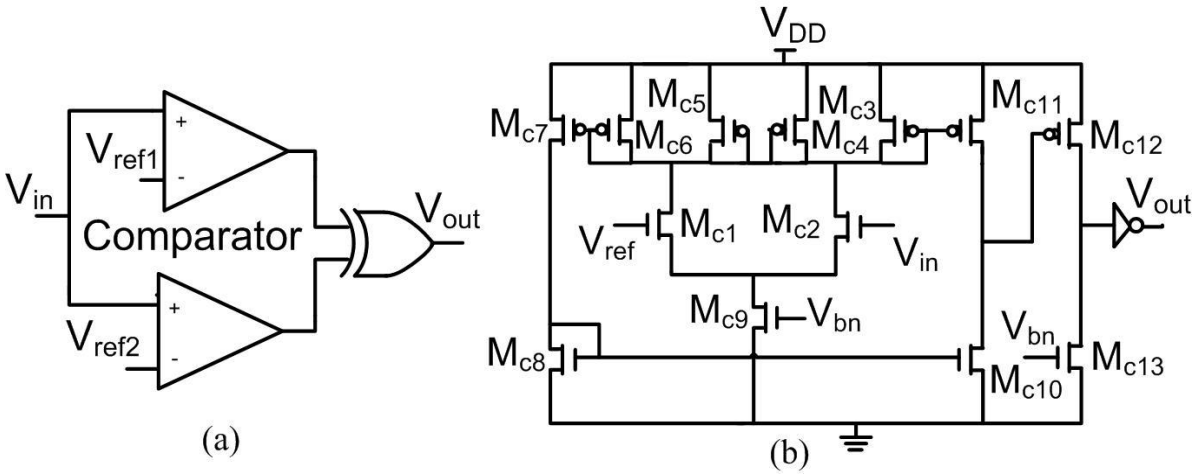

Figure 4.6: Schematic diagram of voltage window detector, (b) Circuit design of comparator.

neural activities in a variable time frame. The time frame is tuned externally based on the patient-specific seizure onset frequency for accurate seizure detection with minimum false alarms.

4.5 Experimental and validation results

4.5.1 Circuit validation results

The asynchronous seizure detector has been validated first using discrete components in 50 mm diameter PCB [1], then implemented in 1.5×1.5 mm^2 area micro-chip using CMOS 0.13 µm process. The circuit design and integrated circuit layout were validated using Spectre simulator (Cadence tools) and seizure detection performance was evaluated [2]. Later, two samples of the fabricated micro-chip were used for measurements and the experimental tests promised the consistency of the test results.

Fig. 4.7 illustrates both photograph of the layout and fabricated micro-chip. Experimental result of the analog block's frequency response is demonstrated in Fig. 4.8(a). The random Dc offset of the electrodes and flicker noise of the circuits were reduced in the front-end stage to prevent saturation of the bioamplifier. Thermal noise from analog circuits was attenuated by using a G_m-C low-pass filter. In Fig. 4.8(b), the performance of the asynchronous seizure detector is shown for a set of 15 mV voltage interval, 20 Hz signal frequency, and 1 s time frame. Table 4.1 summarizes the measured specifications of the proposed ASD.

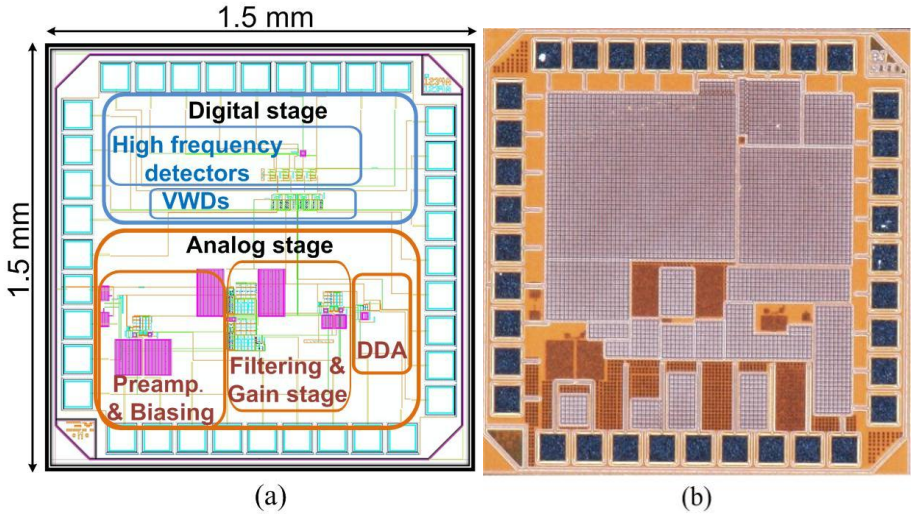

Figure 4.7: The proposed asynchronous seizure detector: (a) Layout of integrated chip, and (b) Photograph of the fabricated chip.

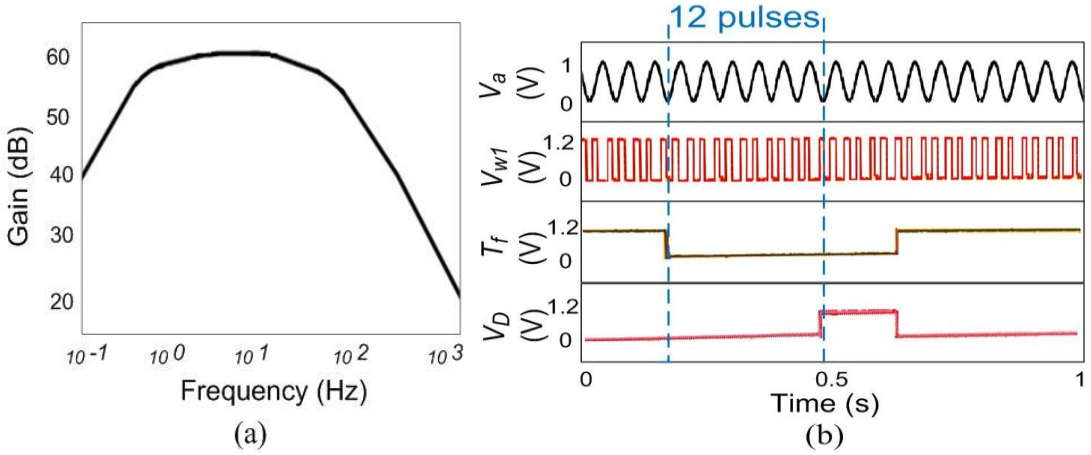

Figure 4.8: Measured results: (a) Gain and frequency response of analog building block, and (b)Validation of asynchronous seizure detector, where V_a is the amplified signal in the output of analog stage, V_{W1} is the output of first voltage window detector, T_f is the time frame, and V_D is the output of first channel changing the state after counting 12 pulses.

Table 4.1: Measured features of fabricated asynchronous seizure detector

Block	Parameter	Value
Filtering and gain stage	Midband gain	60 dB
	High-pass cutoff frequency	< 1 Hz
	Low-pass cutoff frequency	59 Hz
Seizure detection stage	Highest threshold voltage	1.1 V
	Lowest threshold voltage	100 mV
	Threshold incremental step	15 mV
ASD	Supply voltage	1.2 V
	Power consumption	9 µW

4.5.2 Patients description

This study was conducted at Notre-Dame Hospital, Centre Hospitalier de l'Université de Montréal (CHUM) and experimental protocol was approved by ethics committee. Two patients with refractory focal epilepsy were qualified for these studies based on electrographic seizure onset. These patients had previously undergone a complementary non-invasive study of the brain (e.g. video-scalp EEG, brain magnetic resonance imaging (MRI), ictal single photon emission computed tomography (SPECT), positron emission tomography (PET), EEG-functional MRI (EEG-fMRI), and magnetoencephalographic (MEG) study) which were failed to localize the epileptogenic zone effectively. Hence the invasive studies were recommended for better delineation of the epileptogenic zone. In these studies, signals were recorded by implementing intracranial electrodes through a craniotomy or burr holes under general anesthesia. Each patient was monitored about 3 weeks and an average of 7 seizures per patient was recorded. IcEEG recordings of these patients acquired using commercially available equipments (PRO-36 amplifiers, Stellate Harmonie System) with a gain of 1000 V/V, a 0.1–70 Hz bandwidth, 200 Hz sampling frequency, and 8 bits of digitization resolution [83]. Following the recordings, the seizures and epileptogenic zone were marked by epileptologist (Dr. Nguyen). The recorded icEEG of these patients were used for validation of our asynchronous seizure detector.

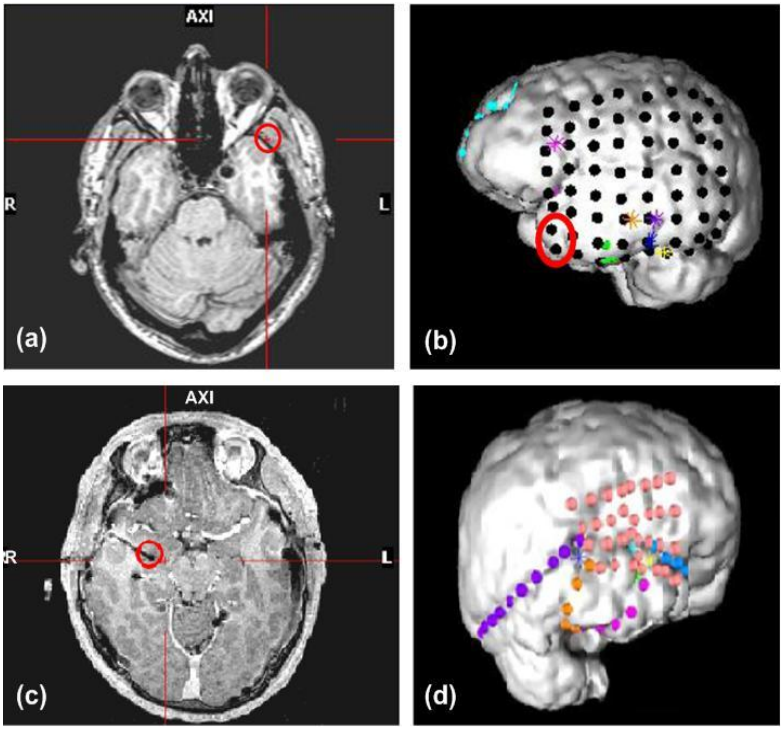

Figure 4.9: The electrode implementation: (a)-(b) MRI and 3D reconstruction of the first patient, and (c)-(d) MRI and 3D reconstruction of the second patient.

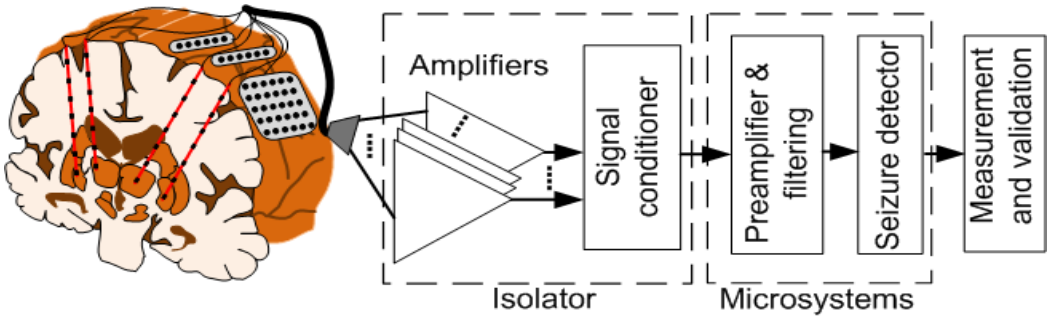

Figure 4.10: Device validation method: icEEG recorded from patients with medically refractory epilepsy were used to test the proposed asynchronous seizure detector.

The first patient was a 36 year-old male with left frontotemporal regional onset seizure since the age of 30 years. The icEEG recording of this patient was characterized by low and high-frequency preictal spiking, and brief electrical seizure activities. Figs. 4.9(a)–(b) show the MRI and 3D images of the implanted electrodes for this patient, respectively. The 3D image of the

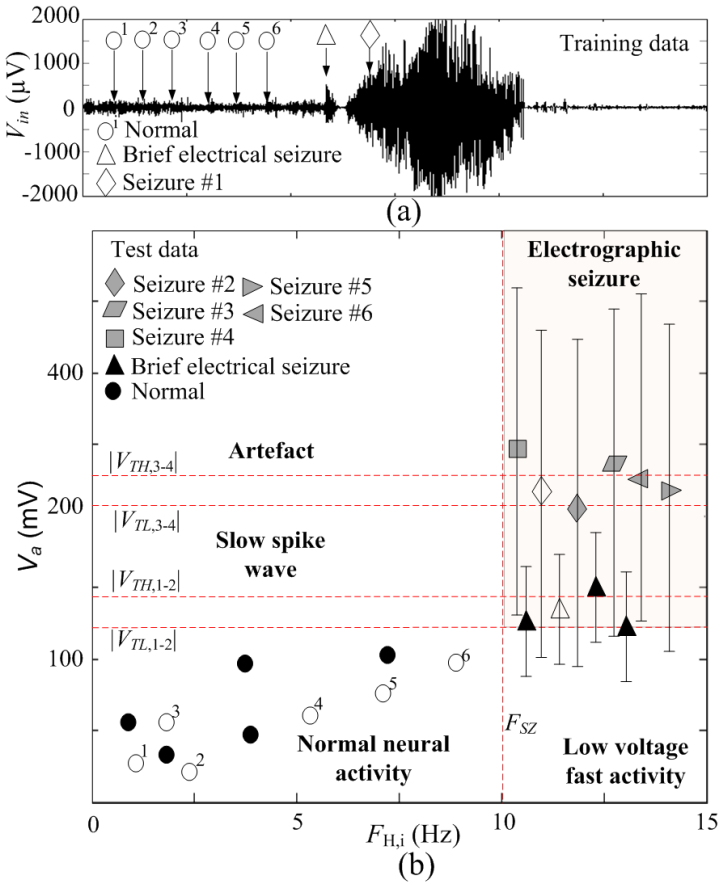

Figure 4.11: Seizure detection performance: (a) Analysis on training data V_{in} and determine detection parameters ($V_{TH/TL,1\text{-}4}$ and F_{SZ}) setting from patients' specific seizure patterns from the time-frequency and time-amplitude analysis, and (b) Decision boundaries formation using $V_{TH/TL,1\text{-}4}$ and f_{SZ} and test detection performance using other 5 seizures, 3 brief electrical seizures and 5 normal activities.

electrodes is reconstructed using grid view software. The circumscribed area in these figures shows the position of two contacts of the subdural grid electrodes, which provided the seizure signals from the epileptogenic zone of the patients.

The second patient is a 24 year-old male with drug resistant partial epilepsy since the age of 18 years. Through a craniotomy, the intracranial electrodes were implemented to sample temporal and insular regions. Several electrical seizures were recorded from the right medial temporal lobe of his brain. The MRI and 3D images of the implanted electrodes for this patient are shown in Figs. 4.9(c)–(d), respectively.

4.5.3 Case study results

The proposed seizure detector was validated using the previously recorded icEEG signals from two patients with refractory focal epilepsy. Electrodes were implemented in the suspected areas of the epileptogenicity to provide the required icEEG signals. A total of 34 recording sets from epileptogenic zone of these patients were used for validation. Among all recordings, 15 recording sets corresponded to seizure activities while the remaining 19 signals were related to variable patient activities such as brief electrical seizures, body movement, and sleep patterns.

Fig. 4.10 illustrates that the icEEG recordings from the contacts positioned over the epileptogenic zones (Fig. 4.9) were amplified and conditioned (isolation: attenuation and converted to micro-level icEEG), and fed into the Microsystem.

In the training process, adjusting the threshold levels is critical in order to prevent the false negative detection rate. In [1], the appropriate parameters of the PCB-based detector in training process were extracted from simulated time-frequency and time-amplitude analysis of a seizure, brief electrical seizure and 5 minutes normal icEEG for each patient. However, each threshold level was tuneable within a limited voltage range that caused a complicated and time-consuming training process. As a result, a novel detection structure is used in the design of the ASD that facilitated the training process and provided a widely adjustable threshold levels in the range of 100-1100 mV. As it is shown in Fig. 4.11, the ASD is adjusted to the specific attributes calculated from the time-frequency and time-amplitude simulations, and validated using the rest of the seizures and other icEEG recordings. This detector introduced effective detection parameters that create several decision boundaries (e.g., normal neural activity, low-voltage fast activity, slow spike wave, brief electrical seizure, and electrograghic seizure). As a result, the detector reduces the number of false detections due to interictal spikes, polyspikes, movement artifacts, physiological rhythms (sleep spindles), and brief asymptomatic high frequency voltage activities or very brief electrical seizures for the patient's specific seizure onset pattern while enhanced the sensitivity. Fig. 4.11(b) shows that all seizure onsets were located inside the electrograghic seizure boundaries without having false detection. Therefore, the proposed algorithm has high detection sensitivity, specificity and avoids false detections.

Fig. 4.12 illustrates the experimental result of the ASD, using an electrical seizure of the 36 years old patient leading to clinical manifestations approximately 30 s after the seizure onset. This icEEG recording was imported into microchip and output of the amplified signal (V_a) was further

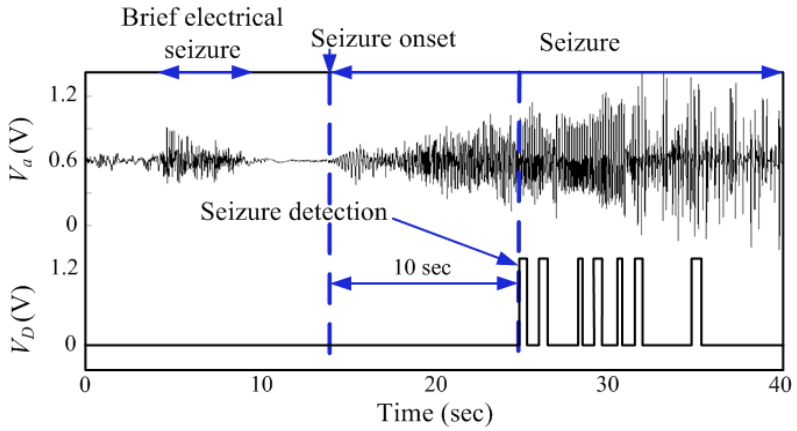

Figure 4.12: Validation of proposed ASD using a recorded seizure of case 1: V_a is the amplified signal at the output of analog stage, and V_D is the seizure detection. The ASD detects seizure with almost 10 s delay that is 19.4 s before patient's clinical manifestation.

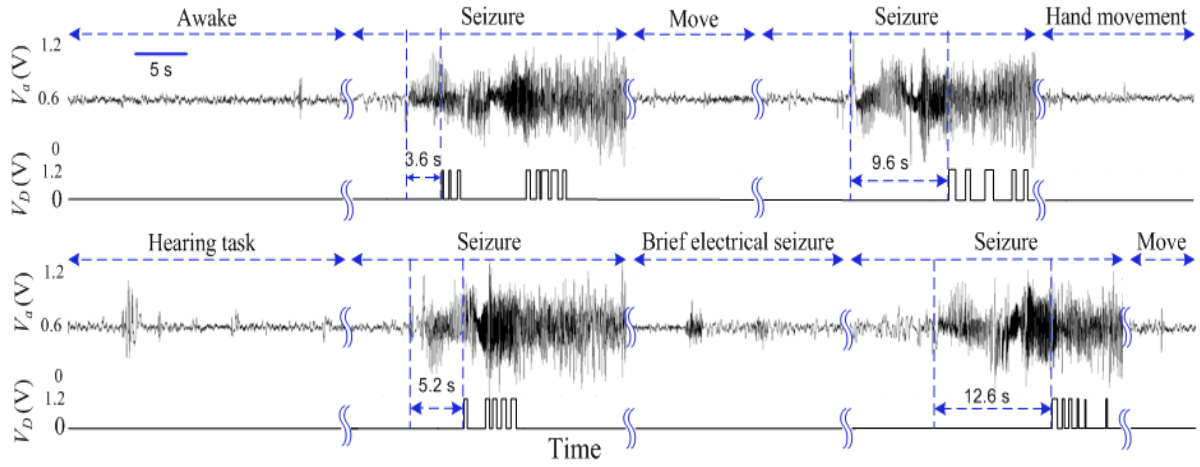

Figure 4.13: Measured seizure onset detection of case2, where V_a is the amplified icEEG signals at output of analog stage and V_D is the seizure detection output showing the non-related seizure activities are ignored and the epileptic seizures are detected by the proposed ASD.

analyzed in time amplitude and frequency domains to find confirmed seizure activities (V_D). During 40 s transient analysis, the first seizure detection was indicated at 25 s in Fig. 4.12 which is early enough (10.6 s after the ictal onset) to have promise of the seizure detection prior to the clinical manifestations (19.4 s earlier). Further experimental tests showed that the non-related seizure activities were ignored while the epileptic seizures were detected by the proposed and fabricated ASD (Fig. 4.13).

Table 4.2: Case study results of two patients

Parameter	Case 1	Case 2
Age/Gender	36/M	24/M
Origin	Left lateral temporal neocortex	Right hippocampus
Seizure characterized by	Arrest of speech and inability to comprehend generalized tonic-clonic seizure	Warmth and dizziness, confusion generalized tonic-clonic seizure
T_f (s)	1	1
T_{CM} [a] (s)	30	47
T_{avm} [b](s)	7	10
T_{avp} [c](s)	8	11
T_{ave} [d](s)	10	17.5

[a] T_{CM} is the duration from seizure onset to first clinical manifestation, [b] T_{avm} is the average detection delay from Matlab, [c] T_{avp} is the average detection delay from post-layout simulation results, and [d] T_{ave} is the average detection delay from experimental tests of two fabricated chips

Table 4.3: Comparison of synchronous and asynchronous seizure detectors

Parameter	Synchronous		Asynchronous	
	PCB-based [103]	Micro-chip [99]	PCB-based [1]	Chip (ASD)
Power consumption	67.6mW	50 µW	47.2 mW	9 µW
Case1- T_{DET} [a] (s)	21	15	16	17.5
Case2- T_{DET} [a] (s)	7	6	9	10
Size (mm^2)	1256.6	2	1963.5	2.25

[a] T_{DET} is the average detection delay

Due to the diversity observed in the signal amplitude and frequencies of the epileptic seizures, two samples of the fabricated micro-chips were verified using various signals of these patients. Sensitivity and specificity of 100% was achieved for 34 recorded icEEG signals of two patients and an average detection delay of 13.7 s was obtained after seizure onset, well before the clinical manifestations. Table 4.2 shows the seizure characteristics and case study results of these two patients. Presented data are based on average values obtained from simulation results and experimental tests.

A comparison of the recently published synchronous seizure detectors [101], [105] with the

experimental results from proposed ASDs (both PCB-based [1] and this integrated chip version) is shown in Table 4.3. In the asynchronous structure, the modulator, demodulator, and frequency divider blocks are not used. Moreover, it keeps several modules OFF in icEEG monitoring mode unless abnormal activity interrupts it (when the amplitude of the neural signals is lower than threshold levels, the output of the VWDs are low and as a result, the high frequency detectors stop counting). In the synchronous systems [101], [105], the clock keeps all the blocks ON. As a result, the power dissipation of the ASD is 40% reduced in power saving mode (icEEG monitoring period). Fig. 4.14(a) illustrates a recorded icEEG signal and Fig. 4.14(b) demonstrates icEEG dependent devices' operation modes and their corresponding average power consumption densities (δ_p) in different devices [1], [101], [105] and this work. The power dissipation density of the proposed ASD is under the maximum safety level (δ_{Pmax}= 6 mW/cm^2 which may cause enough

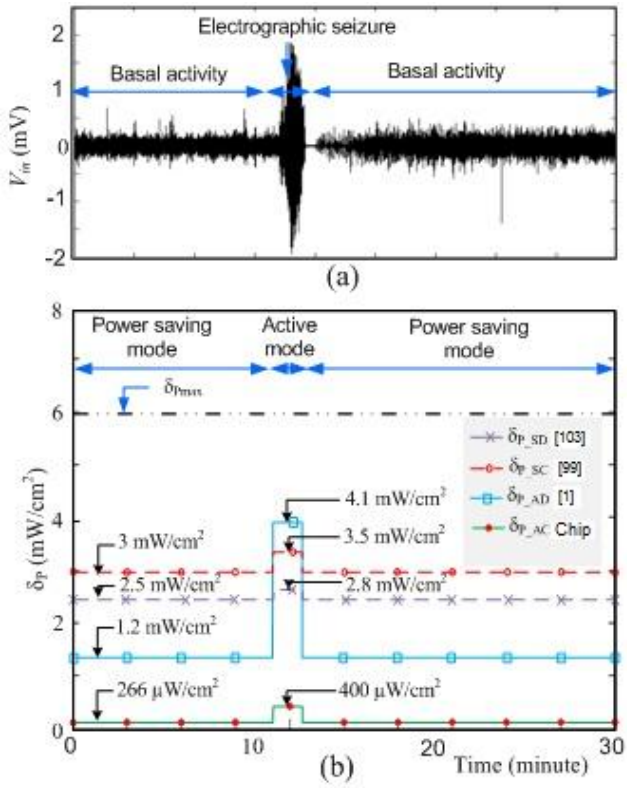

Figure 4.14: Illustration of device operating modes based on the icEEG recording: (a) IcEEG recording of an electrographic seizure and (b) average power consumption densities during power saving and active modes in synchronous devices [103], [99] and asynchronous devices [1] and chip.

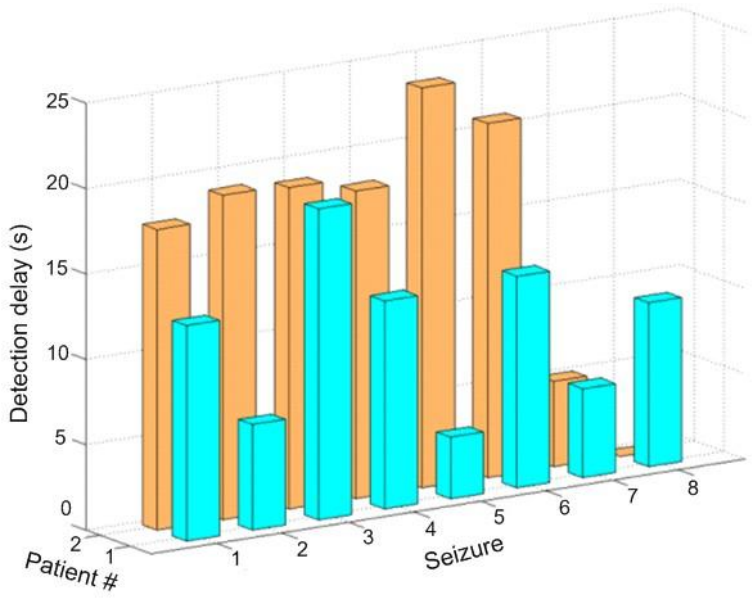

Figure 4.15: Delay plot for Case 1 and Case 2 showing the measured detection delays from seizure onset to the first detection alarm.

heat to damage surrounding tissue) [95]. The individual detection delays of the ASD for Case 1 and Case 2 are shown in Fig. 4.15.

Table 4.4 compares the performance of the recently published CMOS-based seizure detectors [83], [85]–[87], [101], with our experimental results from fabricated ASD. In [85], an implantable method is proposed to detect epileptic seizures and a multiple stage algorithm is used to reduce the false alarms. The hippocampal depth electrode recordings of 6 animals are used to evaluate the performance of this system, which resulted in 95% sensitivity. However, the power consumption and sensitivity are based on simulation results. The low-power seizure detector in [83] is validated using a total of 25 seizures and 24 non-seizure signals. Post-layout simulation resulted in 100% sensitivity and detection delay of 9.7 s after seizure onset. The count-based algorithm in [101] is implemented in CMOS 0.18 µm technology and power consumption of 50 µw is obtained from fabricated device. The validation results on seven patients provided 100 % specificity and an average detection delay of 13.5 s. However, these methods are using a synchronous algorithm, which results in unnecessary signal transition and power consumption. The seizure detector in this work provides a power saving mode (icEEG monitoring period) where transistors do not change their state until an event occurs. As a result, power consumption of the proposed ASD reduced significantly compared to other seizure detectors. Moreover, specificity of 100 % is obtained for

Table 4.4: Comparison of the latest low-power seizure detectors

Reference	Electrode	Location	Amplifier		Detector		Total PC [a]	Sen [b]	Detection delay (s)
			Process	PC [a]	Process	PC [a]			
[101]	Subdural and depth	Lateral temporal, mesial temporal, and frontal lobe	CMOS 0.18 µm	50 µW	CMOS 0.18 µm	44.8 nW	50 µW	100%	13.5
[83]	Subdural and depth	Lateral temporal, mesial temporal, and frontal lobe	CMOS 0.18 µm	6.5 µW (Sim)	CMOS 0.18 µm	0.57 µW (Sim)	7.07 µW (Sim)	100%	9.7
[85]	Depth	Hippocampus	Data acquisition system interfaced to a desktop computer	N/A	MIT 180 nm	350 nW (Sim)	N/A	95%	8.5 (Sim)
[86]	Subdural and depth	Frontal, temporal, and partial lobe	Neurofile NT digital video EEG system	N/A	CMOS 0.13 µm	2.7 µW	N/A	94%	N/A
[87]	Ag/AgCl	Scalp	CMOS 0.18 µm	72 µW	CMOS 0.18 µm	48.1 µW	48 µW	93%	8.2
This work	Subdural and depth	Lateral temporal, mesial temporal, and frontal lobe	CMOS 0.13 µm	7.5 µW	CMOS 0.13 µm	1.5 µW	9 µW	100%	13.7

[a]PC is power consumption, [b]Sen is sensitivity, and [c]Sim is simulation.

two epileptic patients and a better sensitivity was achieved compared to [85], [86], [87]. Total power consumption of the chip is 9 µW and average detection delay is 13.7 s after seizure onset. Although this delay is slightly higher than the value of some other methods, it is early enough before the onset of the clinical manifestations.

The good overall results presented in this paper are achieved using the advantages of the asynchronous algorithm and count-based detection method. The asynchronous structure provides a reduction of 40% in power saving mode and the count-based detection method decreases the false detection rate of the proposed system, which is caused by unrelated seizure activities. The presented asynchronous micro-chip was validated using icEEG recordings from two patients. However, our study on PCB-based asynchronous seizure detector was based on icEEG recordings from seven patients. Both of the systems have same seizure detection algorithm and similar detection performance. Therefore, validation of the further detection performance long icEEG recordings from the rest of patients was avoided, but different scenarios were evaluated carefully for the clinical applications.

4.6 Conclusion

An integrated low-power asynchronous seizure detector demonstrated power consumption reduction in an accurate detection system for implantable device therapies. The presented micro device was fabricated using 0.13 µm CMOS technology and validated using recorded icEEG from two patients with refractory focal epilepsy. This system has widely programmable parameters that facilitate the specific tuning to electrographic seizure onset of a patient. As a result, specificity of the system were improved (100 % for two patients). Experimental results have shown 100% sensitivity of the fabricated seizure detector. The power consumption, noise and performance of the system were improved compared to the PCB-based detector and some other recently published detectors.

Further validation in an animal model of epilepsy is warranted. To note, seizure onset patterns may vary in terms of onset morphology, discharge frequency, and spread pattern. However, low-voltage fast-activity patterns at seizure onset are commonly encountered. The proposed seizure detector is applicable for this type of patterns and it is worth further investigating on patients suffering from epileptic seizure characterized by high-voltage fast-activity, rhythmic spiking, and other patterns.

4.7 Acknowledgment

The authors acknowledge support from NSERC and Canada Research Chair in Smart Medical Devices, and are grateful for the support provided by CMC Microsystems with 130 nm CMOS technology and engineering services.

CHAPTER 5 EXPERIMENTAL TESTS AND VALIDATION RESULTS

5.1 Experimental results of the PCB-based seizure detector

Our group proposed an asynchronous algorithm that offers the advantage of the reducing the total power dissipation and minimizing the false alarms. The system was assembled with discrete components on a circular PCB. Performance of this device was proved using the icEEG signals recorded from seven patients with different electrical seizures. The power consumption of the detector was reduced by 45% in power saving mode [1]. Table 5.1 shows the measured results of the PCB-based seizure detector.

Table 5.1: Measured features of the PCB-based seizure detector

Block	Parameter	Value
Filtering and gain stage	Midband gain	60 dB
	High-pass cut-off frequency	3 Hz
	Low-pass cut-off frequency	51 Hz
Seizure detection stage	Highest threshold voltage	3.3 V
	Lowest threshold voltage	50 mV
	Threshold incremental step	20 mV
PCB	Supply voltage	3.3 V
	Power consumption	67.6 mW

The PCB-based asynchronous seizure detector was validated using icEEG recordings from seven patients and the study on the asynchronous micro-chip was based on icEEG recordings from two epileptic patients (Case1 and Case2). From these seven patients, the detection setups of the PCB-based seizure detector for three patients are available and shown in Tables 5.2 to 5.7. A total of 11 icEEG signals are recorded from Case1, 23 icEEG signals are recorded from Case2, and 25 icEEG signals are recorded from Case3. The recorded signals of Case1 and Case 2 are also used for validation of the microchip (Table 4.2). The icEEG signals of Cases 2, 3, 5, 6 and 7 are recorded using depth electrodes while for Cases 1 and 4, the subdural strip electrodes are used for recording the icEEG signals. Different scenarios (e.g., movement artifacts and brief electrical seizure during sleep) in addition to seizure activities have been used for validation.

In Tables 5.2 to 5.7, the threshold voltages of the first window detector are V_{a1} and $V_{a2,}$ the threshold voltages of the second window detector are V_{b1} and $V_{b2,}$ the threshold voltages of the third window detector are V_{c1} and $V_{c2,}$ and the threshold voltages of the fourth window detector are V_{d1} and V_{d2}.

Table 5.2: Different settings of the voltage window detector for Case 1

Setting no.	**V_{a1}**	**V_{a2}**	**V_{b1}**	**V_{b2}**	**V_{c1}**	**V_{c2}**	**V_{d1}**	**V_{d2}**
1	970 mV	940 mV	880 mV	850 mV	430 mV	400 mV	330 mV	300 mV
2	940 mV	910 mV	850 mV	820 mV	400 mV	370 mV	300 mV	270 mV
3	910 mV	880 mV	820 mV	790 mV	370 mV	340 mV	270 mV	240 mV

Table 5.3: Detection performance of the PCB-based seizure detector for Case 1

File name	**Setting no. 1**	**Setting no. 2**	**Setting no. 3**
bes	0	0	1
bes2	1 (FP)	0	0
s1	1	1	1
s2	1	1	0 (FN)
s3	1	1	1
s4	1	1	1
s5	1	1	1
S6_breif	1 (FP)	0	0
s7_bes	1 (FP)	0	1 (FP)
sleep	0	0	0
sleep2	0	0	0

T_f=1 Hz

In Table 5.3, signals S_1-S_5 are the epileptic seizures while other 5 signals are the normal activities of the brain or very brief high-frequency discharges which do not lead to clinical manifestations. In this table, for three different settings, symbol "1" shows that the output of the PCB-based seizure detector declares seizure activity while symbol "0" shows that the output of the PCB-based seizure detector declares normal activity. As it is shown in Table 5.3, due to the FP and FN detections for settings 1, 3, only sitting 2 is used to improve the detection performance of the PCB-based seizure detector.

Table 5.4: Different settings of the voltage window detector for Case 2

Setting no.	**V_{a1}**	**V_{a2}**	**V_{b1}**	**V_{b2}**	**V_{c1}**	**V_{c2}**	**V_{d1}**	**V_{d2}**
1	870 mV	840 mV	770 mV	740 mV	400 mV	370 mV	300 mV	270 mV
2	900 mV	870 mV	800 mV	770 mV	430 mV	400 mV	330 mV	300 mV
3	930 mV	900 mV	830 mV	800 mV	460 mV	430 mV	360 mV	330 mV

Table 5.5: Detection performance of the PCB-based seizure detector for Case 2

File name	**Setting no. 1**	**Setting no. 2**	**Setting no. 3**
S1	1	1	1
S2	1	1	1
S3	1	1	1
S4	1	1	1
S5	1	1	1
S6	1	1	1
S7	1	1	1
S8	1	1	1
SL_awake_1	0	0	1 (FP)
SL_awake_2	0	0	0

SL_awake_3	0	0	0
SL_sleep_1	0	0	0
SL_sleep_2	0	0	0
SL_sleep_3	0	0	0
SL_move_1	0	0	0
SL_move_2	0	0	1 (FP)
SL_move_3	0	0	1 (FP)
SL_relax_1	0	0	1 (FP)
SL_relax_2	0	0	0
SL_relax_3	0	0	0
Hearing	0	0	0
Right hand moves	0	0	0
Left hand moves	0	0	0

T_f=1 Hz

In Table 5.5, signals S_1-S_8 are the epileptic seizures while the other signals are the recorded normal activities of the brain or very brief high-frequency discharges that do not lead to clinical manifestations. In this table, for three different settings, symbol "1" shows that the output of the PCB-based seizure detector declares seizure activity while symbol "0" shows that the output of the PCB-based seizure detector declares normal activity. Due to the FP detections for setting 3, only sittings 1 or 2 should be used to improve the detection performance of the PCB-based seizure detector.

Table 5.6: Different settings of the voltage window detector for Case 3

Setting no.	$\mathbf{V_{a1}}$	$\mathbf{V_{a2}}$	$\mathbf{V_{b1}}$	$\mathbf{V_{b2}}$	$\mathbf{V_{c1}}$	$\mathbf{V_{c2}}$	$\mathbf{V_{d1}}$	$\mathbf{V_{d2}}$
1	920 mV	890 mV	820 mV	790 mV	460 mV	430 mV	360 mV	330 mV
2	890 mV	860 mV	790 mV	760 mV	430 mV	400 mV	330 mV	300 mV
3	860 mV	830 mV	760 mV	730 mV	400 mV	370 mV	300 mV	270 mV

Table 5.7: Detection performance of the PCB-based seizure detector for Case 3

File name	Setting no. 1	Setting no. 2	Setting no. 3
S1	1	1	1
S2	1	1	1
S3	1	1	1
S4	1	1	1
S5	1	1	1
S6	1	1	1
S7	1	1	1
S8	1	1	1
eyeopen1	1 (FP)	0	0
eyeopen2	0	0	0
Lefthand	0	0	0
righthand	0	0	0
look_left	0	0	0
Look_right	0	0	0
move1	0	0	0
move2	0	0	0
relax1	0	0	0
relax2	0	0	0
relax3	0	0	0
sleep1	0	0	0
sleep2	0	0	0
sleep3	0	0	0
sleep4	0	0	0

sleep5	0	0	0
sleep6	0	0	0

T_f=1 Hz

In Table 5.7, signals S_1-S_8 are the epileptic seizures while the other signals are the recorded normal activities of the brain or very brief high-frequency discharges that do not lead to clinical manifestations. In this table, for three different settings, symbol "1" shows that the output of the PCB-based seizure detector declares seizure activity while symbol "0" shows that the output of the PCB-based seizure detector declares normal activity. Due to the FP detection for setting 1, sittings 2 or 3 should be used to improve the detection performance of the PCB-based seizure detector.

Table 5.8: Comparison of the average detection delay from PCB-based seizure detector and Matlab simulations [1]

Case no.	**Age/Gender**	**Average detection delay (s)**	
		Experimental measurement	**Matlab simulation**
1	36/M	16	10
2	24/M	9	7
3	41/M	22	12
4	44/M	18	7
5	49/F	15	18
6	32/M	13	11
7	15/M	22	19

Table 5.8 shows the average detection delay of the PCB-based seizure detector using signals of seven patients and the corresponded Matlab simulation results. In each case, there is a difference between experimental and Matlab results. In general, due to the noise figure, the detection delay of the PCB-based seizure detector is longer than Matlab results.

5.2 Post-layout simulation and experimental results of the chip

The asynchronous seizure detector has been validated in a PCB and its results persuaded us to

design an integrated version of our previous system to improve power management, noise, and performance of the asynchronous seizure detector.

5.2.1 Post-layout simulation results

The low amplitude icEEG signals are amplified by two gain stages to provide a total midband gain of 61.9 dB while the random Dc offset of the electrodes is eliminated in the front-end stage. The general structure of the ASD including the analog and digital building blocks is shown in Fig. 3.7. Table 5.9 summarizes the power consumption of the implemented blocks and Table 5.10 shows the measured features of the ASD obtained from post-layout simulations. V_{bp1} and V_{bn2} are the bias voltages produced internally by bias stage.

Table 5.9: Power consumption of the ASD obtained from post-layout simulations

Parameter	**Value**
Bias stage	11.6%
Amplifier stages	51.6%
Filter & DDA	23.3%
Digital stage	13.5%
Total power consumption	7.1 µW

Table 5.10: Measured features of the ASD obtained from post-layout simulations

Block	**Parameter**		**Value**
Bias stage	Internally generated	V_{bp1}	883 mV
		V_{bn2}	176 mV
	Externally generated	V_{bp2}	600 mV
		V_{bn1}	300 mV
Filtering and gain stage	Midband gain		61.9 dB
	High-pass cut-off frequency		1.1 Hz
	Low-pass cut-off frequency		57.6 Hz
Digital stage	Highest threshold voltage		1.1 V
	Lowest threshold voltage		100 mV
	Threshold incremental step		5 mV
PCB	Supply voltage		1.2 V
	Power consumption		7.1 µW

The system noise is attenuated by using a Gm-C low-pass filter. A total input referred noise of 4.4 µVrms (Fig. 5.1) is obtained for the 3-dB bandwidth of 56.5 Hz.

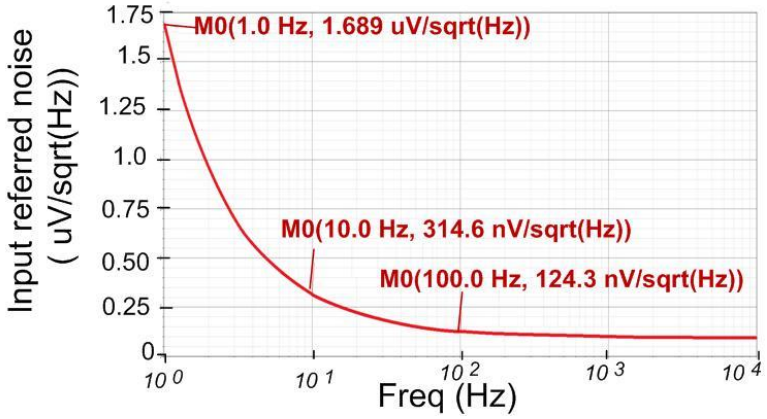

Figure 5.1: Total input referred noise of the ASD from Post-layout simulations.

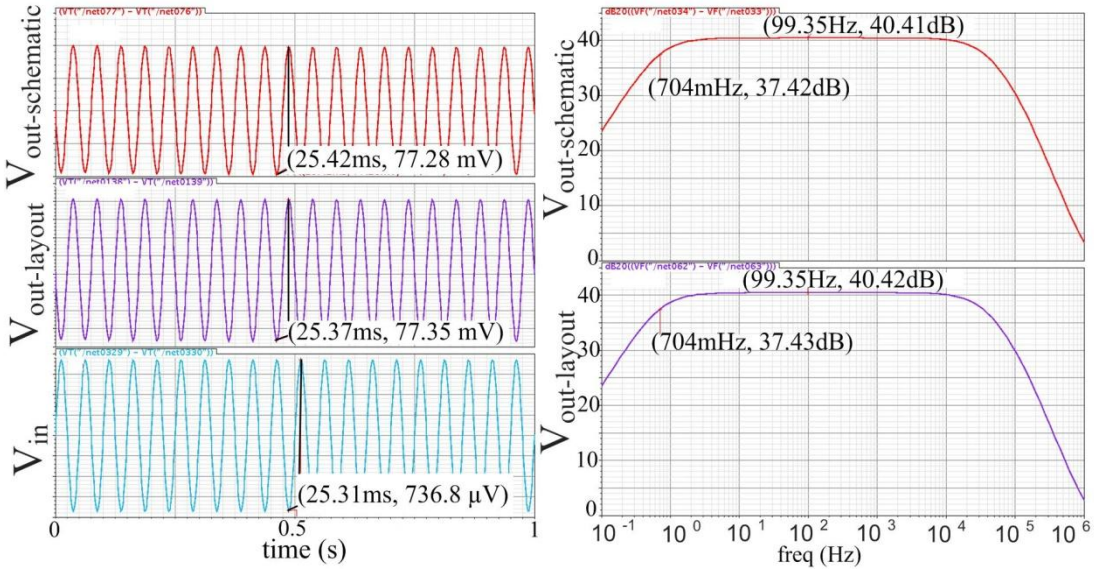

Figure 5.2: Frequency and transient analysis of the first amplification stage obtained from schematic and post-layout simulations.

In Fig. 5.2, the left side shows transient analysis of the first amplification stage while the right side shows its gain plot. For an input sinusoidal wave (V_{in}), the transient outputs of both schematic design and layout design are shown in left up and left middle of this figure, respectively. As it is illustrated, the transient outputs of schematic and layout have the same amplitudes around 77.3 mV. The gain plots obtained from schematic and layout simulations are also shown in the right up

and down side of the Fig. 5.2, respectively. The simulation results show the consistency of gain around 40.4 dB for both schematic and layout designs.

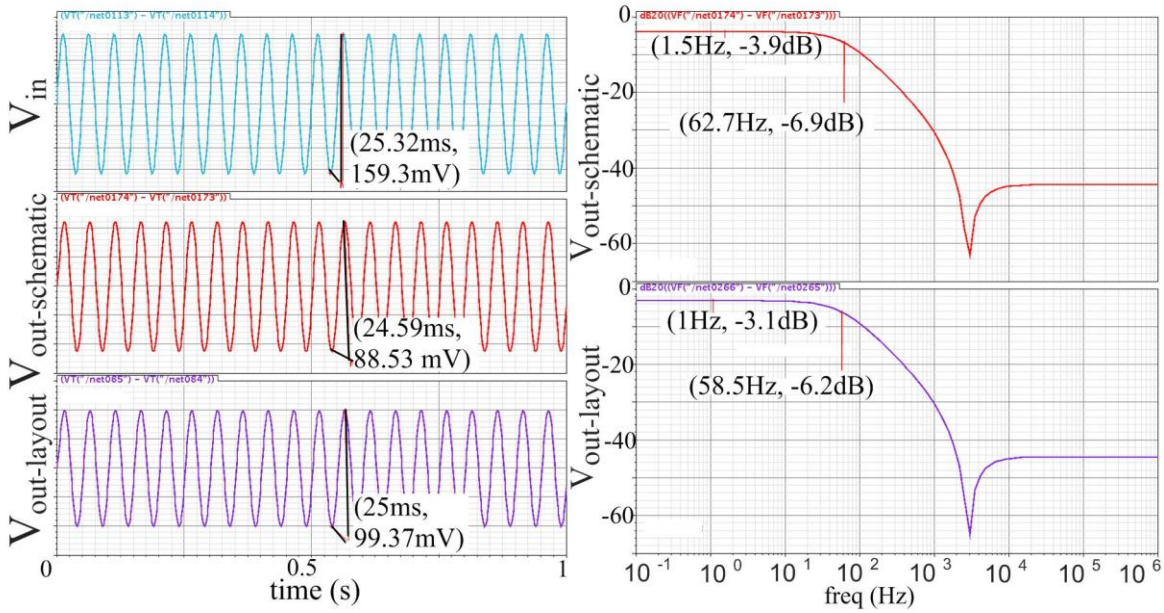

Figure 5.3: Frequency and transient analysis of the Gm-C low-pass filter obtained from schematic and post-layout simulations.

In Fig. 5.3, the left side shows transient analysis of the Gm-C low-pass filter while the right side shows its gain plot. For an input sinusoidal wave (V_{in}), the transient outputs of both schematic design and layout design are shown in left middle and left down side of this figure, respectively. Simulation results show that, amplitude of the signal in the output of the schematic design (88.5 mV) is in the range of the layout design (99.3 mV). In addition, the gain plots obtained from schematic and layout simulations are shown in the right up and down side of Fig. 5.3, respectively. The simulation results also show the consistency of gain around -3 dB for both schematic and layout designs.

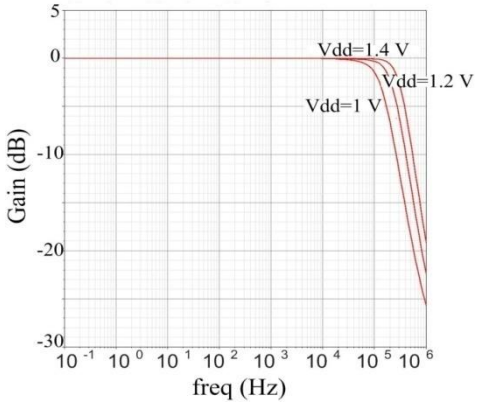

Figure 5.4: Frequency response showing the effect of the V_{dd} variation on DDA.

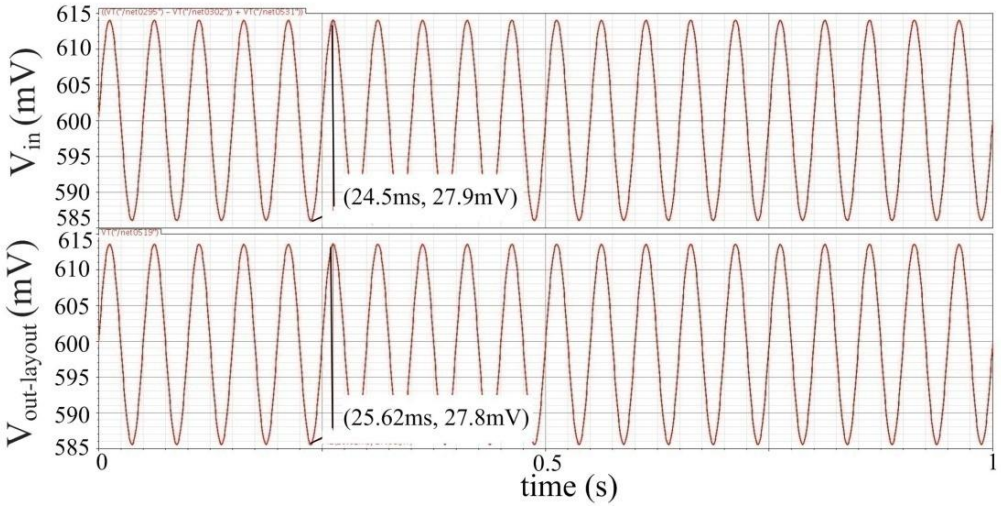

Figure 5.5: Transient analysis of the DDA from post-layout simulations.

Fig. 5.4 shows the effects of the V_{dd} variations (1 V, 1.2 V, and 1.4 V) on the frequency response of the differential difference amplifier (DDA). However, a Low-pass filtering stage is used to provide cutoff frequency of 57.6 Hz and as a result, this V_{dd} variations doesn't affect the frequency response of the asynchronous seizure detector. For a sinusoidal input signal, the supply voltage is set on 1.2 V and the output of the DDA is verified in Fig. 5.5. As the post-layout simulation result shows, the input and output of the DDA has the same amplitude (around 27.9 mV) in Fig. 5.5.

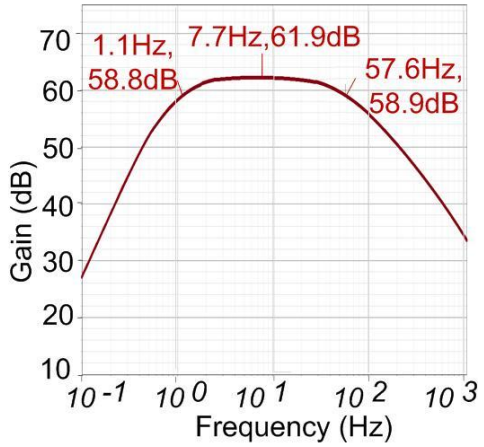

Figure 5.6: Frequency and gain response of the analog building block.

Fig. 5.6 demonstrates that the analog building block has the overall gain of 61.9 dB for 3-dB bandwidth of 56.5 Hz. The Monte carlo simulation results (Fig. 5.7) shows the possible gain and frequency response of the analog building block including the mismatch and process variation for 100 runs. As it is shown, the gain of the analog building block varies in the range of 58.8 dB and 62.8 dB. The low-pass cutoff frequency is around 1.1 Hz and the high-pass cutoff frequency varies between 53.6 Hz and 58.4 Hz. Since the required gain, high-pass, and low-pass cutoff frequencies are 60 dB, 1Hz, and 55Hz, respectively, the consistency of the Monte carlo simulation results promised the good performance of the analog stage. Otherwise, it is required to modify the design of the schematic and layout in order to provide the acceptable ranges.

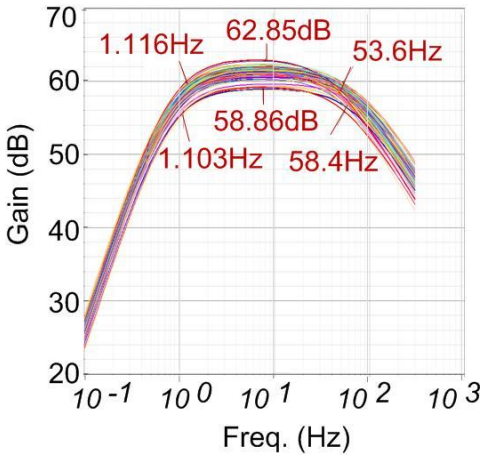

Figure 5.7: Monte carlo simulation results of the analog building block for 100 runs.

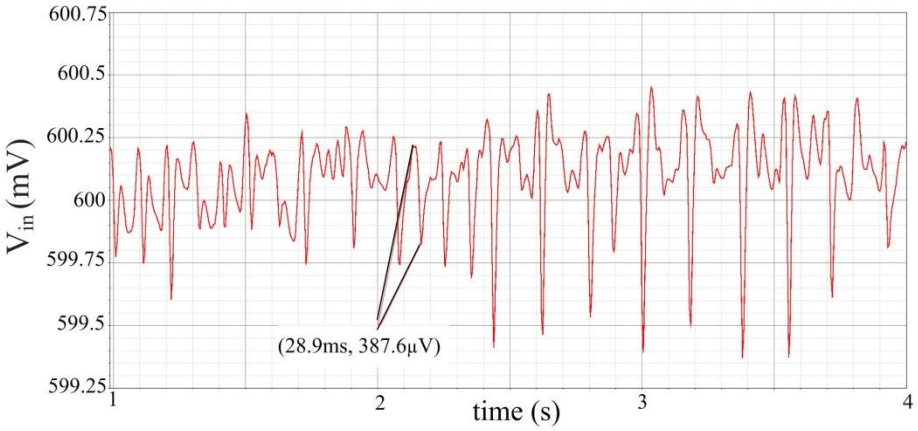

(a)

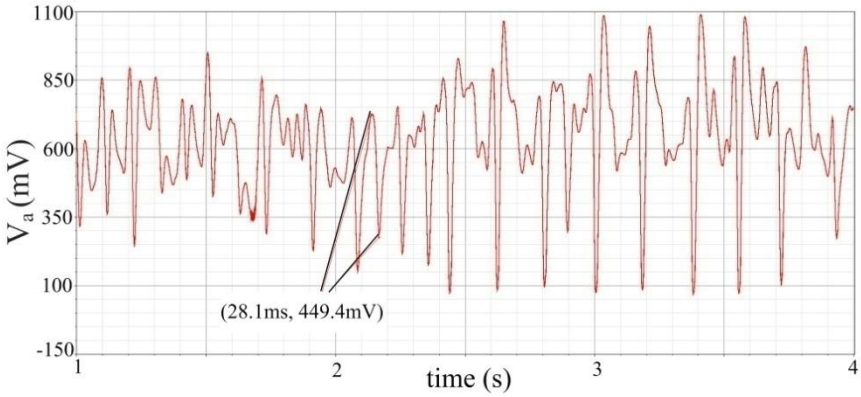

(b)

Figure 5.8: (a) A recorded icEEG signal in the input of the ASD and (b) The amplified signal in the output of the analog building block.

Since the amplitude and frequency of the neural signals are variable, in Fig. 5.8 a recorded icEEG signal is used instead of the sinusoidal wave to verify the performance of the integrated design. Fig.5.8 (a) shows the recorded icEEG signal used as the input of the ASD and Fig. 5.8 (b) illustrates the output signal of the analog building block that is amplified with the gain of around 61 dB.

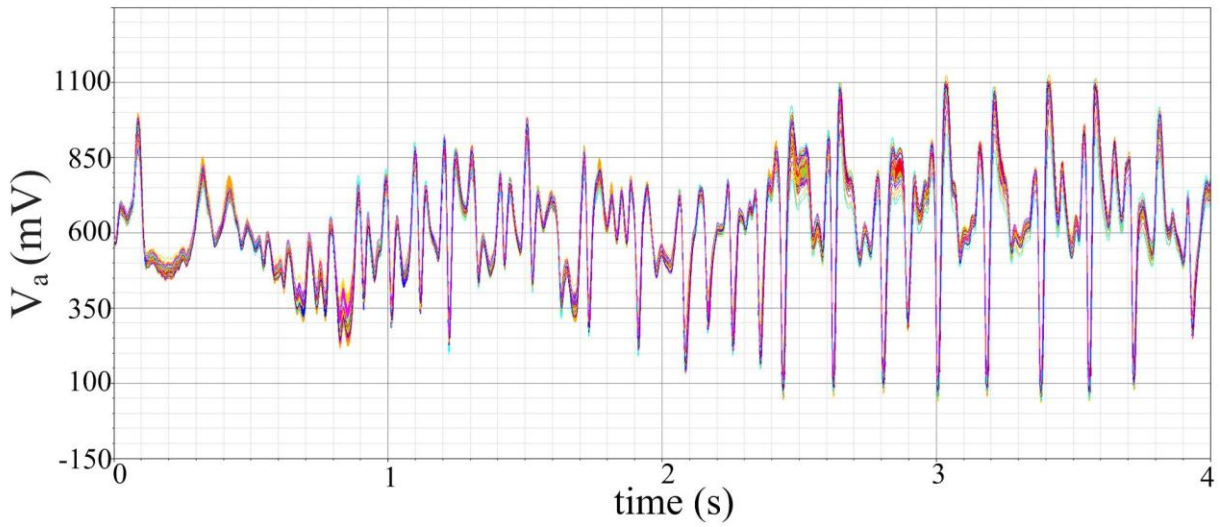

Figure 5.9: Monte carlo simulation results (100 runs) of the stabilized analog stage using an icEEG signal of the epileptic patient

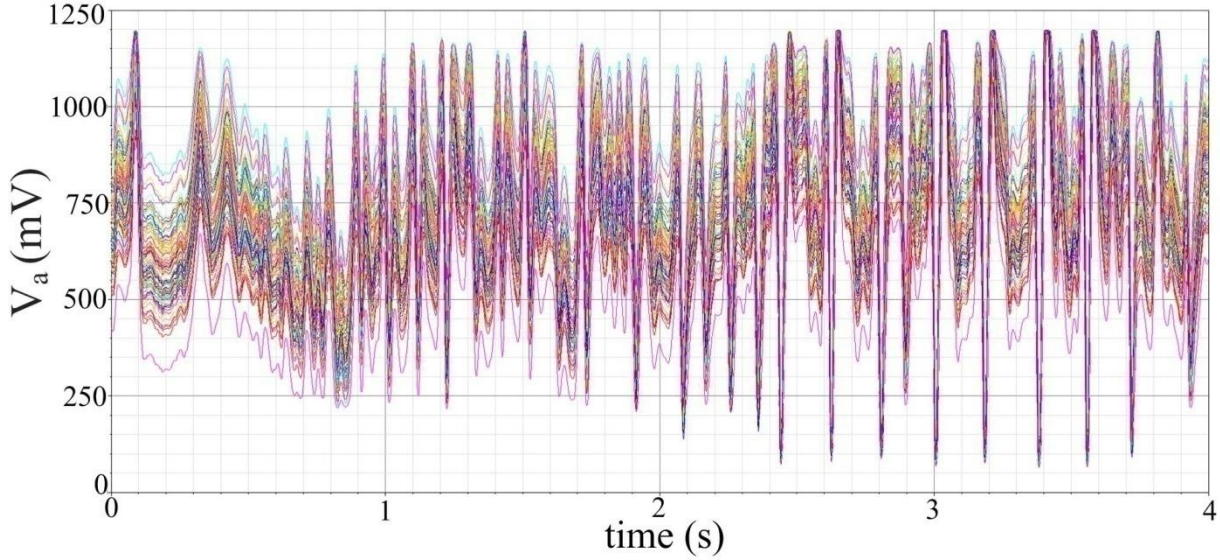

Figure 5.10: Monte carlo simulation results (100 runs) of the unstable analog stage using an icEEG signal of the epileptic patient

Fig. 5.9 illustrates the Monte carlo simulation results (100 runs) of the icEEG signal shown in Fig. 5.8. For 100 runs, the DC level and amplitude of the icEEG signal in Fig. 5.9 are in the same range as shown in Fig. 5.8. That shows the consistency of the simulations in a stabilized analog stage. However, Fig. 5.10 demonstrates that mismatches and process variations affect the Dc offset and

amplitude of the icEEG output signal for an unstable circuit.

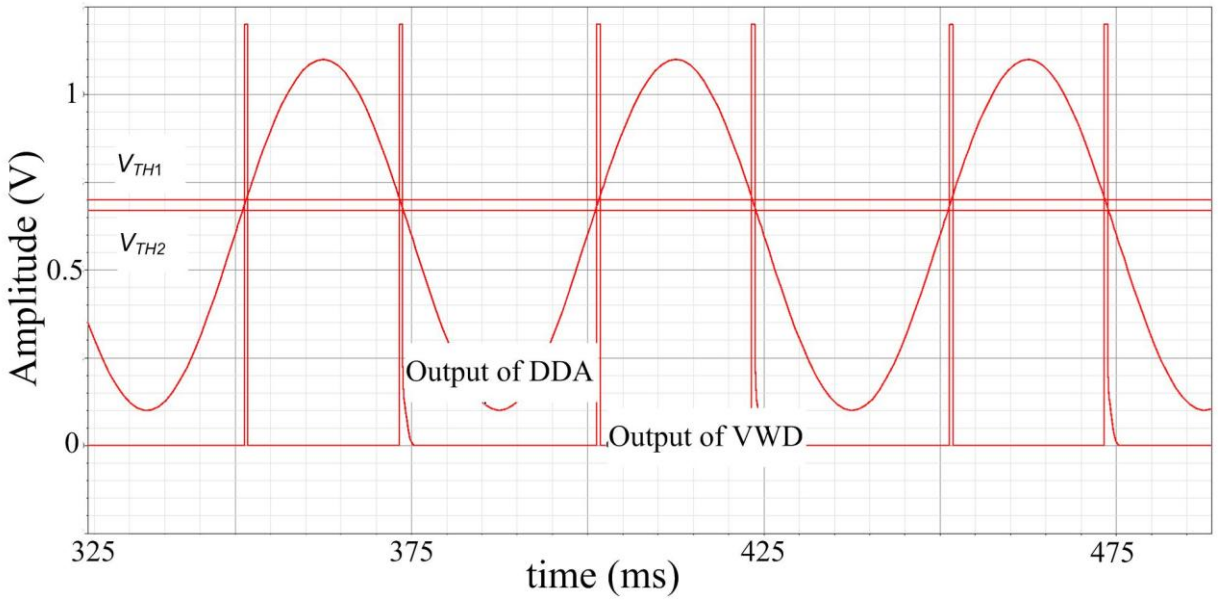

Figure 5.11: Output of the voltage window detector for threshold levels of 670 mV and 700 mV

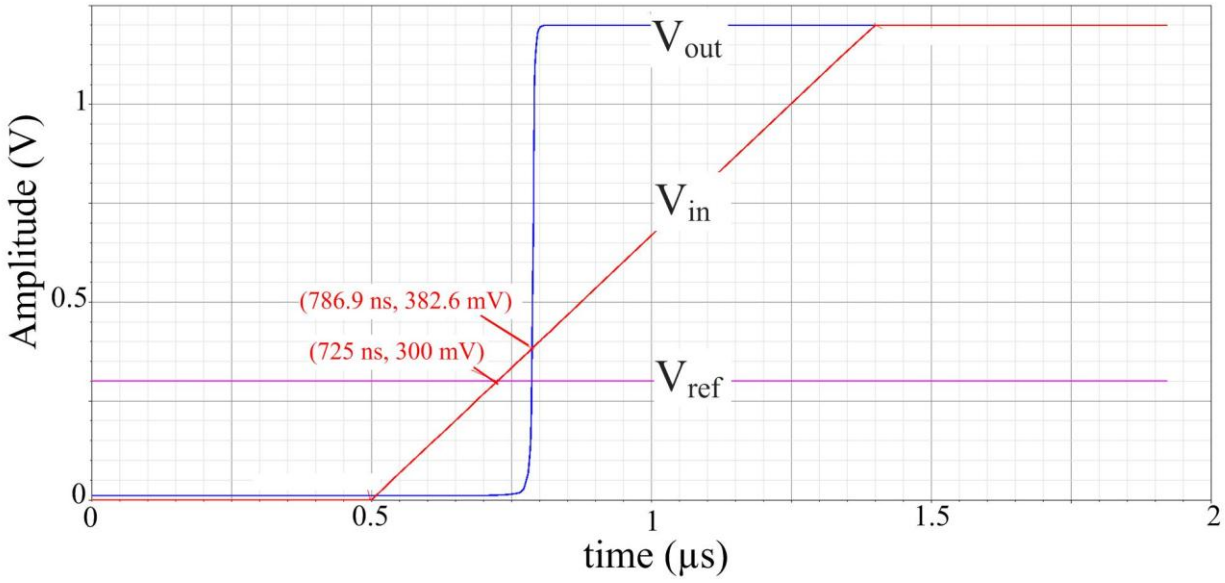

Figure 5.12: Delay of the comparator to switch its output

In Fig. 5.11, a sinusoidal wave is used as the input of the VWD and two threshold levels V_{TH1} and

V_{TH2} are set on 700 mV and 670 mV to verify the performance of the VWD. As it is shown, the VWD is able to detect this voltage interval of 30 mV. The VWD composed of two comparators. The output of an ideal comparator changes the state when the input signal passes the threshold level while a practical comparator exhibits delay and DC offset as shown in Fig. 5.12.

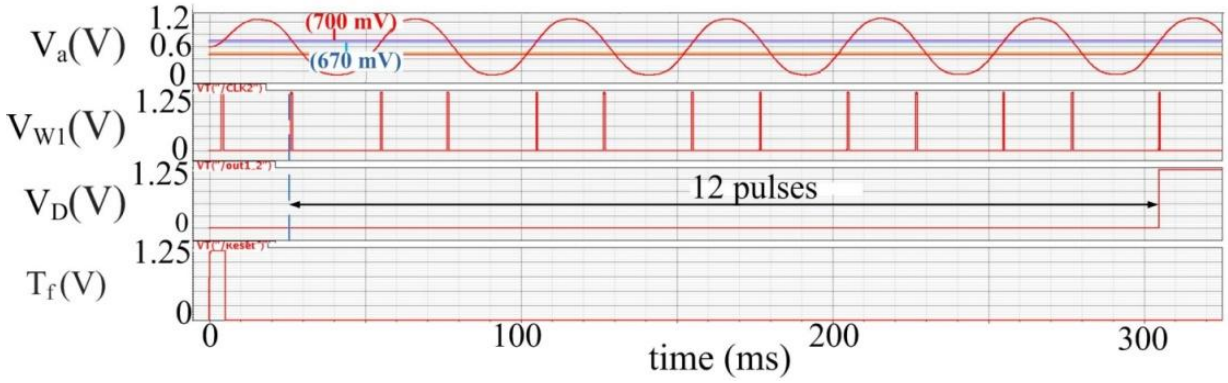

Figure 5.13: Output of the counter and logic gates which counts 12 pulses

Fig. 5.13 shows the performance of the counter where V_a is the amplified signal in the output of the analog stage, V_{W1} is the output of the first voltage window detector, T_f is the time frame used to reset the counter , and V_D is the output of the first channel changing the state after counting 12 pulses. Based on Matlab simulation results [1] and in order to reduce the power consumption, the counter stops working after counting 12 pulses.

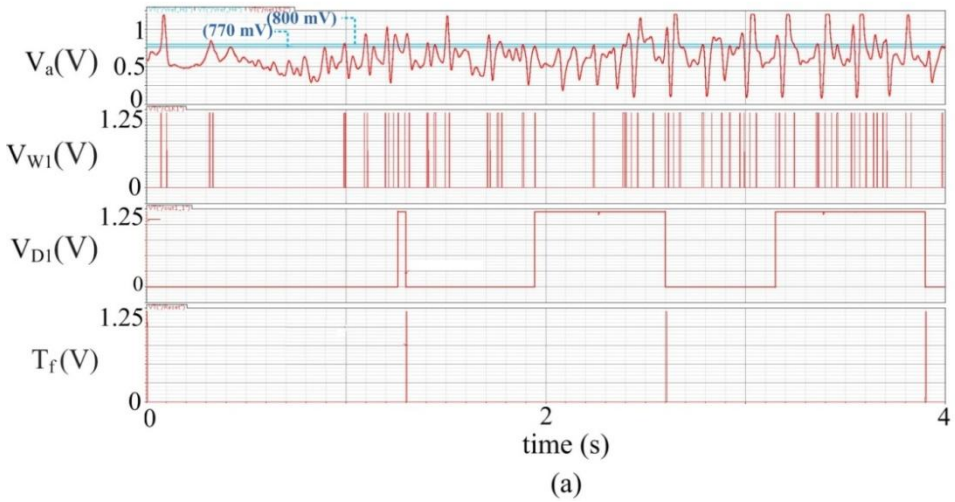

(a)

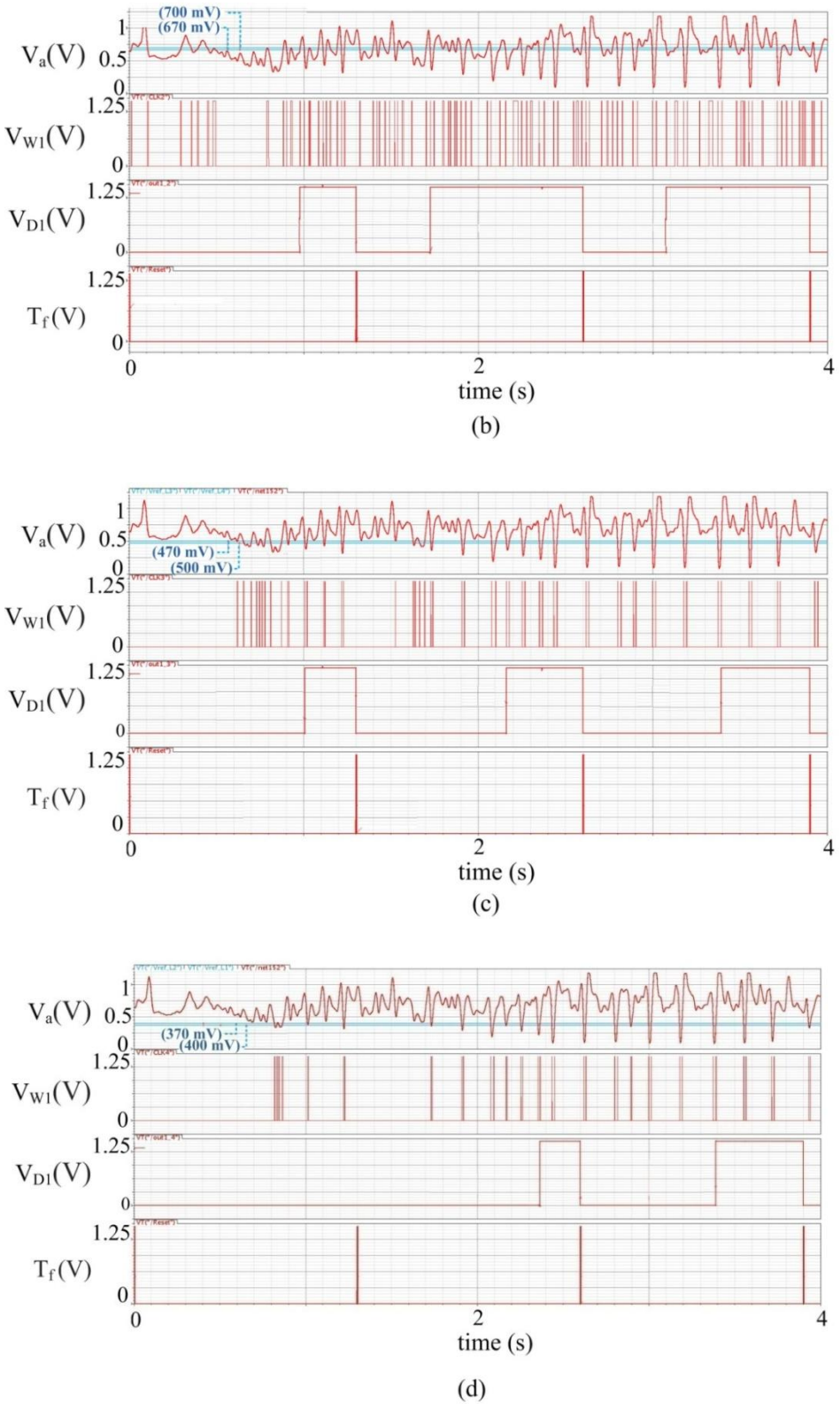

Figure 5.14: Output of four channels of the asynchronous seizure detector using icEEG recording of an epileptic patient and variable threshold levels to extract seizure activities.

Fig. 5.14 (a) - (d) shows the first test result of the ASD that the performance of the analog and digital building blocks are verified together by using an icEEG recorded signal. This signal was imported into microchip and output of the amplified signal (V_a) was further analyzed (V_{Wi}) in time amplitude and frequency domains through four channels of the high-frequency detectors. For each channel, different threshold voltages are used to find the confirmed seizure activities (V_{Di}) of the channel, where i = 1, 2, 3, 4 and a variable time frame (T_f) and total of eight variable threshold voltages are used. As it is shown in Fig. 5.14, all channels are able to extract seizure onset information.

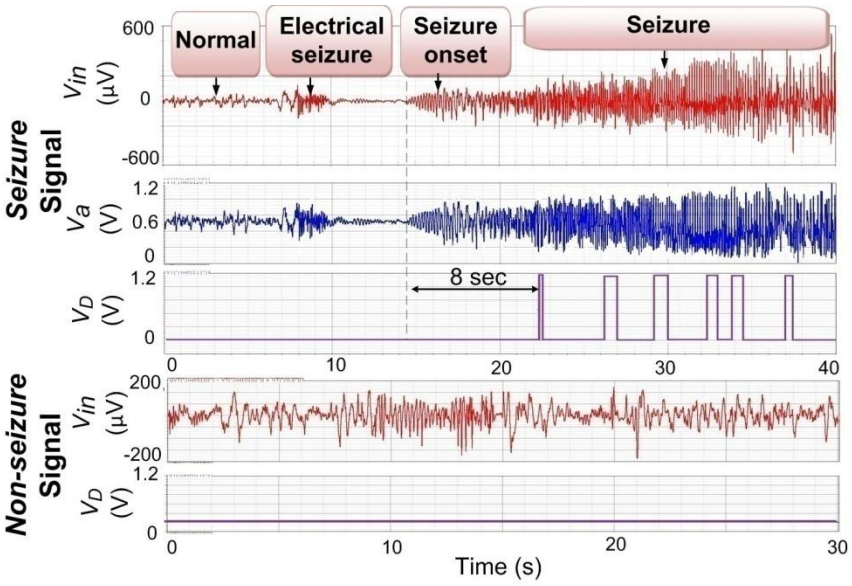

Figure 5.15: Validation of the proposed ASD by post-layout simulation of Case 1: V_{in} is the recorded icEEG signal, V_a is the amplified signal in the output of the analog stage, V_D is the final output of the ASD.

Further experimental tests from two patients with drug resistant partial epilepsy are used to verify the performance of the ASD using the normal and seizure activities. The icEEG recording of the first patient (36 year-old) is characterized by high-frequency preictal spiking, low frequency preictal spiking, and brief electrical seizure activities. Fig. 5.15 illustrates an electrical seizure and a normal signal of this patient. The seizure leaded to clinical manifestations approximately 30 sec after the ictal onset (marked by epileptologist). This signal (V_{in}) was imported offline into Cadence to validate the performance of the system. During 40 sec transient analysis of the seizure

signal, the asynchronous seizure detector (Fig. 5.15) has detected six pulses. The quantity of these pulses is related to the progressive increase of the magnitude and frequency for each patient. For this case, the first detection delay is 8 s after the seizure onset so that the proposed ASD recognized the seizure early enough to have promise of the seizure detection prior to the clinical manifestations (22 sec earlier).

It is important to mention that the progressive increase of frequency is measured indirectly. As an instance, by setting T_f around 1 s and using a 1 Hz sinusoidal signal, the counter counts the number of times the signal falls inside the voltage window. Providing the same T_f, voltage window, and amplitude of sinusoidal signal while increasing only the frequency of the signal will result in increasing the number of times the signal falls inside the voltage window. On the other hand, increasing the number of times the signal falls inside the voltage window implies a signal with progress increase of frequency/amplitude.

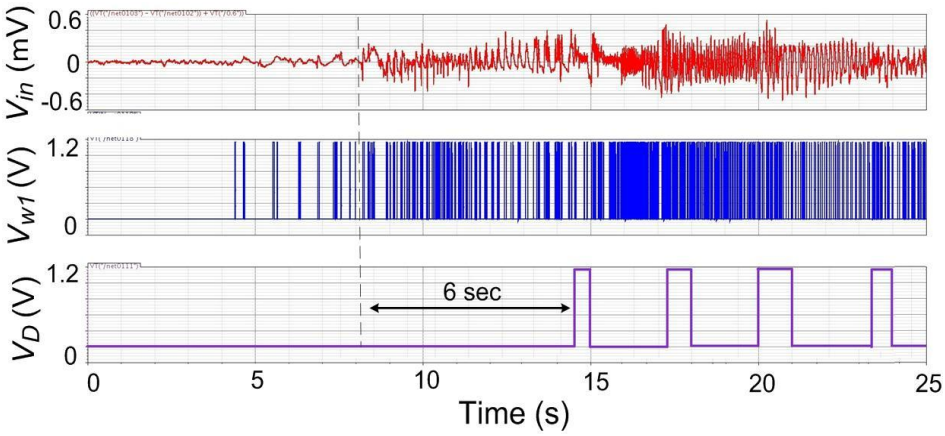

Figure 5.16: Validation of the proposed ASD by post-layout simulation of Case 2: V_{in} is the icEEG signal of the partial seizure, V_{W1} is the output of the first voltage window detector, and V_D is the final output of the ASD.

Through a craniotomy, intracranial electrodes were implemented to sample temporal and insular regions of the second patient (24 year-old male). Several electrical seizures were recorded from the right medial temporal lobe. The magnitude and frequency analysis of a recorded icEEG signal of this patient is shown in Fig. 5.16. The proposed system detected the seizure 6 sec after the ictal onset.

A total of 8 signals including 4 long normal signals and 4 electro-clinical seizures from these two epileptic patients were processed for post-layout simulations and an average detection delay of 9.5 s was obtained after seizure onset. Table 5.11 compares the epileptic seizure detectors in [83] and [112] with the experimental results from PCB-based detector [1] and those we got from the post-layout simulation of the ASD [2].

Table 5.11: Comparison of the seizure detectors

Parameter	**Power consumption (mW)**	**Input referred noise (µVrms)**	**T_{DET}[a] (s)**
[83]	0.0070	N/A	10.7
[112]	7.21	N/A	0.65
[1][b]	67.6	6	12.5
This work[c] [2]	0.0071	4.4	9.5

[a] T_{DET} is the overall average detection delay, [b] The experimental results from PCB-based detector, and [c] Post-layout simulation results of the integrated ASD.

5.2.2 Experimental results

Fig. 5.17 illustrates that the icEEG recordings from the contacts positioned over the epileptogenic zones were selected, stored on a Tektronix 715 Logic analyzer and converted to 8-bit digital signals. Then, a digital to analog converter (DAC) circuit was used to reconstruct the icEEG signals of the patients. By using an attenuator, these signals are converted to micro-level analog form and streamed to the fabricated seizure detector. The asynchronous seizure detector was adjusted to the specific attributes on time frequency and time amplitude analysis of the icEEG data for each patient.

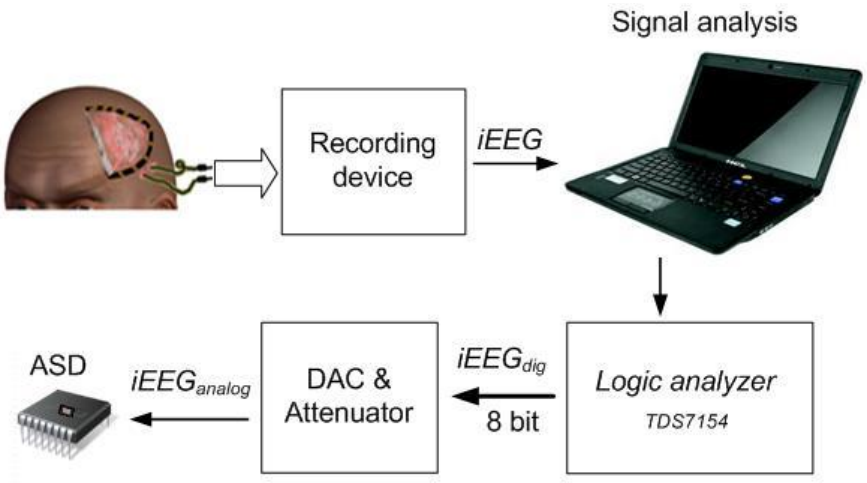

Figure 5.17: Test-bench setup to test fabricated ASD

In Fig. 5.18, a sine wave with frequency of 30 Hz was fed to the fabricated micro-chip. The output of the analog building block provided the required gain (60 dB) to amplify this signal.

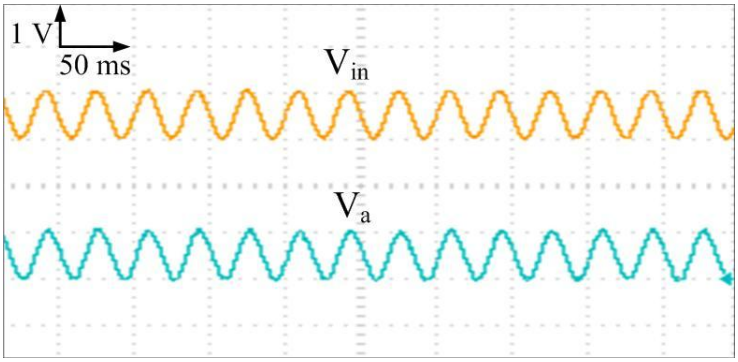

Figure 5.18: V_{in} is a sine wave (F=30 Hz) used as the input of the ASD and V_a is the output of the analog stage

Fig. 5.19 shows that for a sine wave with frequency of 59 Hz, the output of the analog stage is filtered (3dB low-pass cut off frequency).

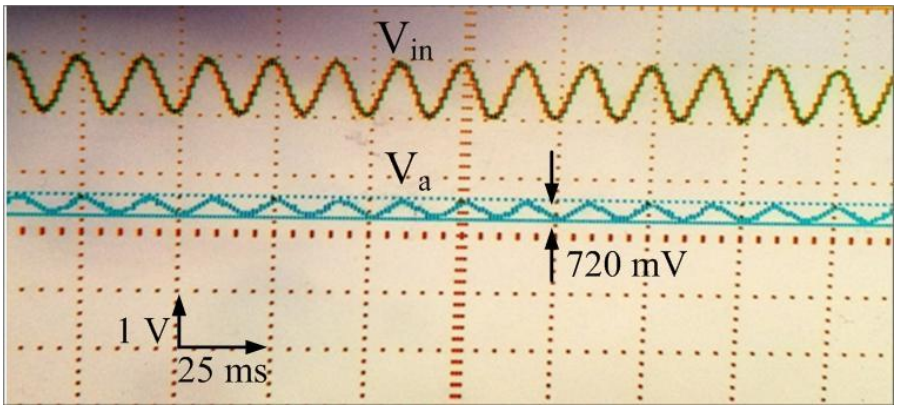

Figure 5.19: 3-dB low-pass cut off frequency of the filter

Fig. 5.20 demonstrates a sine wave with frequency of 1 Hz as the input of the ASD and the amplified and filtered output of the analog stage showed that the high-pass cut off frequency of the chip is less than 1 Hz.

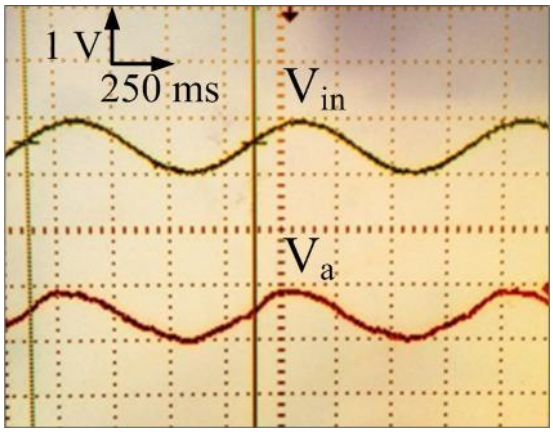

Figure 5.20: The output of the analog stage for a sine wave with frequency of 1 Hz

The signal amplitude and frequency of the brain activities are variable so that more experimental results of the fabricated micro-chip were illustrated in chapter 4 [3].

GENERAL DISCUSSION

Although antiepileptic drugs provide the first line of treatments for epilepsy many of these patients suffer from systemic side effects and remaining of them are drug resistant. Epilepsy surgery is an alternative treatment option for the refractory patients but patients who have multifocal epilepsy or have risks from surgery due to loss of the brain functionalities are continuously disable due to the lack of treatment option. Thus, researchers are looking for other alternative treatments for conventionally untreatable patients, such as implantable responsive devices delivering focal treatment upon automated detection of the electrographic seizures. The first step of constructing a reliable responsive device is to design an electrographic seizure detector. Recently, the epileptic seizure prediction methods are more interesting for researchers since detecting seizure activities prior to clinical manifestation could warn patients and provide the release of the medication in order to suppress seizure activities. Therefore, the automatic self-triggering detector must exhibit high sensitivity and low false alarms.

Efficacy of the implantable microsystems for treatment of the refractory patients depends on precise evaluation of the EEG and accurate identification of the predefined electrographic patterns. The automated evaluation and detection performance can be improved by reducing the noises which may degrade self-triggering devices. Flicker noise due to fundamental physics property of the instrumentation and thermal noise due to internal resistance of the instrumentation and wire resistance contribute major amount. In this work, a low-noise front-end bioamplifier is used which eliminates the Dc offset due to electrode-tissue interface. Moreover, the 60 Hz noise is attenuated using low-pass filter. Following the amplification and filtering stages, recordings are further evaluated to detect abnormal electrographic patterns precisely.

Power management of the automatic seizure detectors is one of the other major issues of the implantable devices. Since power consumption could be managed by two main parameters, short circuit currents due to transistor switching and signal transitions in parasitic capacitances, we proposed in this thesis an asynchronous system to reduce power consumption of the seizure detector by eliminating unnecessary clock skew and clock tree.

The proposed system provides a suitable therapy for patients who suffer from focal epilepsy and are not good candidates for surgery or are refractory to antiepileptic drugs. From patient to patient, seizure onset patterns may vary in terms of onset morphology, discharge frequency, and

spread pattern. The proposed system is designed to detect low-voltage high-frequency discharge that is the most common seizure onset pattern in epileptic patients.

The Prototype-based asynchronous seizure detector was first designed and validated using discrete components on PCB. The performance of the PCB was verified using icEEG signals recorded from 7 patients with different electrical seizures. The results persuaded us to design, in a second step, an integrated version of the asynchronous seizure detector to improve power management, noise, and performance of the seizure detector.

Then, the integrated asynchronous seizure detector is designed to be part of an implantable integrated device intended to identify electrographic seizure onset and trigger a focal treatment to block the seizure progression. This system eliminates the unnecessary clock tree and reduces power dissipation in the power saving mode. The hardware implementation of the integrated system is done in 0.13 µm CMOS technology with total die area of 1.5×1.5 mm^2. This system contains low-noise front-end preamplifier, digital signal processor and a detector. Some programmable parameters are used to extract electrographic seizure onset information from real-time EEG recordings. Sensitivity of the detector is enhanced by optimizing the variable parameters based on specific electrographic seizure onset activities of each patient. Performance of the integrated asynchronous seizure detector is validated using post-layout simulations.

The icEEG signals from two patients including 15 seizures and 19 non-seizure datasets were recorded. A test bench is used to reconstruct the recorded icEEG signals and test the chip offline. Two samples of the fabricated device were used which demonstrated proper performance of the system and early detection of the seizure onset prior to the clinical manifestations.

The overall results in this work are achieved using the advantages of the following techniques:

- A patient-specific detection method is used where electrographic signals of each patient are used to improve the sensitivity and specificity of the system.
- The count-based detection algorithm decreased the false detection rate of the system, which is caused by unrelated seizure activities.
- The asynchronous structure provides a reduction of 40% in power saving mode.
- Both positive and negative parts of the icEEG signals are analyzed using programmable parameters to facilitate the specific tuning to electrographic seizure onset of each patient.

CONCLUSION AND FUTURE WORKS

An integrated low-power asynchronous seizure detector has been proposed where low amplitude icEEG signals are amplified by two gain stages to provide a total midband gain of 60 dB. The random Dc offset of the electrodes is eliminated in the front end stage and noise of the system is attenuated by using a Gm-C low-pass filter. A sensitivity of 100% was achieved using various signals of the epileptic patients and an average detection delay of 13.7 s was obtained after seizure onset, well before the clinical manifestations. The power consumption of the proposed asynchronous seizure detector is improved compared to the PCB-based and other seizure detectors. The experimental results demonstrated that the microsystem can identify electrographic seizure onset precisely and trigger an electrical stimulator for focal treatment prior to the clinical manifestations.

Due to the diversity observed in the signal amplitude and frequencies of the epileptic seizures, two samples of the fabricated micro-chips are verified which showed the consistency of the measurements in digital and analog building blocks. However, it is worthwhile testing more patients or providing longer dataset of these patients.

The seizure onset patterns may vary in terms of the onset morphology, discharge frequency, and spread pattern from patient to patient. Since low-voltage fast-activity patterns at seizure onset are the most frequently encountered ones, the proposed seizure detector is designed for this type of patterns and it is worth further investigating on patients characterized by high-voltage fast-activity, rhythmic spiking, and other patterns.

Future works based on our studies and experiments in this thesis can proceed in four directions as follow.

The proposed asynchronous seizure detector is tested off-line using the recorded icEEG signals of two epileptic patients. The future work could contain the validation of the proposed device in an animal model of the epilepsy.

In the design of the proposed system, several test pads are used to verify the performance of different blocks. This resulted in using larger silicon area to design the integrated chip. Since the performance of this asynchronous seizure detector is approved, it is possible to reduce the number of the test points and minimize the size of the device.

The differential difference amplifier stage that works as a buffer between analog and digital stages didn't work properly so an external buffer (INA 118) is used to connect the analog and digital blocks together. It is suggested to design a new differential difference amplifier stage or reproduce the layout of the previous one with a better matching and verify the functionality of this stage.

In the layout of the asynchronous seizure detector, the pads are used as terminals but these pads do not provide electrostatic discharge protection. It is suggested to provide this protection and check design rule to meet the requirements.

REFERENCES

[1] Salam, M. T., Mirzaei, M., Ly, M. S., Dang Khoa, Nguyen, & Sawan, M. (2012). "An Implantable Closed-loop Asynchronous Drug Delivery System for the Treatment of Refractory Epilepsy." *Neural Systems and Rehabilitation Engineering, IEEE Transactions on* 20(4): 432-442.

[2] Mirzaei, M., Salam, M. T., Nguyen, D. K., & Sawan, M. (2012, November). An integrated low-power asynchronous epileptic seizure detector. In Biomedical Circuits and Systems Conference (BioCAS), (pp. 152-155).

[3] Mirzaei, M., Salam, M. T., Nguyen, D. K., & Sawan, M. (2013). A Fully-Asynchronous Low-Power Implantable Seizure Detector For Self-Triggering Treatment. Submitted to *Biomedical Circuits and Systems, IEEE Transactions (TBCAS).*

[4] Yadav, R. (2012). Automatic Detection and Classification of Neural Signals in Epilepsy. Doctoral dissertation, Concordia University.

[5] Venkataraman, V. (2012). Brain Dynamics Based Automated Epileptic Seizure Detection, Thesis (M.A.Sc), Arizona state university.

[6] Dorai, A., and Ponnambalam, K. (2010, June). Automated epileptic seizure onset detection. *In Autonomous and Intelligent Systems (AIS)*, 2010 International Conference on (pp. 1-4), IEEE.

[7] Litt, B. and K. Lehnertz (2002). "Seizure prediction and the preseizure period." Current opinion in neurology 15(2): 173-177.

[8] Gardner, A. B. (2004). A novelty detection approach to seizure analysis from intracranial EEG. Doctoral dissertation, Georgia Institute of Technology.

[9] Qu, H. (1995). Self-adapting Algorithms for Seizure Detection During EEG Monitoring [microform], Thesis (Ph.D.)- McGill University.

[10] Zijlmans, M., Jacobs, J., Kahn, Y. U., Zelmann, R., Dubeau, F., & Gotman, J. (2011). Ictal and interictal high frequency oscillations in patients with focal epilepsy. *Clinical Neurophysiology*, *122*(4), 664-671.

[11] Gotman, J. (1985). Seizure recognition and analysis. *Electroencephalography and clinical neurophysiology*. Supplement, 37, 133.

[12] Tzallas, A. T., Tsipouras, M. G., Tsalikakis, D. G., Karvounis, E. C., Astrakas, L., Konitsiotis, S., & Tzaphlidou, M. (2012). Automated Epileptic Seizure Detection Methods: A Review Study. Epilepsy - Histological, Electroencephalographic and Psychological Aspects, Dr. Dejan Stevanovic (Ed.), ISBN: 978-953-51-0082-9, InTech, Available from: http://www.intechopen.com/books/epilepsy-histological-electroencephalographic-and psychologicalaspects/automated-epileptic-seizure-detection-methods-a-review-study.

[13] Gotman, J., & Gloor, P. (1976). Automatic recognition and quantification of interictal epileptic activity in the human scalp EEG. *Electroencephalography and clinical neurophysiology*, *41*(5), 513-529.

[14] Ktonas, P. Y. (1983). Automated analysis of abnormal electroencephalograms. Crit Rev Biomed Eng, 9(1), 39-97.

[15] Faure, C. (1985). Attributed strings for recognition of epileptic transients in EEG. Int J Biomed Comput, 16(3-4), 217-229.

[16] Pon, L. S., Sun, M., & Robert, J. S. (2002). The bi-directional spike detection in EEG using mathematical morphology and wavelet transform. Paper presented at the 6th International Conference on Signal Processing.

[17] Xu, G., Wang, J., Zhang, Q., Zhang, S., & Zhu, J. (2007). A spike detection method in EEG based on improved morphological filter. Comput Biol Med, 37(11), 1647-1652.

[18] Hesse, C. W., & James, C. J. (2007). Tracking and detection of epileptiform activity in multichannel ictal EEG using signal subspace correlation of seizure source scalp topographies. Med Biol Eng Comput, 45(10), 909-916.

[19] Ossadtchi, A., Baillet, S., Mosher, J. C., Thyerlei, D., Sutherling, W., & Leahy, R. M. (2004). Automated interictal spike detection and source localization in magnetoencephalography using independent components analysis and spatiotemporal clustering. Clin Neurophysiol, 115(3), 508-522.

[20] Kobayashi, K., Akiyama, T., Nakahori, T., Yoshinaga, H., & Gotman, J. (2002a). Systematic source estimation of spikes by a combination of independent component analysis and RAP-MUSIC. I: Principles and simulation study. Clin Neurophysiol, 113(5), 713- 724.

[21] Webber, W. R., Litt, B., Wilson, K., & Lesser, R. P. (1994). Practical detection of epileptiform discharges (EDs) in the EEG using an artificial neural network: a comparison of raw and parameterized EEG data. Electroencephalogr Clin Neurophysiol, 91(3), 194- 204.

[22] Castellaro, C., Favaro, G., Castellaro, A., Casagrande, A., Castellaro, S., Puthenparampil, D. V., et al. (2002). An artificial intelligence approach to classify and analyse EEG traces. Neurophysiol Clin, 32(3), 193-214.

[23] Oikonomou, V. P., Tzallas, A. T., & Fotiadis, D. I. (2007). A Kalman filter based methodology for EEG spike enhancement. Comput Methods Programs Biomed, 85(2), 101-108.

[24] James, C., Kobayashi, K., & Gotman, J. (2000). Seizure Detection with the Self-Organising Feature Map. In Artificial Neural Networks in Medicine and Biology (pp. 143-148). Springer London.

[25] Lopes Da Silva, F. H., Dijk, A., & Smits H. (1975). Detection of nonstationarities in EEGs using the autoregressive model – an application to EEGs of epileptics. G. Dolce, H. Künkel (Eds.), CEAN: Computerized EEG Analysis, Verlag, Stuttgart, 180–199.

[26] James, C. J., Jones, R. D., Bones, P. J., & Carroll, G. J. (1999). Detection of epileptiform discharges in the EEG by a hybrid system comprising mimetic, self-organized artificial neural network, and fuzzy logic stages. *Clin Neurophysiol, 110*(12), 2049-2063.

[27] Exarchos, T. P., Tzallas, A. T., Fotiadis, D. I., Konitsiotis, S., & Giannopoulos, S. (2006). EEG transient event detection and classification using association rules. *Information Technology in Biomedicine, IEEE Transactions on*, *10*(3), 451-457.

[28] Mukhopadhyay, S., & Ray, G. C. (1998). A new interpretation of nonlinear energy operator and its efficacy in spike detection. IEEE Trans Biomed Eng, 45(2), 180-187.

[29] Malarvili, M. B., Hassanpour, H., Mesbah, M., & Boashash, B. (2005). A Histogram-Based Electroencephalogram Spike Detection. Paper presented at the Proc. 8th Intern. Symp. on Sig.l Proc. & Its Applic.

[30] Durka, P. J. (2004). Adaptive time-frequency parametrization of epileptic spikes. Phys Rev E Stat Nonlin Soft Matter Phys, 69(5 Pt 1), 051914.

[31] James, C. J. (1997). Detection of epileptiform activity in the electroencephalogram using the electroencephalogram using artificial neural networks. University of Canterbury, Christchurch.

[32] Tzallas, A. T., Oikonomou, V. P., & Fotiadis, D. I. (2006). Epileptic spike detection using a Kalman filter based approach. Conf Proc IEEE Eng Med Biol Soc, 1, 501-504.

[33] Yadav, R. (2012). Automatic Detection and Classification of Neural Signals in Epilepsy, Concordia University.

[34] Willming, D. A. and B. C. Wheeler (1990). "Real-time multichannel neural spike recognition with DSPs." Engineering in Medicine and Biology Magazine, IEEE 9(1): 37-39.

[35] Chandra, R. and L. M. Optican (1997). "Detection, classification, and superposition resolution of action potentials in multiunit single-channel recordings by an on-line real-time neural network." Biomedical Engineering, IEEE Transactions on 44(5): 403-412.

[36] Wood, F., M. J. Black, et al. (2004). "On the variability of manual spike sorting." Biomedical Engineering, IEEE Transactions on 51(6): 912-918.

[37] Kaneko, H., H. Tamura, et al. (2007). "Tracking Spike-Amplitude Changes to Improve the Quality of Multineuronal Data Analysis." Biomedical Engineering, IEEE Transactions on 54(2): 262-272.

[38] Wolf, M. T. and J. W. Burdick (2009). "A Bayesian Clustering Method for Tracking Neural Signals Over Successive Intervals." Biomedical Engineering, IEEE Transactions on 56(11): 2649-2659.

[39] Chan, H.-L., T. Wu, et al. (2010). "Unsupervised wavelet-based spike sorting with dynamic codebook searching and replenishment." Neurocomputing 73(7–9): 1513-1527.

[40] McSharry, P. E., He, T., Smith, L. A., & Tarassenko, L. (2002). Linear and non-linear methods for automatic seizure detection in scalp electro-encephalogram recordings. Med Biol Eng Comput, 40(4), 447-461.

[41] Polat, K., & Gunes, S. (2007). Classification of epileptiform EEG using a hybrid system based on decision tree classifier and fast Fourier transform. Applied Mathematics and Computation, 187(2), 1017–1026.

[42] Ocak, H. (2009). Automatic detection of epileptic seizures in EEG using discrete wavelet transform and approximate entropy. Expert Systems with Applications, 36(2), 2027– 2036.

[43] Guo, L., Rivero, D., & Pazos, A. (2010). Epileptic seizure detection using multiwavelet transform based approximate entropy and artificial neural networks. J Neurosci Methods, 193(1), 156-163.

[44] Wang, D., Miao, D., & Xie, C. (2011). Best basis-based wavelet packet entropy feature extraction and hierarchical EEG classification for epileptic detection. Expert Systems with Applications (8), 14314–14320.

[45] Iscan, Z., Dokur, Z., & Tamer, D. (2011). Classification of electroencephalogram signals with combined time and frequency features. Expert Systems with Applications, 38, 10499–10505.

[46] Nigam, V. P., & Graupe, D. (2004). A neural-network-based detection of epilepsy. Neurol Res, 26(1), 55-60.

[47] Srinivasan, V., Eswaran, C., & Sriraam, N. (2005). Artificial neural network based epileptic detection using time-domain and frequency-domain features. J Med Syst, 29(6), 647- 660.

[48] Subasi, A., & Kiymik, M. K. (2010). Muscle fatigue detection in EMG using time–frequency methods, ICA and neural networks. *Journal of medical systems*, *34*(4), 777-785.

[49] L., Rivero, D., Dorado, J., Munteanu, C. R., & Pazos, A. (2011). Automatic feature extraction using genetic programming: An application to epileptic EEG classification. Expert Systems with Applications, 38, 10425-10436.

[50] Tzallas, A. T., Tsipouras, M. G., & Fotiadis, D. I. (2009). Epileptic seizure detection in EEGs using time-frequency analysis. IEEE Trans Inf Technol Biomed, 13(5), 703-710.

[51] Adeli, H., Ghosh-Dastidar, S., & Dadmehr, N. (2007). A wavelet-chaos methodology for analysis of EEGs and EEG subbands to detect seizure and epilepsy. IEEE Trans Biomed Eng, 54(2), 205-211.

[52] Subasi, A., & Gursoy, I. (2010). EEG signal classification using PCA, ICA, LDA and support vector machines. Expert Systems with Applications 37, 8659–8666.

[53] Lima, C. A., & Coelho, A. L. (2011). Kernel machines for epilepsy diagnosis via EEG signal classification: A comparative study. Artif Intell Med.

[54] Pauri, F., F. Pierelli, et al. (1992). "Long-term EEG-video-audio monitoring: computer detection of focal EEG seizure patterns." Electroencephalography and Clinical Neurophysiology 82(1): 1-9.

[55] Gotman, J. (1982). "Automatic recognition of epileptic seizures in the EEG." Electroencephalography and Clinical Neurophysiology 54(5): 530-540.

[56] Gotman, J. (1990). "Automatic seizure detection: improvements and evaluation." Electroencephalography and Clinical Neurophysiology 76(4): 317-324.

[57] Harding, G. W. (1993). "An automated seizure monitoring system for patients with indwelling recording electrodes." Electroencephalography and Clinical Neurophysiology 86(6): 428-437.

[58] Osorio, I., M. G. Frei, et al. (1998). "Real-time automated detection and quantitative analysis of seizures and short-term prediction of clinical onset." Epilepsia 39(6): 615-627.

[59] Khan, Y. U. and J. Gotman (2003). "Wavelet based automatic seizure detection in intracerebral electroencephalogram." Clinical Neurophysiology 114(5): 898-908.

[60] Saab, M. E. and J. Gotman (2005). "A system to detect the onset of epileptic seizures in scalp EEG." Clinical Neurophysiology 116(2): 427-442.

[61] Iasemidis, L. D. (2003). "Epileptic seizure prediction and control." Biomedical Engineering, IEEE Transactions on 50(5): 549-558.

[62] Navakatikyan, M. A., P. B. Colditz, et al. (2006). "Seizure detection algorithm for neonates based on wave-sequence analysis." Clinical Neurophysiology 117(6): 1190-1203.

[63] Aarabi, A., R. Fazel-Rezai, et al. (2009). Seizure detection in intracranial EEG using a fuzzy inference system. Engineering in Medicine and Biology Society, 2009. EMBC 2009. Annual International Conference of the IEEE.

[64] Duun-Henriksen, J., T. W. Kjaer, et al. (2012). "Channel selection for automatic seizure detection." Clinical Neurophysiology 123(1): 84-92.

[65] Majumdar, K. K. and P. Vardhan (2011). "Automatic seizure detection in ECoG by differential operator and windowed variance." Neural Systems and Rehabilitation Engineering, IEEE Transactions on 19(4): 356-365.

[66] Qu, H., & Gotman, J. (1997). A patient-specific algorithm for the detection of seizure onset in long-term EEG monitoring: possible use as a warning device. *Biomedical Engineering, IEEE Transactions on*, *44*(2), 115-122.

[67] Wendling, F., J. J. Bellanger, et al. (1996). "Extraction of spatio-temporal signatures from depth EEG seizure signals based on objective matching in warped vectorial observations." Biomedical Engineering, IEEE Transactions on 43(10): 990-1000.

[68] Wendling, F. and F. Bartolomei (2001). "Modeling EEG signals and interpreting measures of relationship during temporal-lobe seizures: an approach to the study of epileptogenic networks." Epileptic Disorders 3.

[69] Wendling, F., F. Bartolomei, et al. (2003). "Epileptic fast intracerebral EEG activity: evidence for spatial decorrelation at seizure onset." Brain 126(6): 1449-1459.

[70] Shoeb, A., H. Edwards, et al. (2004). "Patient-specific seizure onset detection." Epilepsy & Behavior 5(4): 483-498.

[71] Wilson, S. B. (2005). "A neural network method for automatic and incremental learning applied to patient-dependent seizure detection." Clinical Neurophysiology 116(8): 1785-1795.

[72] Wilson, S. B. (2006). "Algorithm architectures for patient dependent seizure detection." Clinical Neurophysiology 117(6): 1204-1216.

[73] Shi, L., R. Agarwal, et al. (2004). Model-based seizure detection method using statistically optimal null filters. Engineering in Medicine and Biology Society, 2004. IEMBS'04. 26th Annual International Conference of the IEEE, IEEE.

[74] Zandi, A. S., M. Javidan, et al. (2010). "Automated real-time epileptic seizure detection in scalp EEG recordings using an algorithm based on wavelet packet transform." Biomedical Engineering, IEEE Transactions on 57(7): 1639-1651.

[75] Salam, M. T. (2012). Implantable Micro-Device for Epilepsy Seizure Detection and Subsequent Treatment, Doctoral dissertation, École Polytechnique de Montréal.

[76] Pellock, J. M., Bourgeois, B. F., Dodson, W. E., and Nordli, D. R. (2008). *Pediatric epilepsy: diagnosis and therapy*. New York: Demos Medical Publishing.

[77] Schachter, S. C., Guttag, J., Schiff, S. J., Schomer, D. L., & Summit Contributors. (2009). Advances in the application of technology to epilepsy: the CIMIT/NIO epilepsy innovation summit. Epilepsy & Behavior, 16, 3–46.

[78] Berdakh, A., & Don, S. H. (2009). Epileptic seizures detection using continuous time wavelet based artificial neural networks. ITNG - Int. Conf. Inf. Technol.: New Gener, 1456-1461.

[79] Sukhi, G. & Jean, G. (2005). An automatic warning system for epileptic seizures recorded on intracerebral EEGs. Clinical neurophysiology, 116, 2460–2472.

[80] Aksenova, T. I., Volkovych, V. V., & Villa, A. E. P. (2007). Detection of spectral instability in EEG recordings during the preictal period, J. Neural Eng., 4, 173.

[81] Nandan, M., Sachin, S. S., Myers, S., Ditto, W. L., Khargonekar, P. P., & Carney, P, R. (2010). Support vector machines for seizure detection in an animal model of chronic epilepsy. J. Neural Eng., 7, 036001.

[82] Polychronaki, G. E., Ktonas, P. Y., Gatzonis, S., Siatouni, A., Asvestas, P. A., Tsekou, H., Sakas, D., & Nikita, K. S. (2010). Comparison of fractal dimension estimation algorithms for epileptic seizure onset detection. J. Neural Eng., 7, 046007.

[83] Safi-Harb, M., Salam, M. T., Nguyen, D. K., & Sawan, M. (2011). An implantable seizure-onset detector based on a dual-path single-window count-based technique for closed-loop applications. *Emerging and Selected Topics in Circuits and Systems, IEEE Journal on*, *1*(4), 603-612.

[84] Salam, M. T., Sawan, M., Hamoui, A., & Nguyen D. K. (2009). Low-power CMOS-based epileptic seizure onset detector. IEEE-NEWCAS, pp. 1-4.

[85] Raghunathan, S., Gupta, S. K., Ward, M. P., Worth, R. M., Roy, K., & Irazoqui, P. P. (2009). The design and hardware implementation of a low-power real-time seizure detection algorithm. Journal of Neural Engineering, 6(5), 1-13.

[86] Patel, K., Chua, C. P., Fau, S., & Bleakley, C. J. (2009, April). Low power real-time seizure detection for ambulatory EEG. In *Pervasive Computing Technologies for Healthcare, 2009. PervasiveHealth 2009. 3rd International Conference on* (pp. 1-7). IEEE.

[87] Verma, N., Shoeb, A., Bohorquez, J., Dawson, J., Guttag, J., & Chandrakasan, A. P. (2010). A micro-Power EEG acquisition SoC with integrated feature extraction processor for a chronic seizure detection system. IEEE Journal of Solid-State Circuits, 45(4), 804-16.

[88] Meier, R., Dittrich, H., Schulze-Bonhage, A., *et al.* (2008). Detecting epileptic seizures in long-term human EEG: a new approach to automatic online and real-time detection and classification of polymorphic seizure patterns," *J. Clin. Neurophysiol.,* vol. 25, no. 3, pp. 119-131.

[89] Zandi, A. S., Dumont, A. G., Javidan, M., & Tafreshi, R. (2009). An entropy-based approach to predict seizures in temporal lobe epilepsy using scalp EEG. *Proc. Annu. Int. Conf. IEEE Eng.Med. Biol. Soc.: Eng. Future Biomed., EMBC*, 228-231.

[90] Tito, M., Cabrerizo, M., Ayala, M. *et al.* (2009). Seizure detection: an assessment of time- and frequency-based features in a unified two-dimensional decisional space using nonlinear decision functions. *J. Clin. Neurophysiol.,* vol. 26, pp. 381-91.

[91] Nielsen, L. S. & Sparso, J. (1999). Designing asynchronous circuits for low power: an IFIR filter bank for a digital hearing aid. *Proceedings of the IEEE,* vol. 87, no. 2, pp. 268-81.

[92] Texas Instruments. (2013). Datasheet. Precision, Low Power Instrumentation Amplifier. Retrieved from http://www.ti.com/lit/ds/symlink/ina118.pdf.

[93] Gosselin, B., Sawan, M., & Chapman, C. A. (2007). A low-power integrated bioamplifier with active low-frequency suppression. *Biomedical Circuits and Systems, IEEE Transactions on*, *1*(3), 184-192.

[94] Baker, R. J. (2011). CMOS: Circuit design, layout, and simulation (Vol. 18). Wiley-IEEE Press.

[95] Harrison, R. R. (2008). The design of integrated circuits to observe brain activity. *Proceedings of the IEEE*, *96*(7), 1203-1216.

[96] Omeni, O., Rodriguez-Villegas, E., & Toumazou, C. (2005). A micropower CMOS continuous-time filter with on-chip automatic tuning. *Circuits and Systems I: Regular Papers, IEEE Transactions on*, *52*(4), 695-705.

[97] Goel, S., Elgamel, M. A., & Bayoumi, M. A. (2003, September). Novel design methodology for high-performance XOR-XNOR circuit design. In *Integrated Circuits and Systems* Design, 2003. SBCCI 2003. Proceedings. 16th Symposium on (pp. 71-76). IEEE.

[98] Modulo N Counter, "Frequency Divider," Modulo N Counter, Retrieved from: http://reviseomatic.org/help/s-advanced-logic/Logic%20Modulo%20N%20Counter.php. [Retrieval date: 15 August 2013].

[99] CS411 Downloadable Source and Executables, "D flip flop - six nand gate model," CS411 Downloadable Source and Executables, Retrieved from:

http://www.csee.umbc.edu/~squire/s98-411/cs411_down.shtml. [Retrieval date: 15 August 2013].

[100] Spencer, S. S., Nguyen, D. K., & Duckrow, R. B. (2009). Invasive EEG in presurgical evaluation of epilepsy. *The Treatment of Epilepsy, Third Edition*, 767-798.

[101] Salam, M. T., Sawan, M., & Nguyen, D. K. (2011). A novel low-power-implantable epileptic seizure-onset detector. *Biomedical Circuits and Systems, IEEE Transactions on*, *5*(6), 568-578.

[102] Mormann, F., Lehnertz, K., David, P., & E Elger, C. (2000). Mean phase coherence as a measure for phase synchronization and its application to the EEG of epilepsy patients. *Physica D: Nonlinear Phenomena*, *144*(3), 358-369.

[103] Elger, C. E., & Lehnertz, K. (2001). Seizure prediction by non-linear time series analysis of brain electrical activity. *European Journal of Neuroscience*, *10*(2), 786-789.

[104] Iasemidis, L. D., Shiau, D. S., Chaovalitwongse, W., Sackellares, J. C., Pardalos, P. M., Principe, J. C., Carney, P. R., Prasad, A., Veeramani, B., and Tsakalis, K. (2003). Adaptive epileptic seizure prediction system. *Biomedical Engineering, IEEE Transactions on*,*50*(5), 616-627.

[105] Salam, M. T., Hamie, A. H., Nguyen, D. K., & Sawan, M. (2012). A Smart Biological Signal-Responsive Focal Drug Delivery System for Treatment of Refractory Epilepsy. *Advances in Science and Technology*, *85*, 39-46.

[106] Salam, M. T., Mounaïm, F., Nguyen, D. K., & Sawan, M. (2012). A Low-Power Miniaturized Seizure Detector with Responsive Neurostimulation for the Treatment of Refractory Epilepsy. Journal of Low Power Electronics: Special Issue on Emerging Technologies, *8*(2).

[107] Yoo, J., Yan, L., El-Damak, D., Altaf, M. A. B, Shoeb, A., Yoo, H. J., and Chandrakasan, A. (2012, February). An 8-Channel Scalable EEG Acquisition SoC With Patient-Specific Seizure Classification and Recording Processor. *In Solid-State Circuits Conference Digest of Technical Papers (ISSCC)*, 2012 IEEE International (pp. 292-294), IEEE.

[108] Altaf, M. A. B., Tillak, J., Kifle, Y., & Yoo, J. (2013, February). A 1.83μJ/classification nonlinear support-vector-machine-based patient-specific seizure classification SoC. *In Solid-State Circuits Conference Digest of Technical Papers (ISSCC)*, 2013 IEEE International (pp. 100-101). IEEE.

[109] Chen, W. M., Chiueh, H., Chen, T. J., Ho, C. L., Jeng, C., Chang, S. T., ... & Wu, C. Y. (2013, February). A fully integrated 8-channel closed-loop neural-prosthetic SoC for real-time epileptic seizure control. In Solid-State Circuits Conference Digest of Technical Papers (ISSCC), 2013 IEEE International (pp. 286-287), IEEE.

[110] Charles, C. T., & Harrison, R. R. (2003, February). A floating gate common mode feedback circuit for low noise amplifiers. In *Mixed-Signal Design, 2003. Southwest Symposium on* (pp. 180-185).

[111] Sackinger, E., & Guggenbuhl, W. (1987). A versatile building block: the CMOS differential difference amplifier. *Solid-State Circuits, IEEE Journal of*, *22*(2), 287-294.

[112] Chen, T. J., Chiueh, H., Liang, S. F., Chang, S. T., Jeng, C., Hsu, Y. C., & Chien, T. C. (2011). The Implementation of a Low-Power Biomedical Signal Processor for Real-Time Epileptic Seizure Detection on Absence Animal Models. *Emerging and Selected Topics in Circuits and Systems, IEEE Journal on*, *1*(4), 613-621.